MAPPING OF PRESSURE LOSSES THROUGH MICROCHANNELS WITH SWEEPING-BENDS OF VARIOUS ANGLE AND RADII

by

CHASE JONATHAN HANSEL
B.S. University of Central Florida, 2006

A thesis submitted in partial fulfillment of the requirements
for the degree of Masters of Science in ThermoFluids
in the Department of Mechanical, Materials, and Aerospace Engineering
in the College of Engineering and Computer Science
at the University of Central Florida
Orlando, Florida

Spring Term
2008

ABSTRACT

MEMS (Micro Electro Mechanical Systems) have received a great deal of attention in both the research and industrial sectors in recent decades. The broad MEMS category, microfluidics, the study of fluid flow through channels measured on the micrometer scale, plays an important role in devices such as compact heat exchangers, chemical and biological sensors, and lab-on-a-chip devices. Most of the research has been focused on how entire systems operate, both experimentally and through simulation. This paper strives, systematically, to map them through experimentation of the previous to untested realm of pressure loss through laminar square-profile sweeping-bend microchannels. Channels were fabricated in silicone and designed so a transducer could detect static pressure across a very specific length of channel with a desired bend. A wide variety of Reynolds numbers, bend radii, and bend angles were repeatedly tested over long periods in order to acquire a complete picture of pressure loss with in the domain of experimentation. Nearly all situations tested were adequately captured with the exception of some very low loss points that were too small to detect accurately. The bends were found to match laminar straight-duct theory at Reynolds numbers below 30. As Reynolds numbers increased, however, minor losses began to build and the total pressure loss across the bend rose above straight-duct predictions. A new loss coefficient equation was produced that properly predicted pressure losses for sweeping-bends at higher Reynolds numbers; while lower flow ranges are left to laminar flow loss for prediction.

This work is dedicated to my parents for nurturing and supporting me through the years and for always being my greatest teachers in life. To Gavin, the best brother I never had. To Jon for sharing in the laughs and datas. And to Dr. Chew for letting me get away with a lot of shenanigans in the lab.

TABLE OF CONTENTS

LIST OF FIGURES

LIST OF TABLES

LIST OF ACRONYMS/ABBREVIATIONS

CFD	Computation Fluid Dynamics
Kn	Knudsen number: Ratio of mean free path over channel length
MEMS	Micro Electro Mechanical Systems
Micron	Short for micrometers
PDMS	PolyDiMethylSiloxane: A type of silicon used to cast microchannels
PSI	Pounds per Square Inch: A unit of pressure
Re	Reynolds number: A nondimensional ratio of viscous and inertial forces

CHAPTER ONE: INTRODUCTION

MEMS (Micro Electro Mechanical Systems) have shown to be an extremely promising avenue of technology that produces machines which are often physically too small to be seen by the human, and perform tasks never before thought possible. Modern Inkjet printers, DMD® and DLP® displays, airbag accelerometers, and many optical switching technologies are all perfect examples of MEMS devices that are available to the consumer level and can be found in the average household. The automotive industry has become wise to the advantages MEMS sensors can provide, resulting in a large source of funding for this field of study. MEMS-based sensors allow scientists to measure biological and chemical components with an increasing level of sensitivity theoretically reaching parts per billion of certain gasses. These devices operate between one millimeter and a micrometer, or 10^{-6} meters. At this scale many standard physics intuitions do not hold true. For example, due to scale, vibration frequencies are extremely high, and heat transfer occurs nearly instantaneously. One of the many avenues in microscale research and development is in the area of fluid flows. Microfluidics, as it is referred to in industry, deals with fluid ducts that are in the micrometer scale. The average human hair is from 50 to 100 micrometers in diameter, and the channels required by MEMS applications are often of this size if not smaller.

Applications of microfluidics are in a few main categories. The first, and probably the largest, involves chemical and biological sensors that can be scaled down to microscopic sized. These lab-on-a-chip would be hyper sensitive and cheap to produce while remaining small enough that they could be embedded into nearly anything, The Lab-on-a-chip dream is

unfortunately still years from full completion, but the idea is very much alive and the technology gaps are closing rapidly. The basic idea is that all the sensing equipment needed to test for a certain substance could be placed on a single microchip. These chips could be distributed all over the world to act as weathers sensors, track carbon dioxide levels or act as an advanced early warning system for biological and chemical weapons. A single chip could be injected inside the body and monitor insulin levels for a diabetic patient with out the need for constant blood drawing. As mentioned earlier, the scale makes these devices more sensitive to even the most minute changes of a particular substance, but even more important than that is that they can be made cheaply. Much like modern computer chips are produced relatively cheaply in bulk, these labs can be made disposable by mass production. The sensors are very complicated, however, and typically are required to draw in fluids from the environment, be it air or liquid, sometimes mix it with required reactants, pump it over a test section, and finally, detect the particular chemical particle or biologic. Nearly all of these tasks are made more complicated by the scale that has afforded them their level of sensitivity.

Another big portion of microfluidics research is heat exchangers. Because of the large surface area to volume ratio any fluid on this scale has lots of surface contact. This surface contact is perfect for the exchange of heat. In addition, the preciseness of the scale allows for nearly perfect even cooling and previously unseen efficiencies. This prevents hot spots from destroying sensitive electronic equipment. Much of the work done in the field of microfluidics is very system oriented. Meaning that lots of people are trying to think up a clever design for a pump, or a mixer, test it via some method, and then publish the results. Though there is a often a considerable amount of thought and complex prediction put forth on these projects they are still trying to grasp big picture with out knowing the true nature of the details. Not enough groups

really try to focus on the fundamental understanding of how fluids act on this level, or at least generate enough useful data to be able to take an empirical approach. Though some work has been done on basic straight-ducts, sudden area changes, and other common plumbing geometries, much of it is conflicting, and over all it provides a very incomplete picture. It is the aim of this research to help fill in the gaps by doing more of these required fundamental tests. The focus will be on taking pressure loss data of sweeping-pipe bends of square-profile microchannels at various flow rates, bend radii, and bend angles. With this data it is hoped that a set of useful empirical data, and loss correlations can be generated in order to fill the gaps of understanding in this new field of study.

CHAPTER TWO: LITERATURE REVIEW

Microfluidics is an important sector of MEMS development. Many have documented the current research and potential future uses of microfluidics in MEMS based devices [1-4]. The aim of these small systems is often in sensing of a whole range of chemical and biological materials as well as providing compact and highly efficient heat exchangers. Electrophoresis can be used to separate out DNA material for small and quick testing. Sensors can be placed cheaply and easily nearly anywhere for detection of biological and chemical weapons. They can be distributed in mass to act as weather or pollution sensors, or placed inside the human body to monitor insulin levels in diabetic patients. Many of these similar applications can be summed up as various types of lab-on-a-chip designs; though each individual one presents its own interesting and unique challenges that must be overcome before the device can be realized. Detection and sensor applications are a large source of the driving force behind microfluidics research, but there are others. Heat exchangers benefit greatly from the scaling effects, and can very efficiently and quickly regulate microchip temperatures allowing for greater advances in computer processing power. Researchers have developed tiny fuel cells and jet engines that operate on the microscale with the hopes that power generation for portable devices could be better served by a re-fuelable cycle of some sort instead of chemical batteries which require time to recharge.

All of these applications require a great amount of understanding and development before they can be fully realized. For sensors to be able to detect anything with in the body or atmosphere they must pull in gas or liquids from the surrounding environment. To do this they

require efficient reliable and powerful pumps with some sort of valve system that can operate in a variety of environmental conditions. Many designs exist, but more will need to be created and refined before the dream can be realized. Many of the biological sensors require certain chemical reactions to take place before testing can occur. This may include mixing, heating, or separation. Mixing is very difficult on this level due to the low Reynolds number of fluids on the microscale, heating is relatively easy, but fine control is often needed which can be difficult, and finally separation of particles like DNA can be done via electrophoresis but other methods would still be preferred. A simpler component that every single one of these devices will have in common is ducting. No matter what type of microfluidics application is being tackled there will have to be piping and duct work to move fluids and materials around. Understanding and prediction of the various straight-duct pipes, bends, expansions, contractions and other pipe features is necessary to the furthering and development of any microscale fluids devices. How can a pump be designed if its requirements are not known?

Physics as it has been developed provides laws that appear to be unbreakable under any circumstances. To the every day observer many of these laws like gravity affect every aspect of daily life. A life with out gravity would be completely different and difficult to live. Scale, however, changes things. In the microscale, a whole new counterintuitive set of effects take over. Gravity becomes almost completely negligible and surface forces like capillarity, wetting and adhesion reign supreme [5]. Why would a simple scale change make all the surface effects more dramatic? Thinking about a simple microscale object such as a cube; the volume of said box would be the length of a side cubed or X^3. Similarly the surface area of a box would be the area of each side multiplied by the number of sides, or $6*X^2$. For an object with side length of 1 meter, the surface area to volume ratio would be 6, while this same ratio for a box with sides of 1

micrometer would be 6,000,000. Dramatic ratio differences like this can seriously change how certain physical phenomenons behave. It is because of this many orders of magnitude difference between the two scales that a person can not stand on water, but a small bug can zip across the surface of a pond as if it were concrete. Effects like this along with some experimental results have led some to believe that the micro flow regime operates completely differently that that of the macro scale [6-9]. Yet others have done similar testing and have concluded that with few exceptions the flow follows standard laminar pipe theory [10-12].

One of the reasons there could be deviation from classic flow theory is the increased effects viscous forces are allowed to have. When a duct is increasingly scaled down the ratio between surface area and volume becomes larger. This combined with a no-slip wall condition assumptions would lead towards a laminar flow nearly always occurring. Using the standard Reynolds (Re) number equation a typical microchannel scenario reveals an exceedingly laminar regime. A 100μm diameter duct with water at STP, and delivering 100 $\mu L\ min^{-1}$ has a Re of just 26. Refer to Appendix A for calculation details. Values this low are rarely if ever seen in standard engineering practices, and most moody charts don't begin to approach this scale. In a physical sense the Reynolds number is a ratio of inertial forces over viscous forces. Numbers this low suggest that the viscous forces are very rapidly catching up to any internal instability caused by flow. To confound matters further, with viscous forces playing such a dominant role in flow characteristics, the temperature of the fluid becomes highly important. A 10ºC deviation from STP causes a 20% change in the viscosity, and this viscosity change can affect the Reynolds number by up to 30% [13]. The high level of viscosity sensitivity due to temperature change was also greatly noted by Koo and Kleinstreuer [14]. This high variation makes it very

difficult to predict heat exchanger performance and adds another layer of variability to the task of flow mapping.

The question can easily be begged, if there is a difference in micro versus macro flow, when does a small channel become a 'microchannel'? Experimental observations backed by computational simulation confirmed that a channel 222μm by 694μm acted in accordance with normal macro scale duct theory [15]. This means that the flow losses could be predicted accurately by a standard moody chart and CFD. The experiment carried out by Qu and Mudawar shows that if "micro" ducts do operate differently than standard practice dictates they do so at a smaller hydraulic diameter than was tested. Herwig and Hausner [16] suggested that there was no "special micro-effect", but rather that there was a scaling effect that was either not fully understood, or not being taken into account. The arguments were mostly based off of heat transfer which is not the focus of their paper, but two of them were general flow issues. One was that there are pressure dependent properties, but the writers never really go on to explain what these are. The other is an issue with wall roughness and its specific distribution. This suggestion appears to fit in line with many of the previous conclusions on the reasoning behind any observed deviation from typical macro scale expectations.

Judy et al.[12] unhappy with the variations of straight-duct microchannel data they had seen previous to their work set out to test a very wide range of flow conditions. Their experiments included flow tests on both stainless steel and fused silica through a hydraulic diameter range of 15 to 150 micrometers; with 7 variations in between. In addition to a large number of pipe choices, they used not only water, but methanol and isopropanol. Their experiment tested whole pipe lengths very similarly to how previous groups had done via fixing the microduct to the end of a tube such that the test liquid had no choice but to flow through the

microchannel. A syringe pump then supplied set amounts of fluid, and by measuring the time it took for that fluid to show up at the exit a flow rate could be calculated. A pressure transducer was placed in between the syringe pump and microchannel to obtain pressure loss data. An interesting procedure they had that appears to be missed on most groups is the taking of temperature data not just on the fluid, but more specifically on the difference between the inlet and outlet fluid. This method would detect viscous heating through the channel; any of which would affect the viscosity and density of the fluid causing adverse changes to the Reynolds number calculations which will highly affect the flow. During the setup many small tests were done to see what had to happen to minimize the over all uncertainty. A highly important one was the testing of normal water versus degassed water. Some groups [9] have gone to great lengths to degas the water with the suggestion that micro bubbles could form in the channel either changing the flow characteristics, or sticking to the side causing a reduction of hydraulic diameter. Their testing of water that had been boiled under a vacuum for 5 minutes versus water that had not, revealed only a slight 2.2% variation. This was deemed low enough that further degassing procedures would not be necessary. Full swing testing showed that some of the tedious details that were taken into account early in the testing and methodology procedure have come in handy. It was noticed that at higher flow rates when the viscous heating became more pronounced the Reynolds number friction factor (fRe) began to deviate by as much as 7-10%. All the test data of the 3 different fluids, 15 different pipe variations, length ranges, and Reynolds numbers all revealed the same thing. With in a certain range of uncertainty, roughly 5% for the over all data set, pipe flow on this scale shows no major characteristics of deviation from macro scale stokes theory. For every situation, the Reynolds number times friction factor value always stuck very closely and linearly to a value of 64 through out the ranges of Reynolds

numbers tested. These results suggest that many deviations noticed from typical laminar pipe flow are simply the result of greater uncertainty inherent in the scale. For example measuring a feature like surface roughness often requires the use of an electron microscope, and visual estimation. As a result, many are unable to do the test and leave surface roughness as a complete unknown, or walk away with only a vague idea of what the actual surface roughness is.

Another group of researchers Mala and Li [7] did a similar test on stainless steel and fused silica microchannels but came up with different results. They used tubes with diameters ranging from 50 to 254 micrometers with a high degree of Reynolds numbers kept below the critical transition region. The mean uncertainty for both the channel types' diameters was 2 micron, while the surface roughness was 1.7 micron. This level of deviation isn't too big of a deal for the large channel, but that amount of uncertainty can wreak havoc on data taken for the 50 micron channel. Pressure loss would be determined by testing two different lengths of the same tube and comparing the over all pressure differences between the two. This would isolate that difference in length as the cause of any pressure losses. In every tube tested a distinct and noticeable deviation from classic laminar pipe theory was found. All the channels appeared to have a linear pressure loss line at low Reynolds numbers, all be it higher than theory, but the smaller the channel was the earlier turbulent style pressure losses appeared to form. Reynolds number increase and tube diameter decrease both exacerbated the deviations from classical theory. The researchers, after a significant amount of analytical analysis for possibilities, sited surface roughness as a leading contributor to the great deviation. This is highly likely, as their 50 micron duct with uncertainty and surface roughness could deviate by as much as 7.5% meaning that at times the channel could act as either a nozzle or a diffuser. This could easily account for the tube diameter being inversely proportional to deviations, but more is probably to

blame for their results. Though the water was carefully degassed and filtered, there was never any mention of temperature measurements. Viscous heating, especially in the smaller channels has been observed to cause incredible temperature differentials across a channel [11]. Regardless, this data is a perfect illustration of the uncertainty and differences in data taken by groups doing almost the exact same experiment.

Due to some micromachining processes many channels come out as trapezoidal instead of perfect squares or rounded tubes. Many channels are made by etching silicone wafer using various wet etching processes, and then either using the etched silicon piece as a channel, or by using it as a mold and pouring a substance like PDMS (PolyDiMethylSiloxane) on the newly etched area [17, 18]. Though the processes can vary in many ways, they general setup is the same; as is the outcome. First a silicone wafer is coated with a photoresist material that is broken down or cured by UV light. A mask is placed over the wafer with a patter that is desired printed onto it. When the whole thing is bombarded by Ultra Violet light the parts of the photoresist not shielded by the mask are destroyed or cured depending on the type of photoresist. What remains is bare silicone in places where a feature is desired. Acid is then poured on top. The acid can not eat the photoresist, but will etch through the silicone at a much documented rate. The problem is that it has a tendency to eat not only downwards, but also towards the side underneath the photoresist. This “undercut” makes the hole created wider at the top than the bottom. Figure 1 shows a side profile view of a channel etched using this process, and what the undercutting looks like.

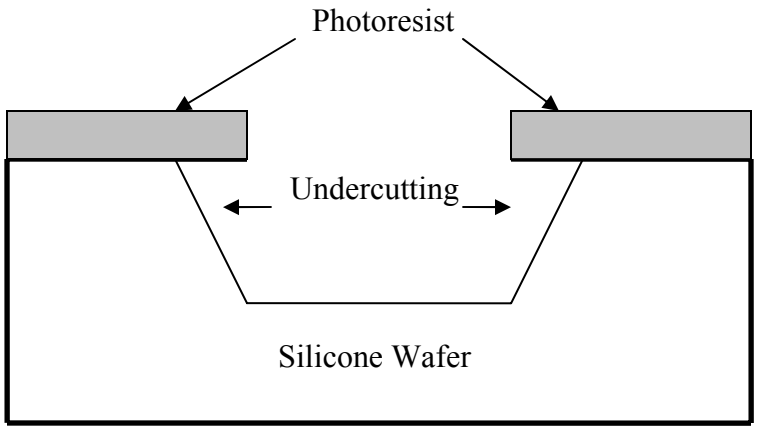

Figure 1: Undercutting

Because of this undercutting it is important to consider trapezoidal shaped ducts heavily in microchannel testing. Weilin et al. [6] did just this by using a silicone substrate wafer capped by a Pyrex glass cover. The dimensions of each channel were carefully measured via a microscope visually to give an uncertainty estimated at around 0.8 micrometers. The hydraulic diameters tested ranged between 50 and 170 micrometers. The 2.5cm channels were fixed between places with pressure transducer ports setup near the entrance and exit of the channel. Pressure drop results through a large range of Reynolds numbers revealed a linear relationship but an increased slope for pressure drop of 18-32%. A set of numerical models is then formed to try an incorporate increased viscosity effects. Though the researchers took great care in mathematically mapping out the differences between a square and a rectangular duct the friction factor appears to a product of the flow conditions and measured pressure losses. Considering the still very real possibility that macro equations do not operate properly in the micro scale, roughness probably should be directly measured. In addition, a true surface roughness is very difficult to determine because the channel was an etched silicon substrate on three sides, and a Pyrex glass sheet on the other. These two materials would be expected to have different surface

characteristics. Regardless of these possible inconsistencies their work agrees almost exactly with that of Shah and London who did a similar study for heat exchangers [19].

Because of the micro fabrication processes, it is common that a group of ducts can only be made to a single depth. This results in the width often being varied to adjust hydraulic diameter. But how much adjustments can be done before it adversely affects the data? Hydraulic diameter is defined as four times the area of the duct divided by the wetted perimeter. It can be expected that a square-duct with an aspect ratio of 1 behaves nicely and can easily predicted. But take that same hydraulic diameter and widen the duct while at the same time make it shallower. The exact same hydraulic diameter can be maintained, but now it has an aspect ratio of say 10. The top and bottom boundary layer are extremely close to each other; while the side walls have almost no effect due to the great distance separating them. It is reasonable to expect that as the aspect ratio approaches infinity the two walls decreasing gap size forms more of a parallel plate situation than a typical duct flow. An infinite aspect ratio is pretty unreasonable, but high aspect ratios are quite common, so to help map out any extraneous deviations caused by aspect ratio Li and Olsen [20] prepared 5 different channels with the same length, all having a hydraulic diameter of 320 micrometers, but with aspect ratios ranging between 0.97, or almost a perfect square, to 5.69. The channels were optically checked for surface roughness and correct dimensions to the effect that there was a small 10 micron uncertainty on the over all duct dimensions, and a small surface roughness in the range of 24 nanometers. MicroPIV (Microscopic Particle Image Velocimetry) was used to measure velocity and boundary layer profile in an attempt to characterize and discover what effects the aspect ratio was having on flow. The boundary layer developments revealed profiles somewhat unlike what is expected in normal scale pipe flow. The profiles all have an obvious slow down at the wall

due to the no-slip condition, but the rest of the flow is extremely flat shaped. Indicating that the viscous forces, at least at low Reynolds numbers, don't reach very far into the flow. As the Reynolds numbers increase, the more classical bullet profile shows up, even through what would be expected to be a laminar turbulent transition region. The ducts with larger aspect ratios maintained their flat profile even through high Reynolds numbers. It is a possibility that the flow is not transiting to turbulent flow. The researchers sited observations made by other groups that the transition can not be observed by simple boundary layer changes. Rather that the true mark of transition occurs when there is a large jump in the mean centerline velocity. This jump was noted in every channel tested; revealing a transition region between the Reynolds numbers of 2400 and 2700. Though this isn't far from the classically held value of 2300, it is reasonable to assume that pressure observations make for finer more accurate indicators of critical transition Reynolds regions. Beyond that, the main focus of the paper was to categorize aspect ratio effects. It was noticed that most of the channels tested performed similarly, but deviations rose with each channel. It can be assumed that as long as the aspect ratio is kept below 3 or 4 that there will be little appreciable difference between two channels of the same hydraulic diameter.

Simulation

Regardless of surface ratios, high viscous forces, and low Reynolds numbers, the micro scale flows should still obey the same physical laws that exist in the macro scale. It is because of this that it is not entirely unreasonable to assume that CFD (Computational Fluid Dynamics) analysis using the Navier stokes equations should confidently provide a good approximation of nearly any micro flow situation. One issue involved with Continuum mechanics is the Knudsen

number (Kn). It is a ratio of the mean free path of the molecules divided by the over all length being analyzed. The importance of this number being that if it is found to fall below Kn < 0.1, then continuum mechanics still holds as a valid prediction method. If however, the values broaches above the 0.1 threshold, then statistical mechanics must be used. If this is the case then the Navier stokes models no longer hold as valid. A Knudsen number calculation was run for the "standard" channel with details available in Appendix A. The result being that with a Knudsen number value of $1.2x10^{-5}$; the use of statistical analysis should not be necessary. Theoretically then continuum mechanics should hold valid and a quality CFD analysis would hold true to experimental observations. It has been suggested that the Knudsen number is only truly relevant for gasses, because the molecules in liquid have much interaction with each other and intermolecular forces cause mean free path to play a large roll in their behavior. It has also been suggested that the only two assumptions should be made for fluids on the micrometer scale in order to reduce invalid oversimplification. One, that all fluid can be assumed to be Newtonian; meaning that stress and strain are directly proportional. The other is Fourier's law of heat conduction; meaning that heat transfer is directly dependent on a temperature differential [21].

Many attempts have been made at trying to use various computation and analytical methods to tackle the microchannel problem with varying results [8, 22-25]. Both Baviere et al. [22] and Bahrami et al. [8] did detailed numerical and analytical analyses while maintaining a high level of focus on boundary layers. Baviere et al. used a regular series of block protrusions from the surface to act as surface roughness. They would then vary the height and spacing of the blocks to simulate different roughness values. Bahrami et al. took a more statistical approach. They assumed that the wall roughness was random and assumed a normal distribution to that point. The pipe radius was considered to be at the mean of the normal distribution and a

roughness factor affected the width of the standard deviations both into and away from the pipe wall. Both groups then compared their simulated data to that of various researchers with a relative degree of success considering the variety of results available from experimentation.

Another approach taken by some is to model a complex microfludic system as a whole instead of looking at only a small section of pipe. Zengerle and Richter tried to model a pump and valve device complete with check valves. Their approach was to model each individual component via large analytical differential governing equations, and then black box that component. Once each component was boxed they could be strung together and solved with a simulation tool known as PUSI. Much of their research focused on the elasticity and compressibility of the fluid suggesting that they had gasses in mind when they were working on modeling. By using high frequency pumps and Pressure Smoothing Elements (PSEs) such as elastic tubing they were able to make the microcomponents act similarly to their macro scale counterparts.

Niklas et al. [24] built, tested and then simulated a heat exchanger consisting of 55 parallel triangular microchannels. Their analysis stared with simulating a simple triangular duct at various flow rates. Then, they added the entrance restriction that was present due to the manifold from the original entrance. Next they started adding exit expansion, and then finally linking groups together till they had worked up in complexity and modeled the whole heat exchanger system. The reason for this slow build up was two fold. One, if there was a convergence problem or glaring error, it would be easier to find as layers were added instead of all at once. More importantly however, is that it is very easy to track how much each additional part affects the pressure losses. For example after the simple pipe was modeled; entrance effects were added, and it was discovered that resulting head loss was not critical, but should be

included for a more complete picture. Their final simulation of the total heat exchanger pointed toward the general understanding that friction factor at lower Reynolds number is the main contributor of pressure loss. According to their data, a Reynolds number of 5 had viscous losses causing nearly 80% of the head loss. When the flow rate was increased dramatically, and Reynolds number was 700; mixing and recirculation dominated at 70% of the loss. It appears friction factor is the highest demon to deal with in what is considered a "normal" microchannel. The simulations with the greatest success also had a high complexity of boundary condition and surface roughness detail.

Early Transition

While the idea of microscale ducts having a different laminar pressure drop than their macroscale counterparts still appears to be up for debate, what is less debatable is a trend of early transition. Traditionally the flow in a pipe will transition from laminar to turbulent flow at a Reynolds number of around 2300. As the Reynolds number increases up to and through this critical transition region the velocity profile changes greatly. Figure 2 shows the general profile of both laminar and turbulent pipe flow.

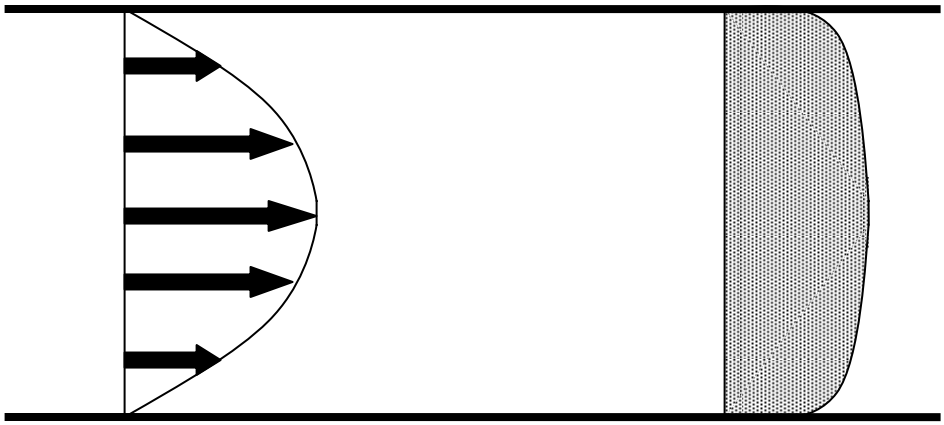

Figure 2: Laminar and turbulent boundary profile

Laminar flow tends to be much faster at the center and slow at the edges where the wall friction holds the fluid and slows it down. This profile development is dependent on viscosity. A good example can be seen if honey is allowed to slide down an inclined plate. The honey will form a natural boundary layer that can be observed as a curved surface at its forefront. As the thick arrows indicate, the fluid is orderly and nearly all traveling in the same direction with only a little deviation due to molecule vibration. Turbulent flow appears as a grey mass because there is only an average over all velocity to it all. Each particle is bouncing around wildly and randomly as the viscous forces fail to keep them under wraps. The turbulent boundary layer has a more even velocity profile with a lot of velocity activity near the surface of the pipe because wall friction has little affect on the mass of highly active particles. This causes the skin friction, or major loss as it is sometimes called, to be much greater for turbulent flow. It could be inferred then that a laminar boundary layer is always desired, but this is not the case. As in external flow, the turbulent flow is able to handle geometry changes more readily with out excessive recirculation and secondary flow. The added surface activity has a huge benefit in heat

exchanger applications where the active particles near the surface can increase the ability of a pipe to add or remove heat by an order of magnitude or more. This all having been said, it is obvious that knowledge and full understanding of transition regions in the microscale is rather important as is boundary layers. More discussion on how boundary layers have been observed in the microscale will continue later, but first; a further analysis of transition number must be made.

Xiong and Chung [10] found evidence of transition occurring in a Reynolds number range of 1500-1700. Their tests were performed on a number of straight and serpentine channels with hydraulic diameters of 209 micron. Regardless of the channel type there was a clean and highly linear relationship between the pressure drop across the whole channel, including entrance and exit, until the Reynolds number passed the 1500 mark. At this point every channel started for a more parabolic trend that was more obvious in the longer channels. A transition to turbulence in the channels would cause the boundary layers to have more wall contact in flow that is already heavily affected by wall conditions due to the high surface area to volume ratios. This is an effect that has been well documented in macroscale ducts, but typically the transition occurs at a Reynolds number of 2300.

Not everyone agrees with the idea of early transition to turbulent flow. Rands et al. [11] cites that there is a wide range of results and opinions in the area of critical Reynolds number, and cites findings from various groups ranging from 300 to 6000. Their work was focused on doing hydraulic diameters below 30 micron because at the time no one had done any work on the critical transition region of ducts below 50 micron. Specifically, four different diameters between 15 and 30 micron were tested with a surface roughness observed via SEM (Scanning Electron Microscope) to be less than 10 nanometers. Their setup was a fairly standard capillary tubing test stand. The tubing was fixed between a highly precise syringe pump and a reservoir

that would measure the output liquid for flow rate estimation. The inlet, exit, and over all length of the tubing would be measured as a pressure transducer was placed between the upstream and downstream pressure ports. The four tube diameters were tested with lengths varying between 1 and 3 cm. For all the channels measured the pressure loss correlated perfectly to the 64 fRe friction factor times Reynolds number standard for macroscale flow when the Reynolds number was kept below 2100-2500. There was slight deviation and wavering, but all points fell on the line expected line well with in the uncertainty range. After the flow rates caused the Reynolds numbers to reach passed the apparent transition range around 2300 the pressure losses climbed considerably which is understood to be a fully developed turbulent flow regime. Additionally, the length had little additional effect on the fRe indicating that the flow had a fully developed laminar boundary layer for nearly the entire length of the duct. According to their results there is no seriously distinguishable deviation from the classical critical Reynolds laminar-turbulent transition number occurring at 2300. Even for channels as small as 16.6 micron, standard flow theory still applies. Another important observation made during testing involved viscous heating. It has been stated that a small temperature change can cause a large viscosity swing which will result in high deviations of Reynolds number. The smaller the tube the more viscosity matters, and in the case of this experiment, some very serious temperature differentials were observed. The largest being 35ºC between the entry and exit port of the 19.7 micron 2.9 cm long duct. Careful observation of the viscous heating appears to be an absolute requirement when taking data on any microchannel; especially as channel size goes down and length increases.

Boundary Layer

Low Reynolds number obviously points towards a laminar flow regime, but such a low Reynolds number could yield a more complex situation than simple laminar theory. Hele-Shaw flow occurs between two plates separated by a very small gap. With flow in this situation of a gap sufficiently small enough the flow takes on new properties. Applying continuum mechanics and an assumption of no vertical flow, then it is quickly seen that vorticity has to be zero in between the plates [5, 26]. The implications of a Hele-Shaw flow regime being present in some or all micro fluidics channels is that certain standard geometries would be highly affected. Classic straight-duct pipe theory doesn't typically call for vorticity, but sudden expansion and contractions do, along with pipe bends. The recirculation regions standard in macro scale sudden expansions would not exist causing the typical theory to fall very short of proper prediction. Similarly pipe bends tend to develop a set of counter circulating along the axis of the bend. If neither of these effects exist in the micro scale, then it is entirely possible that micro pipe bends and sudden expansions are much less lossy than their macro scale counter parts. The evidence does not completely support this theory however. A microchannel was made with a sudden expansion and contraction at its center. The walls of the microchannel were lined with perpendicular off shoots that lead to micro scale piezoelectric pressure transducers. The result being that they could track the static pressure, and therefore the velocity, along the whole channel. It was noticed that the pressure was lowest just after the sudden expansion, and not at the restriction it self. Higher velocity after the restriction has ended would suggest a vena contracta, and recirculation zone. The original microchannels were 1μm high, and 40μm wide. The obstructions varied between a 5μm gap to nearly the full channel width [27]. These results

appear to refute any claims that microchannels in the range down to at least 30μm in diameter should be free of cumbersome Hele-Shaw flow characteristics.

Thompson et al. used a Molecular Tagging Velocimeter to visualize the flow profile in a microchannel [28]. The method uses a UV photoactivated tracer in solution with the flow medium that when bombarded begins to phosphoresce for a certain amount of time. These then show up as streaks which represent the "tagging" of individual molecules through out the flow. If every particle phosphoresces for a certain amount of time, then the length of the streak will reveal that particles velocity. Hundreds of the images are taken to be combined filtered and processed to produce a clear quality idea of what the continuous boundary layer looks like. A 182μm fused silica microtube was placed in a brass holder and surrounded by the flow. The end was then sealed such that flow had to go through the tube to escape. A lens focused the beam from the top down such that it would be strong enough only in a localized area of the capillary tube to minimize the phosphorescent effect in the surrounding fluid. With the camera placed on the side looking in; any extra streaking that existed outside the tube could easily be ignored. Using the setup to take visual snapshots of the boundary layer development, they started at the tube entrance and slowly worked their way away from the inlet. Discritization of the streaky image revealed something very familiar. At the entrance, the flow in the center maintained a flat profile, indicating plug flow. Along the edges of this plug flow exists a zone where the fluid particles appear to stop and swirl. This indicates a vena contracta at the entrance which is typically not seen in macro scale flow at a Reynolds number below 500. The tests were done with flow rates providing Reynolds numbers between 60 and 350. Further away from the entrance effects the flow settled down into a very respectable laminar fully developed flow profile. The distance that it took for the entrance flow to convert from a uniform plug to a fully

developed profile also seemed to fit with standard macro scale understanding being a function of the distance from the entrance divided by the Reynolds number, and hydraulic diameter. This value seems to be about 0.05, which is in line with macro scale laminar development lengths. With the possible exception of the vena contracta, their experiment seems to show that micro scale flow, at least using a hydraulic diameter of 182μm, provides characteristics that are no different than what is observed in normal scale pipe flow.

Boundary layers can be analyzed in great detail via simulation, because extra emphasis can be placed around areas of interest; like walls and bend edges. Xu et al. [29] did a detailed simulation through the use of the incompressible, two-dimensional, steady, time averaged Navier-Stokes equations along with a modified Wolfshtein one-equation turbulence model. Results verification was performed until laminar velocity errors of less than 0.01% were obtained. Then the same operation was carried out for turbulent flow. Simulations were carried out for pipes with diameter ranges of 50 micron to 254 micron. The transition region of Reynolds numbers between 1000 and 2000 were heavily focused on to show the gradual shift in velocity profile. In most cases, the shift was just that, gradual. The smaller ducts only had a slight blunting that could easily be mistaken for a normal laminar flow; while the larger diameters had profiles closer to that of traditional turbulent flow. They appeared broad and flattened with a sharp drop off at the edges connected to the walls. For these simulations the non-dimensional turbulence kinetic energy was also recorded with some interesting results. In every single simulation the energy was lowest at the center, would hump around 25% away from the wall, and then spike again at the walls. This double hump profile only changes slightly with respect to Reynolds number. Aside from the profile, the amount of energy each section had was quite different. Though the lower diameter sections appear to have earlier transition regions the

amount of energy present is much less than that of the larger ducts. The paper concludes that the one-equation turbulence model is well suited for simulation of the microducts, and that ducts with diameters lower than 130 micron should be considered in the micro regime. Though it has been suggested that there is a transition region between micro and macro theory, this is one of the few instances where the researchers tried to draw a definitive line.

Macro Bend Theory

Pipe bends of every shape size and angle have been used for centuries, and their performances are widely published in hand books and guides for engineers [13, 30-32]. Through years of experimentation and observation a number of odd characteristics appear to occur in most pipe flow. These different forces and effects show up to greater and lesser degrees depending on factors like the angle of the bend, the pipe diameter, and radius of curvature. Figure 3 shows the important characteristics of a pipe elbow. Pipe elbows with a radius of curvature of zero are referred to as miter-bends.

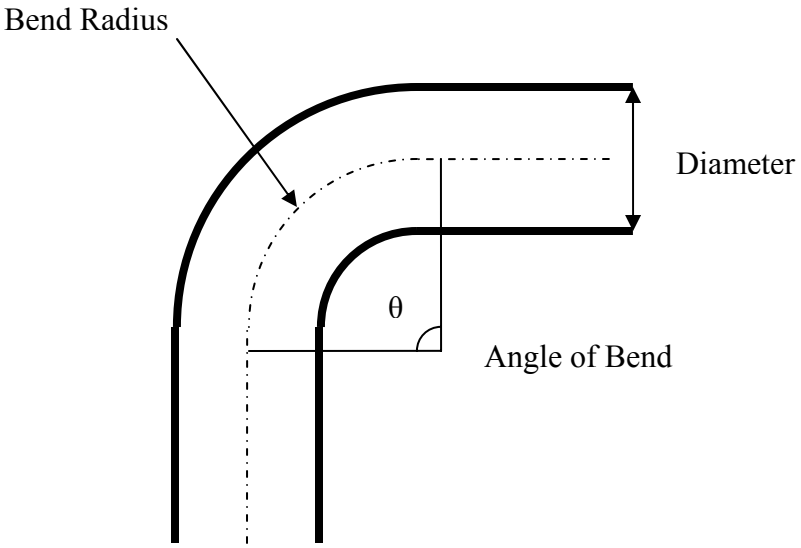

Figure 3: Pipe bend nomenclature

When flow enters a bend there is a centrifugal force that acts on the turning fluid. Much in the same way that water will stay in a bucket if it swung vertically any fluid in the pipe will be slung to the outer edge. In a duct the force directs fluid from the center of curvature to the outer wall of the pipe causing static pressure to be higher on the outer edge than in the inner. These centrifugal forces cause the fluid to have a sort of circulation as it goes through the turn, and a pair of vortexes that are symmetric around the center line of the pipe elbow form. Figure 4 illustrates the basic idea of what this double swirl in a pipe bend looks like.

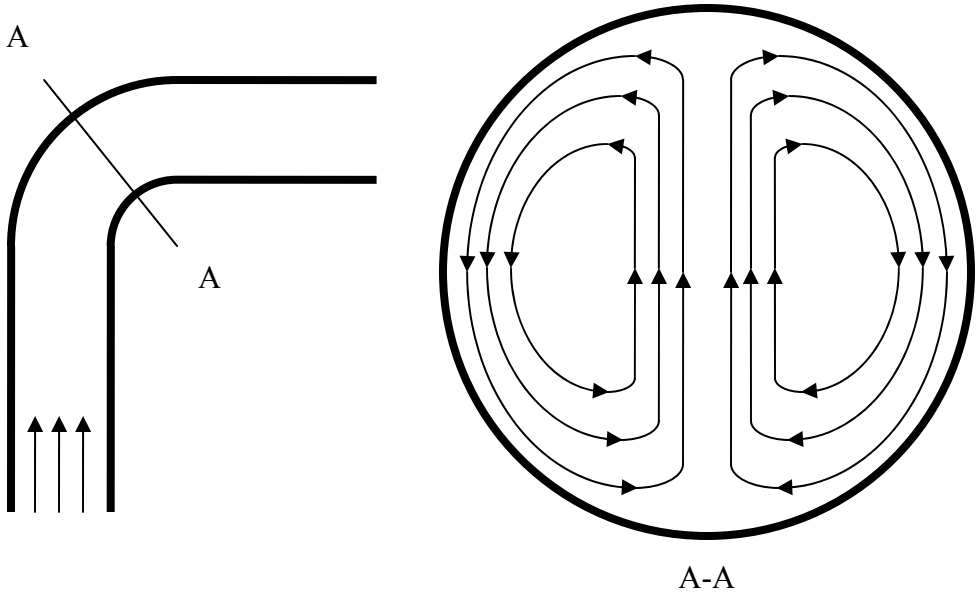

Figure 4: Vortex pair in pipe elbow

These secondary flows cause the pressure losses to go above and beyond normal straight-duct pipe flow. Energy is required to accelerate the fluid in these constantly changing swirl patterns, so losses start as soon as a bend is initiated. Total velocity against the walls is increased by this new component which makes the wall friction losses greater. To keep the double swirl going the natural viscous dampening forces must be continually overcome. The sources of loss quickly add up in pipe flow causing it to have much greater pressure losses when compared to an equivalent distance of straight-duct flow. Finding the exact amount of pressure loss created by this effect can be tricky, because the swirl continues downstream after the pipe. The full loss effects are not felt until the fluid has stopped swirling completely. In normal pipe flow this can take as long as 50 pipe diameters in distance down stream from the bend feature that created the swirl.

To further complicate pipe bends is the difference in distance the flow must travel as it goes around a turn. Along the centerline of a bend there is no distance change, but when a path closer to the inside of the bend is taken the distance to be traveled shortens. This acts as a sort of nozzle, and similarly the outer edge has a diffusion effect on the flow. Completely counter to this, however, is the recirculation zones that tend to form that will reverse this effect. Depending on the bend radius the diffuser effect at the outer edge will cause flow separation and a recirculation bubble contoured to the outside of the bend. In addition, the inside edge of a bend with a radius too small will act like a sudden expansion. The flow can't make the turn fast enough, and another recirculation zone just down stream of the bend will be created. Figure 5 shows both of these possible recirculation zones.

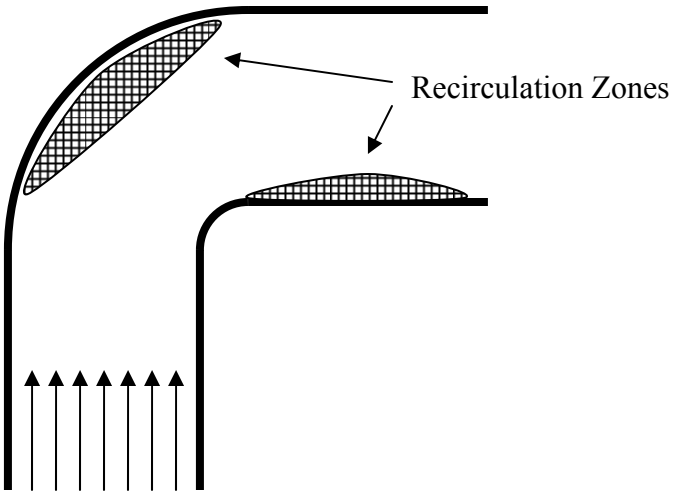

Figure 5: Elbow recirculation zones

Zones like those possible in pipe bends do two different things. The first is that they reduced the effective diameter of a pipe because the over all flow rate though a recirculation zone is negligible. Reduced diameter means lower possible flow rates and higher pressure losses. The second outcome is the standard story when ever secondary flows are present; it takes

energy to keep changing that fluids direction and they are constantly fighting viscous dampening forces. This is added to the double vortex swirl caused by centrifugal forces makes pipe bends extremely lossy features that should be either avoided if at all possible, or carefully designed for.

With the total loss of a section tabulated it can be displayed in a number of ways. Often the loss is referred to as head loss which is essentially a loss of over all total pressure in a flow system. Anther popular term is the resistance or loss coefficient K [33]. Instead of the bend being converted to some sort of equivalent length it is completely separated form the flow network and given its own loss value. This value is then multiplied by the dynamic pressure to provide head loss. The loss values are often as a function of some sort of ratio being characteristic of their geometry and Reynolds number. The reason fittings are handled this way can seem odd when constructing continuous flow networks in microchannels, but in light of how larger pipe work is done it makes more sense. In processes like lithography the entire plumbing set is all made as a continuous piece at the same time, and path length of the network is easy to back out. In most "normal" applications, however, plumbing is assembled from standard pieces. A few 10 foot pipes come together at a standard 90º elbow then are reduced to a different diameter via another standard coupler. So from an engineering point of view the losses must be calculated across 20 feet of pipe and 2 different fittings. It is easy to invoke a moody diagram for the two straight pipes and then add to that calculation two K loss coefficients for the fittings at a particular Reynolds number. The result will be a total pressure loss across the flow network. If more fittings or valves are added the proper loss coefficients can simply be thrown in and no consideration has to be given to their path length or diameter or anything. This form of black boxing can be a little cumbersome to produce for every fitting type, but once done makes calculating pressure losses extremely quickly.

Classical pipe theory for a smooth bend in a round duct follows as such [34]. For pipe bends of 45º or 90º and with a radius over diameter ratio between 0.5 and 11.7, the loss coefficient equation with a Reynolds number between 500 and 2000 is between 1 and 2. There is a linear relationship between the loss coefficient starting at a Reynolds number of 15 with a K value of 200 till 500 when the K value settles out. It is also suggested that this trend will also work for 180º bends if the K value is simply doubled.

Micro Bends

Most lab-on-a-chip technologies require the mixing or separation of fluids and particles via electrokinetic manipulation. The method uses a positive and negative charge at different places along the flow. Fluid particles become charged by the one contact and are drawn towards the other in a process known as electrophoresis. Tsai et al. [35] studied common designs aimed at mixing and processing fluids, and noticed the compactness required often led to a large amount of serpentine channels. Glass plates were etched using fairly standard micromachining wet etching to form the entry points and bends to be analyzed. The channels them selves were simple 100 micron parallel straight-ducts separated by 1 millimeter. The ducts were connected by a 180º bend with different diameters that were driven by the electrophoresis device. A bend ratio was decided to be the ratio between the original duct size, and the reduced duct size of the bend portion. Essentially it was thought that perhaps a smaller duct size in the bends could induce more secondary flow and mixing. A flow visualization technique similar to that of Thompson et al. [28] was used to measure particle movement and determine mixing effectiveness. The main focus of the paper, however, was on a complex simulation of the

electrophoresis process and how the bends were affected down stream by it. Straight-duct flow was first analyzed to act as a starting point between the software, traditional convention, and the testing apparatus. Straight-ducts appeared to have a boundary layer profile closer to that of turbulent flow than that of a fully developed laminar boundary layer. This is probably due to the electrophoresis acting more like a body force than a pressure driven term. The profile is characterized as having a mostly flat profile with a standard no slip boundary causing a rapid velocity drop off at the edges. Starting with a bend ratio of 1, the visualization shows the plug flow starting off normal, but by half way through the turn it has become highly distorted. Flow along the outer edge has slowed somewhat, and flow towards the middle has greatly accelerated. This stretches and stresses the profile to appear like a thin diagonal line that once out of the bend is at a 30º angle to the side walls. As the bend ratio was increased, however, the profile seemed to remain more and more in tact. It could easily be that the smaller areas have much greater trouble overcoming viscosity. By the time the bend duct was at 25 micron or one fourth the diameter of the original straight-ducts the flow profile looked very similar to that of the inlet. The only differences could be attributed to the effects of the nozzle and diffuser leading into and out of the bend. The paper refers to this effect as band tilting, and it appears to be a bit more of a function of the way the flow is induced. Regardless, it glimpses further into the life of bent ducts and what secondary flows occur in them.

Yi and Bau [36] tested simple 90º sharp "L" shaped bends using a Navier-stokes based commercial CFD package called CFD2000. These are also known as miter bends Their testing showed that typical vortices were created during the bend, but due to the high viscous dampening forces present in low Reynolds number. At a Reynolds number of 80, the vortex strength decayed by 3 orders of magnitude with in six hydraulic diameters down stream of the bend. At

Reynolds numbers below 15 they found that the pressure losses were actually less in the pipe bend than in the straight pipe, probably due to the increase of area. Above that threshold secondary flow started to kick in and vortices caused the pressure losses to increase. As the Reynolds number increased, and bends were stacked in series, they calm vortices became indefinable chaos. The point of the simulation was to confirm was had been suspected, and somewhat observed empirically; typical macro scale secondary flow occurs in pipe bends if to a somewhat lesser extent. Next, they attempted to generate a series of these pipe bends using ceramic tapes to test the validity of their code models. Unfortunately the type of structure they built was 3-D; sort of a coil with only sharp 90º bends. The ceramic tape only allowed them to view the very top and very bottom sections of the pipe bend geometry. This in addition to the use of red dye and clear water made it very difficult for them to confirm or measure any sort of results. There was a small amount of viable mixing after about 5 bends with the Reynolds number above 10, but this was the only real conclusion of the experiment.

Another group to work with these sharp miter-bends was Xiong and Chung [10]. Their experimental procedure involved making first a set of straight-duct micro channels to test over all friction factors. Next, the ducts would begin to serpentine, with each new duct having more switchbacks than the one before it. Duct hydraulic diameter ranged between 200μm and 550μm, and the pressure was taken at the over all entrance and exit to the switchback holding mechanism. They concluded that the flow losses can be broken into two different categories. When Reynolds number remained below 100 there exist no secondary flow or eddies, and the over all pressure losses through the device are minimal. Then, at a critical Reynolds number between 100 and 200 circulation appears on the inner and outer walls of the bend and pressure drop increases dramatically with Reynolds number. Yi and Bau [36] had a similar conclusion,

but their critical range was around 15 instead of 100. the major difference between the two tests aside from empirical versus numerical was that Xiong and Chung [10] used much larger microchannels. There must be some critical hydraulic diameter region where the macro scale assumptions deviate and a new set of micro scale relations take over.

In addition to liquids, compressible gasses have been tested in microchannels to see the effects and flow rate losses. Raju and Roy [37] use a hydrodynamic algorithm developed by the Computational Plasma Dynamics Laboratory to test a microchannel with two 90º bends. Their models simulated nitrogen gas, and ended up with an outlet Knudsen number of 0.0585. This is many orders of magnitude higher that what is expected in incompressible flow microchannels that are the focus of this thesis. With the model they simulated gas flow up to a Reynolds number of 0.04, using both a no-slip wall condition, and first-order slip boundary. Small recirculation zones were present regardless of the low Reynolds number flow, and the over all results suggested that the mass flow rate had been reduced by around 160% compared to a straight microchannel.

Lee et al. [38] did an actual empirical test with gas to determine flow losses. They flowed argon through a 20 by 1 micron duct consisting of a 90º miter-bend, a 60 micron radius bend, or a "double-turn" bend made of two 45º bends separated by a 50 micron straight-duct. Each turn had 6 built in MEMS based pressure transducers that were used to help determine flow characteristics through out the turn. First, a calculation of flow losses due to a straight pipe of this length and hydraulic diameter was calculated. Next, the ducts were tested, and pressure losses compared to that of the theoretical straight-duct. Both the double-turn bend and sweeping-bend were found to have a flow rate at roughly 95% of the straight-duct theory at a given pressure loss. This indicates that the turn does induce some sort of secondary losses

beyond normal friction. Also, the sharp miter-bend induced an even greater loss than the previous two having a flow rate of only 80% of the theoretical straight-duct. Lastly, a comparison was made between the pressure measurements taken on the inside of the turn, and those taken on the outside of the turn. At the same distance along the turn, there was a distinct pressure differential between the inside and outside surfaces. The differences were noticeable in nearly all parts of every type of bend. Flow separation and recirculation regions in the various bend geometries appear to be the only explanation for the pressure observation. This again confirms the importance of geometry in duct flow, and, at least for gas flow of this scale.

Some attempts have been made at simulating bends in microchannels have been made. Wang and Liu [39] attempted to tackle what they called "slightly curved" microchannels using state of the art numerical simulations. The channels in question were set at 100 microns deep, had widths ranging from 500 to 1,000 micron, and were curved with a bend radius of 33 to 53 mm. Though these dimensions make it difficult to consider the work done as true microchannel research, the depth dimension is very small, and this could have a great impact on the double swirl present in pipe bends. Also, with the extreme size of the bend radii it is difficult to think of a situation in which this research could be applied because of the typically small footprint required by most microfluidics applications. Great amounts of work were done to prepare the mesh and ensure that every painstaking detail was captured and understood by the code. The main focus was on detailing what was happening inside the ducts disturbance wise, and to apply specific dean numbers to each situation. Their results revealed the classical swirl patterns seen in normal pipe bends, but with an added periodic oscillation. As Reynolds number increased, the oscillation frequency continued to increase until it became intermittent and finally chaotic. The averages even with these peculiar oscillations still appeared to be in the range of normally

expected flow. Even a slight curvature did affect the fRe factor for laminar flow as well as the Nusselt number. So according to the simulations even in microchannels all the normal curvature effects appear, and the channel characteristics are closely tied with the macroscale theory.

Mixing

Goullet et al. [23] attempted to test various mixing scenarios via CFD and Fluent 6. The sections were variations on "T" intersections, and "Y" splits. According to the analysis the best geometries were the ones that produced secondary flow recirculation regions. This is not very surprising, but what was interesting was the inclusion of ribs in mixing, and the rate at which the flow was pulsed. The straight-duct flow degree of mixing was over doubled by the addition of ribs while in constant flow. Pulsing the flow at a very low rate of 5Hz produced dramatic results as well. The 5Hz pulse was varied with phase difference between 90º and 180º the result being that the degree of mixing was again nearly doubled over the constant flow condition with ribbing. It is reasonable to assume that the ribbing probably acts as a set of successive sudden expansions and contractions. Sudden expansion pipe flow, in the macro scale at least, produces a large amount of recirculation, and the pulsing causes the recirculation to create and destroy on both sides of the obstruction over and over again. The effect being that fluid trapped in the recirculation zone could be released, and fluid entering the contraction sections where the flow is fairly behaved will suddenly become an expansion section again, and experience good mixing. The theoretical result is an excellent process for reducing mixer size and increasing effectiveness.

Another, possibly more efficient means of mixing takes advantage of the double swirl effect present in pipe bends. Sudarsan and Ugaz [40] tested trapezoidal channels that averaged 150 micron wide, 29 micron tall spiral ducts at a Reynolds number range from 0.02 to 18.6. Yellow and blue dye was equally injected next to each other at the entrance tunnel which proceeded into an inward spiraling channel that reversed direction when it got to the center. The result was a compact channel that would mix the two side by side fluids in one direction for a set length, and then would reverse the mixing direction as the spiral worked its way from the center back outwards. To test the mixing capabilities, the process was filmed through a CCD camera and then a green filter was applied. The better the yellow and blue fluid mixing was, the greener the image would appear. Intensity was gauged as the width of the green band over the width of the whole channel. If the whole channel was green, then the mixing would be 100% complete. When the Reynolds number was less than 1 there did not appear to be any extraneous mixing beyond simple diffusion which naturally happens in straight-duct flow. Even still, the spiral ducts are advantageous because they increase the effective duct length while still remaining compact. Various spiral distances and radii were tried with a multitude of results, but the over all picture was clear. 80% mixing could easily be achieved at low Reynolds number in a 19mm square footprint, and mixing values as high as 90% were available if higher flow rates were used. There appeared to be a direct correlation to the Reynolds number and secondary flow intensity. Pipe flow in bend sections will be discussed later in this section.

CHAPTER THREE: METHOLODGY

There is a myriad of research in the subject area of microfluidics. Much of the work done is application focused with heat transfer and mixing being two of the main focuses due to their immediate requirement by present and future MEMS devices. Of the detailed avenues to study in microfluidics, straight-duct flow seems to have been heavily looked at, and although there is still room for debate on the laminar flow losses; better arguments seem to side with losses following classical pipe flow theory. The critical transition region is slightly more difficult to get a full grasp on, and probably will require more and varied experimentation before it can be confidently decided upon. An important area that appears to of received little attention is bends in microfluidics.

Much of the focus in the literature review, beyond a "big picture" idea of what the microfluidics research industry is doing, was a heavy focus on bends and turns in microflow. Through extensive searching it was noticed that there were large in glaring holes in the understanding and data available for these most necessary pipe features. The research done so far can be summed as a small hand full of ventures in 90º smooth and miter-bends, a few works of simulation, and various studies of the effectiveness of spirals and miter-bends in mixing. Between changes in bend radius and pipe diameter, there still exists a wide range of smooth 90º bends left uncharted. In addition, different bend angles can be looked at as well. Only one bend test was found that involved compressible flow, so there is an entire avenue to discover in that respect as well. Considering nearly every final design in microfluidics is probably going to have at least one or two curves if not for mixing then just for the sake of compactness and reduction of

chip foot print. It is because of this that the focus of the literature review has been pipe bends, and the experimentation portion will involve a large amount of work with sweeping-pipe bends in microchannels.

Test Fluid

The fluid chosen for testing was water. Water was chosen for its wide range of uses in microfluidics, and by utilizing nondimensional values like Reynolds number all results should be easily related to other incompressible fluids. The specific water used was off the shelf store brand distilled water that was carefully handled and stored so as not to introduce any extra particulate. One of the large concerns in using water for testing is the formation of bubbles. Water's high surface tension gives it a tendency to form small bubbles quite readily and getting rid of them can be quite tricky. The reason this was such a concern had mostly to due with the possibility of a bubble starting or somehow getting lodged in the microchannel it self. The channel surface has a certain amount of roughness, and this could possibly help hold an air pocket in place even after flow is initiated. The reason this is such a large worry is because of area changes. If a normal straight-duct has a small bubble lodged somewhere in it then that bubble will cause it to act like there is a small nozzle and diffuser in the way. This could easily throw off data, and make the channel seem like there are greater losses at hand than there actually are. Now, one thing must be made clear. There is a difference between a liquid having microbubbles and degassed water. Often the papers researched spoke of using degassed water for their tests. The concern for water in solution is that if the pressure should drop greatly; say in a small fast moving channel, the static pressure could drop below the vapor pressure of some

particular gas present in solution. If this did happen, that gas would come out of solution and form bubbles. It is probably a good precautionary measure, although Judy et al. [12] did a rather extensive test using both regular and degassed water with no appreciable difference noticed. Degassing is also difficult, because anytime the fluid is exposed to the atmosphere the partial pressure difference between the gases in the air and the lack of gasses in the water causes them to take nitrogen and oxygen back into solution. As long as the fluid was not agitated so as to force extra gasses and bubbles into it there would only be the normal dissolved gasses at their ratios similar to atmospheric. It was decided that testing "normal" distilled water would be more useful because in the field and in real practical application of MEMS degassed water is rarely if ever available. It was hoped that this decision would produce data, though probably more variable, closer to that of a real world applications.

Fluid Delivery

With the fluid selected, a delivery method had to be chosen. A precision controlled syringe pump seemed to be the preferred weapon of choice by many of the researchers reviewed; although other methods existed. Another viable one was the use of elevated fluid sources to provide a pressure difference. In the cases of electrophoresis flow, the driving force was obviously not pressure, but in every other case something along these lines was used. There is a tempting element or two to using elevated water. For one the total pressure can be known accurately with out the use of a single pressure transducer. Another is that through the use of inclined tubes, a great level of precision can be had. The main problem with this method appears to be flow rate. Measuring volumes at this scale must be done over a long period of time so that

there is enough fluid to make an appreciable observation. Also, due to the long times required evaporation can become and issue. Uncertainty when trying to measure small volumes is quite high which leads to the highly important Reynolds numbers having a great degree of variability. This is one of the most important inferred measurements that must be made because it directly relates transition and pressure losses. With funding available and the desire to maximize the accuracy of Reynolds number calculations a syringe pump was the delivery method chosen. The pump used was a New Era Pump Systems, Inc Ne-1000 programmable pump syringe. Figure 6 is the pump fully loaded and pumping for an experiment. The advantage of this particular pump was its programmability, and ability to deliver accurate flow rates.

Figure 6: Pump in action

The research carried out by earlier graduate students was done on this type of unit, so its reliability and capability was well known. The unit would handle between 1 and 60cc syringes and had a flow range capability of 0.73 microliters per hour to 1,705 milliliters per hour. This ensured that no matter what Reynolds number was required the pump would be able to deliver exactly the required flow regardless of the pressure requirements. This particular unit used a highly accurate encoded stepper motor to drive a worm drive slide assembly which resulted in very low uncertainty. Uncertainty analysis and methodology will be discussed in greater detail later on. New era pump systems provided a continuous pump plumbing attachment so that two pumps could be used for continuous delivery. The plumbing is a set of screw on seal tips, known as leur locks, which ensure good seal with the syringe, a set of parallel check valves and splitters that allow two pumps to act together. When one is pumping the other can be withdrawing from a common source, and then allow a switch off. Though infinite continuous pumping isn't required; parts from the plumbing pack were harvested so that the unit would draw from the reserve tank with out pulling in air from the microchannel side, and it could then pump to the microchannel with out fear of test fluid leaking back to the reserve tank. This was done so that refilling of the syringe didn't require anything to be disconnected. The connection to a test fluid storage device is discussed in the next section. Figure 7 is the check valve system that allows the syringe to automatically refill with out pulling air from the test side. Test fluid enters from the top line into the syringe and exits towards the right when pumping.

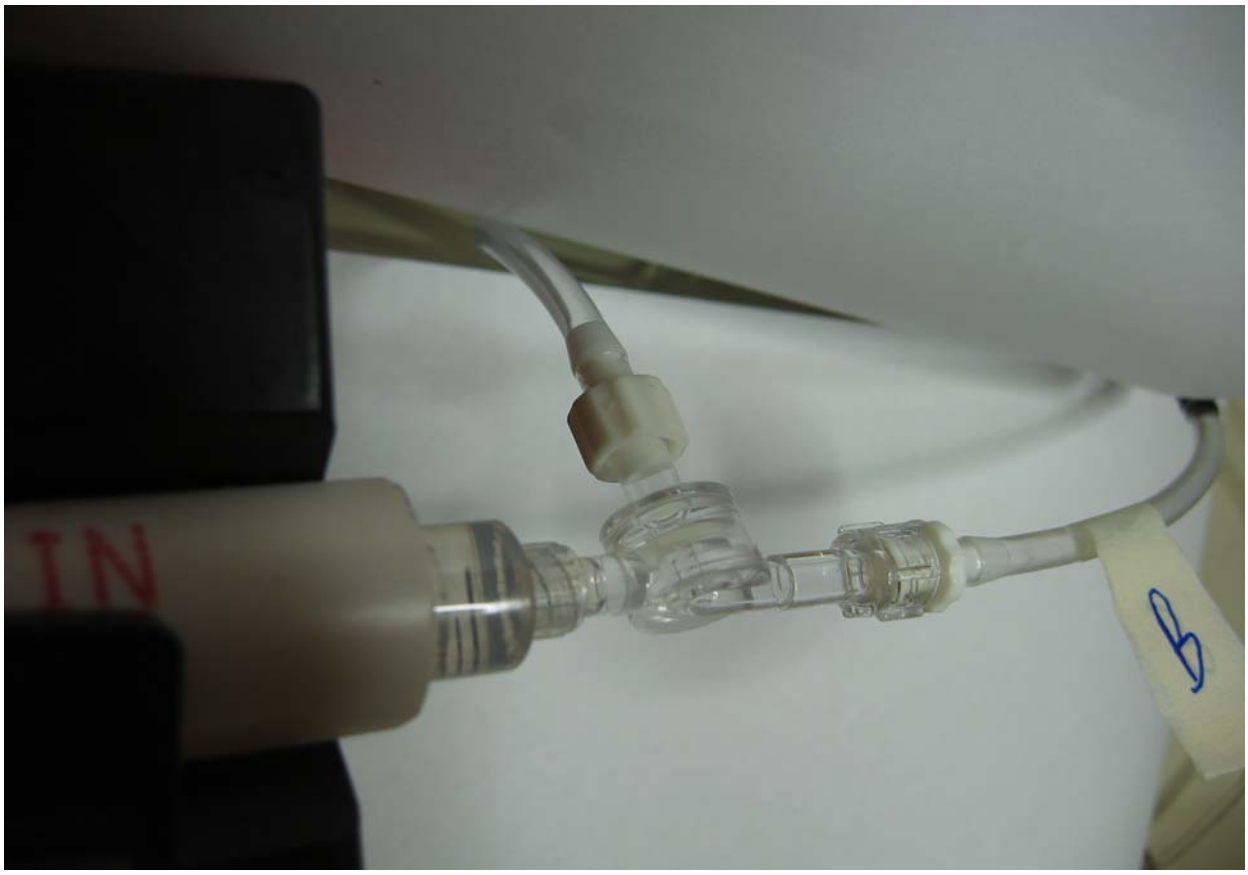

Figure 7: Check valve system

Test Fluid Storage

Water was prepared in 3 quart volumes and placed in a simple storage container. The open bowl was topped with a 1/8 inch sheet of Plexiglas to prevent contaminants from entering the source fluid. The pump system was installed with the ability to withdraw and fill its own syringe with out the need of user interaction; thus helping to further prevent contamination and intrusion of foreign particles. A small hole was drilled in the lid that just barely allowed the syringe withdraw line to pass through. Though the system is by no means 100% air tight; there is no easy way for dust or any other contaminants to enter the container. After months of storage

the test fluid still appears to be completely clear unlike the surface of the Plexiglas which has built up a fine layer of dust. This simple method was chosen for water storage because it increased cleanliness of water and reduced the risk of contamination while remaining inexpensive and easy to build. Figure 8 is the storage tank full of fluid with cover in place and fill line inserted.

Figure 8: Test fluid storage tank

Pressure Measurements

Pressure measurements are the most important direct observation made in this experimental process. The entire focus of the project was to find the pressure drops across a

certain length of microchannel, and then to compare that with a similar channel containing a certain turn. Because of this little expense was spared in the selection of a proper measurement device, and the PX2300-1DI from omega was found to be an ideal candidate. This pressure transducer was carefully chosen for a number of reasons. For starters, it is a "wet-wet" transducer complete with bleed valves. This means that the transducer can have fluid inside both ports and even let water leak out of the ports to ensure that they are full. With the entire pressure line and transducer cavity full of water instead of air it will have a faster response time than if the entire system was full of air. Air would need to be compressed in the lines for a steady state pressure to be reached which takes time. Furthermore if water was pushed up one of the pressure lines and not the other, the height different would add an unmeasured element to the pressure difference. Figure 9 is the pressure transducer wired and plumbed to the test system.

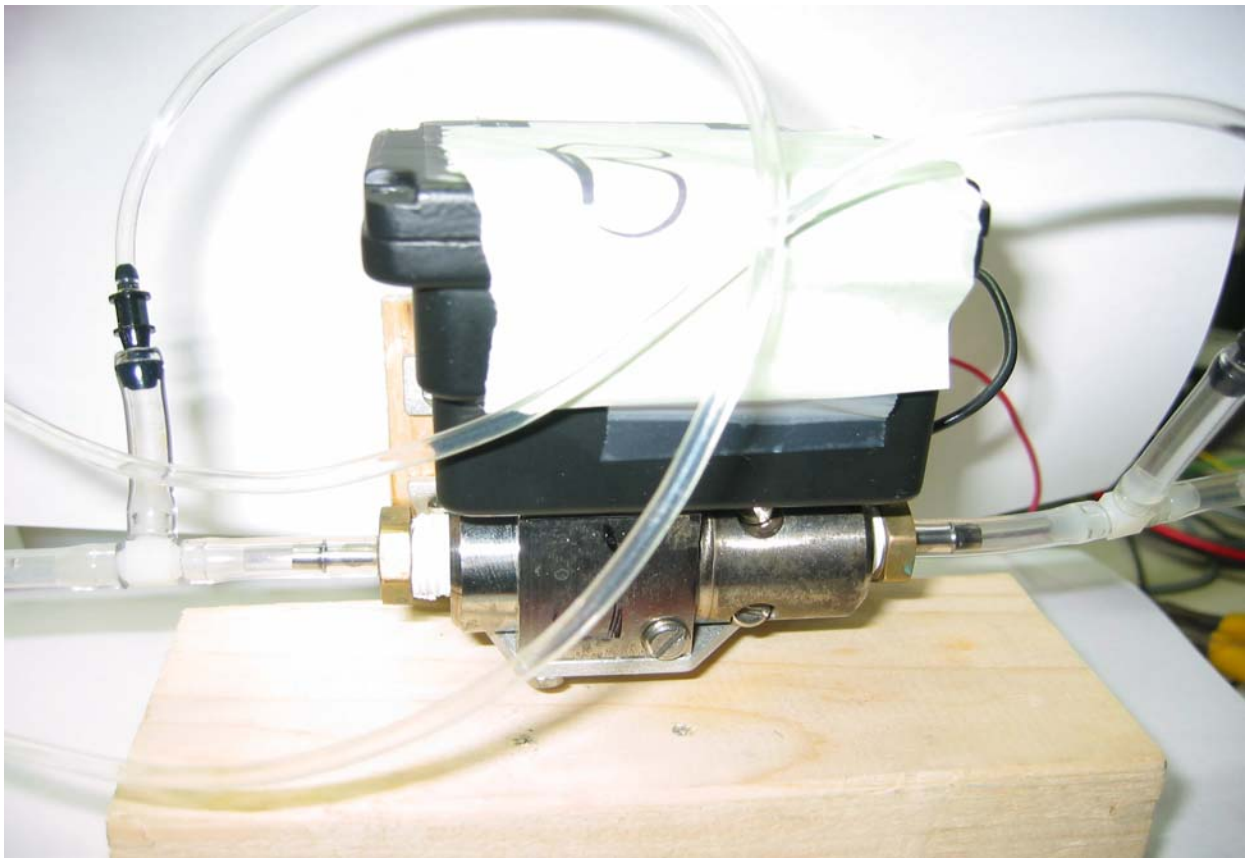

Figure 9: Pressure transducer

More details of how the pressure transducer will interface with the test chamber is included in a later section, but for pressure information to reach the transducer it must pass though a duct with a hydraulic diameter of about 20 micron. Assuming there is a 1 psi (Pound per Square Inch) pressure change that must be detected the air in the lines would have to shrink by roughly 7%, and water would have to rush in through that 20 micrometer pressure duct to fill in the volume that the air has left. Considering a few feet of tubing with cavities in the transducer; it could take many minutes for this exchange to occur. So in the interest of speedy pressure response the wet-wet feature was chosen. Also this transducer was capable of taking a higher than average excitation voltage meaning that it would produce higher and easier to obtain

voltage output data. Finally, a very small full scale range of only 0-2 psi was chosen because earlier studies had shown that the pressure drop across most channels of this size was rarely ever over the capabilities of the transducer. A proper full scale range is extremely important because it dictates resolution. Uncertainty will be discussed in great detail later on. Differential transducers usually come in two types, a one way and a plus minus. The one way transducer has a high port and a low port and only reads if the pressure follows the port rule. The other kind of transducer can read pressure equally in either direction, but the full scale range is doubled. If a plus minus transducer had been used then its resolution capabilities would have been cut in half, and this was not at all an acceptable prospect. The problem that arises from a one way pressure transducer is that the user must keep very careful track of which port is the high port, and which is the low port. Considering there will be no area changes of the duct in between the pressure measurement ports it is reasonable to assume that pressure loss will increase as the duct length increases. So if any two measurements were taken the up stream one would certainly have to be the highest static pressure reading. The reversal of this would cause the pressure transducer to be stressed in a way it was not designed for opening up the possibility of permanent damage to the device, and most assuredly erroneous data. Because of this great care was exercised in making sure proper placement was done.

The excitation voltage of the pressure transducer called for a DC power supply between 15 and 30 volts. A set of PSS-5B, pictured in Figure 10, power supplies from Omega.com were chosen to supply the pressure transducers. The units chosen are specifically designed for pressure transducers and are capable of supplying a highly regulated 24V 1A signal with a voltage accuracy of ±1%. This proved to be the simplest and cheapest available power source available with in a certain range of required accuracy. High frequency data acquisition samples

have shown the produced signal to be very clean and it appears to have no visible periodic tendencies. With the transducers power they would then output their pressure data in the form of a voltage range of 0.6 to 5 volts.

Figure 10: Transducer power supply

On its own this data is useless with out a proper correlation. To correlate and calibrate the pressure transducer a simple U-Tube manometer was used. The manometer was capable of producing water heights of up to 24 inches. The high port of the transducer was put inline with one side of the manometer, and the other sides of both were left open to atmosphere. Voltage measurements were taken every inch of height to produce a calibration curve that can be seen in Figure 11. The slope of this curve was taken and used to convert from recorded voltage data

from the DAQ system to inches of water or what ever pressure units desired. The curve fit generated by MatchCAD produced an r^2 correlation coefficient of 0.99996 which would indicate a very good curve fit and an extremely linear response from the pressure transducer.

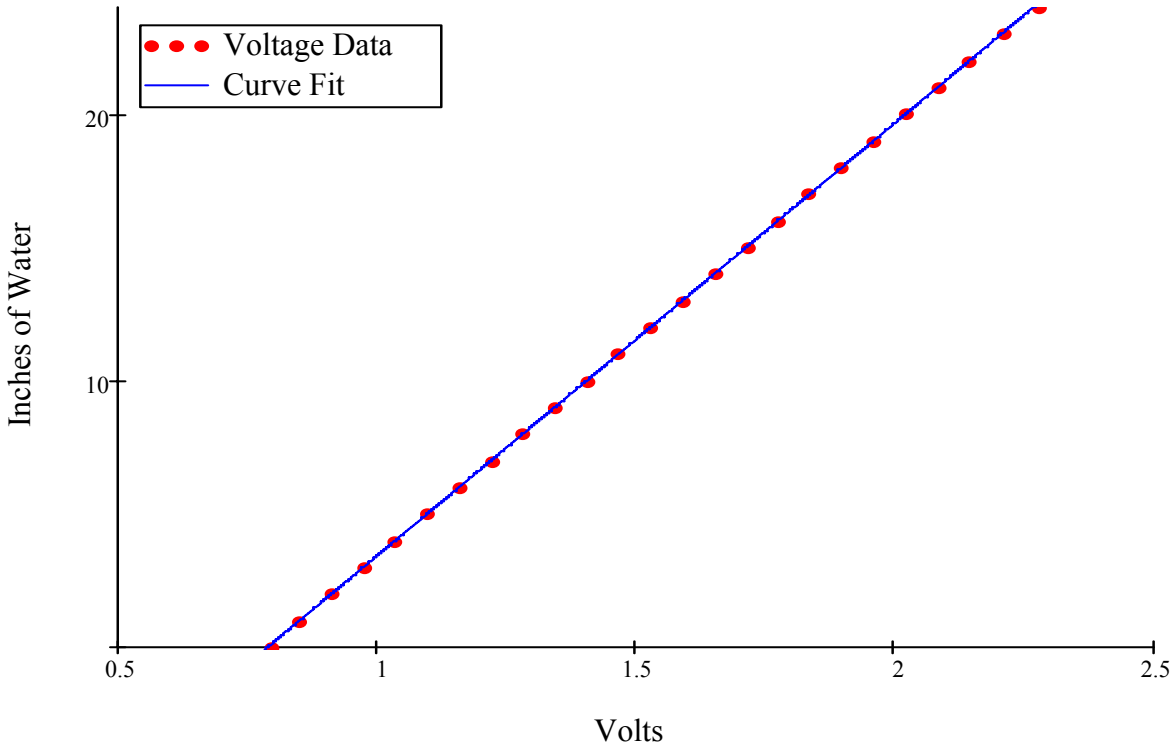

Figure 11: Transducer calibration

Data Acquisition

With a pressure transducer decided upon and output voltage ranges set the data acquisition system could then be chosen. Originally some DAQ work had been done with a National Instruments system power by labview software. It was a system capable of variable voltage detection ranges with 16 bit resolution. The system and software used was designed more for high frequency data sample rates and was capable of up to a 20,000 Hz sample rate.

Though it could be set to something more reasonable for long term data taking like 1 sample a second there was a further difficulty in how it took those samples. Instead of telling it to sample at 1Hz and starting the experiment; a definite number of samples to be taken had to be set. In addition once started the program could not be stopped with out losing all the data. So if something happened half way though either the whole data set had to be scraped or the user would have to wait the full test time to get the good bit from the beginning. To make matters worse it wouldn't display any acquired data until it had finished recording. This means that if something went wrong during testing it probably wouldn't show up until the end. All of this resulted in many hours of wasted test time from either pressure ports not being connected properly, or various other equipment failures. Finally the system was only capable of handling a single voltage input at a time. Some of these problems could probably be worked out via careful coding in labview, but no one close by on staff was very knowledgeable on the subject, and taking the time to learn it could mean months of fidgeting with software.

Instead a simpler solution was found. Omega.com had available a 4 input data logger that was designed for long term data testing and could easily be connected to a computer via the USB port. The OM-CP-QUADVOLT was almost exactly what was needed. While recording the software would automatically back up any recorded data to the hard drive at routine intervals, it would display all the data it has taken in real time, and could be easily started stopped and paused when needed. Though the voltage range is quite high at 0 to 15V the fact that it is a 16 bit board means that the resolution is higher than the accuracy of the pressure transducers being used. Now with a DAQ system ideally suited for long term testing, and highly flexible programmable pump, a new way of testing could be done. The pump was set with a full flow routine that was known to last about two and a half hours. Data acquisition software was set in

such a way that it would properly handle the time sets and allow the user to monitor the results. This meant that testing required the researcher to spend a few minutes prepping a channel set and start the test routine then walk away for hours. Figure 12 is the DAQ board wired with the transducer into a port.

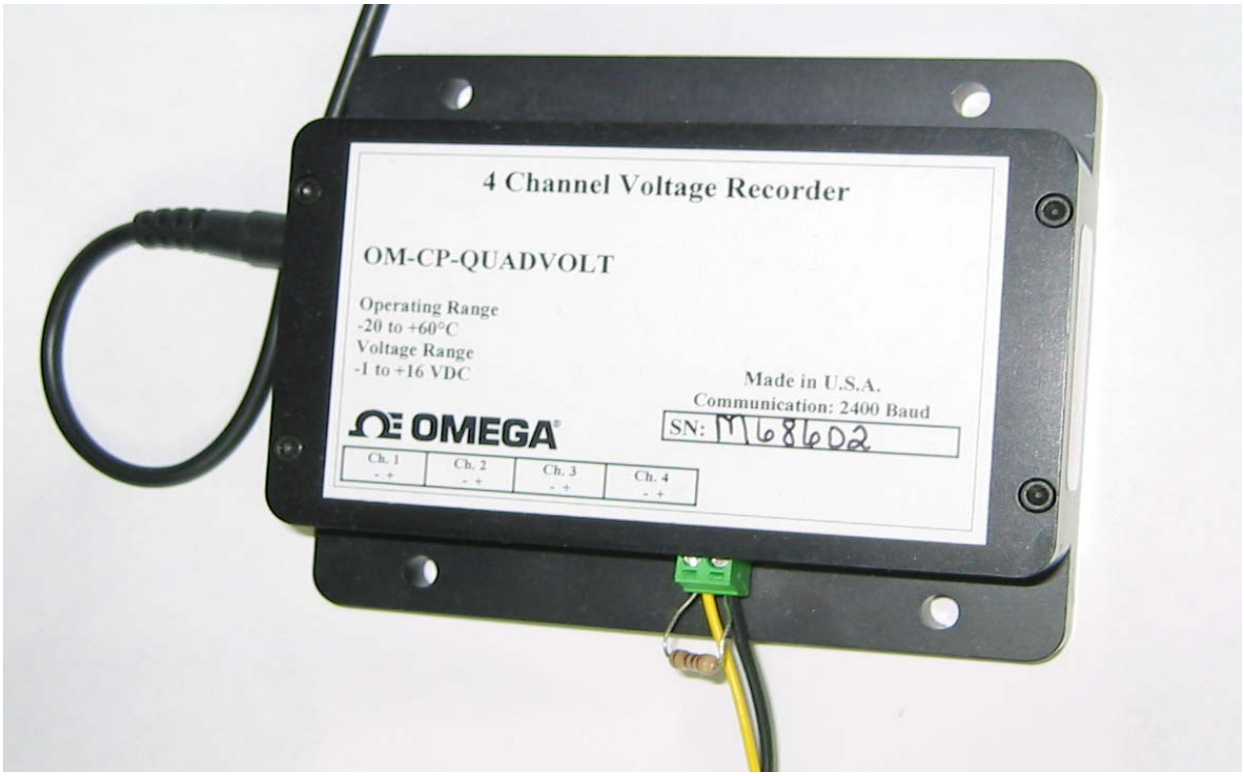

Figure 12: DAQ board

Channel Production

The test sections were produced via a soft casting of PDMS from a master copy similar to the one highlighted in the literature review. First a silicone wafer is fixed and spun at a highly controlled revolution rate. A photoresist material with a viscosity is very well known is placed on the spinning wafer. This produces a photoresist layer of even thickness that can be adjusted

by changing the speed at which the wafer is rotated. Once a desired coating thickness of photoresist has been reached the mask processes can begin. A mask is placed over the wafer that is entirely blacked out except for the portions that are desired to be relief cut.

The entire process was handled by Stanford University's microfluidics foundry in their bioengineering division. A CAD drawing was sent with the desired design inside a 4 inch circular envelope. They were able to manufacture a set of square channels averaging at 100μm with a set of desired bends of various radii and bend angle. Figure 13 below shows a CAD drawing of the first mask created by the Stanford foundry.

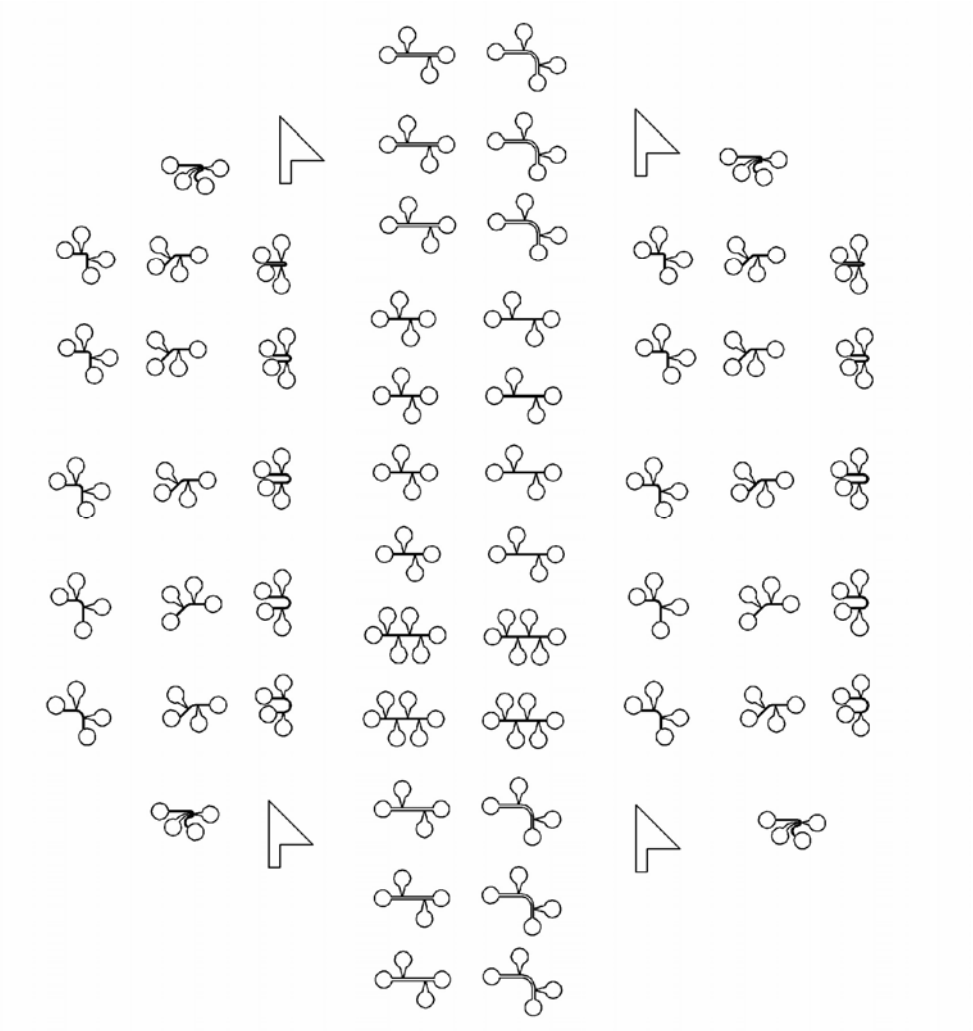

Figure 13: Mask CAD drawing

The layout and channels on the mask may seem strange, but a detailed explanation of why this layout was chosen will be given shortly. With the mask placed over the coated wafer it was then allowed to be bombarded by ultraviolet light. The UV would not touch the photoresist shielded by the black mask, but would react with the resist through the narrow slits and ports that make up the desired channels. This light would cause the photoresist to cure and adhere to the silicon wafer surface. After curing is complete the residual resist is washed away and negative cast is left over. This means that anywhere a channel is desired there is a raised "hill" of

photoresist. Figure 14 below shows this silicon master ready for casting. The shiny grey is the silicon and the brown is raised photoresist.

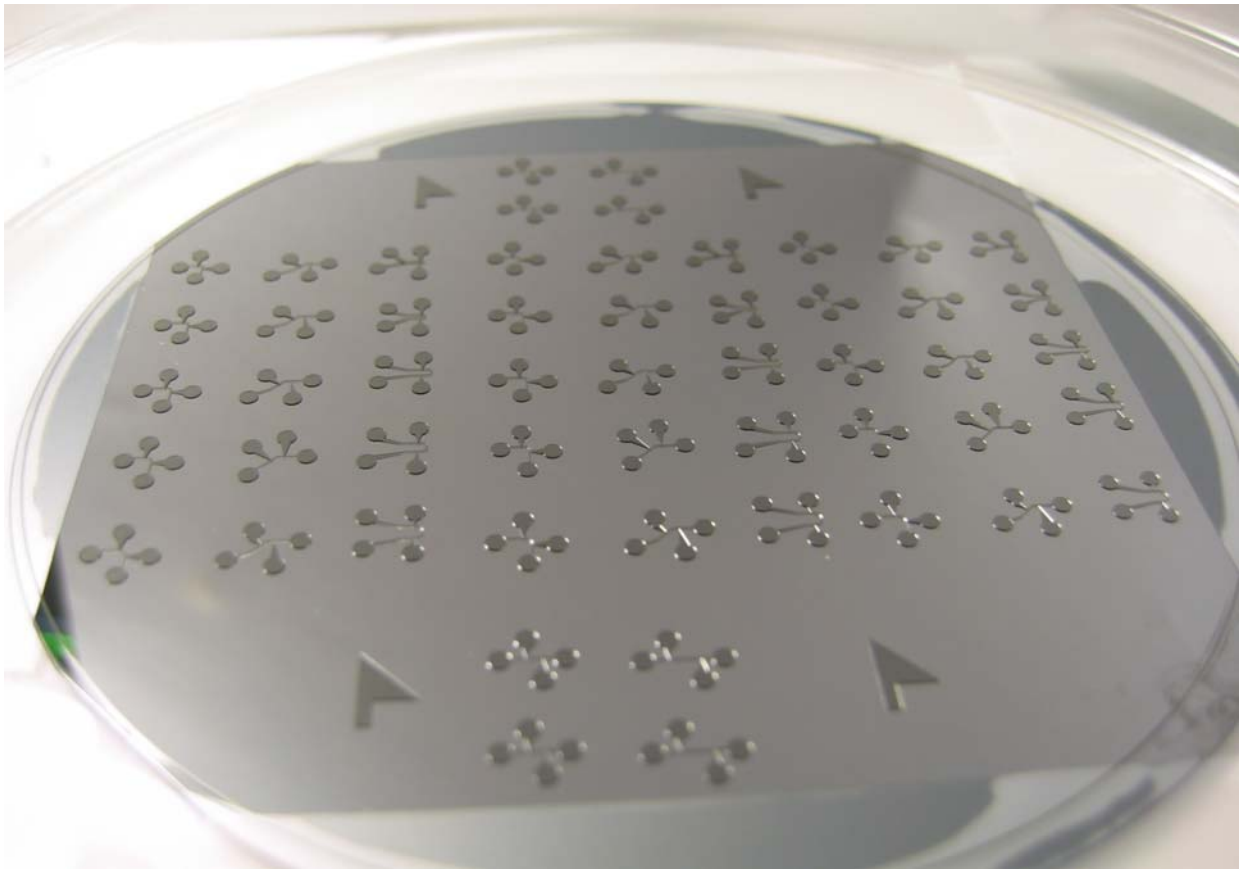

Figure 14: Master Silicone Wafer

PDMS can then be poured on the surface, be allowed to cure, and pulled off with out damage to the wafer or photoresist. Once a casting has been made off the master it is essentially a groove in the silicone. In order for it to be sealed and useful another piece of blank PDMS is bonded to the surface via oxygen plasma. Once the two surfaces are together there is a perfectly sealed microchannel complete with inlet, exhaust and pressure ports. Figure 15 is a picture of a molded and sealed microchannel set in PDMS which from now on will be called a “chip”.

Unfortunately the channels are very small and do not easily reflect light making them very difficult to see.

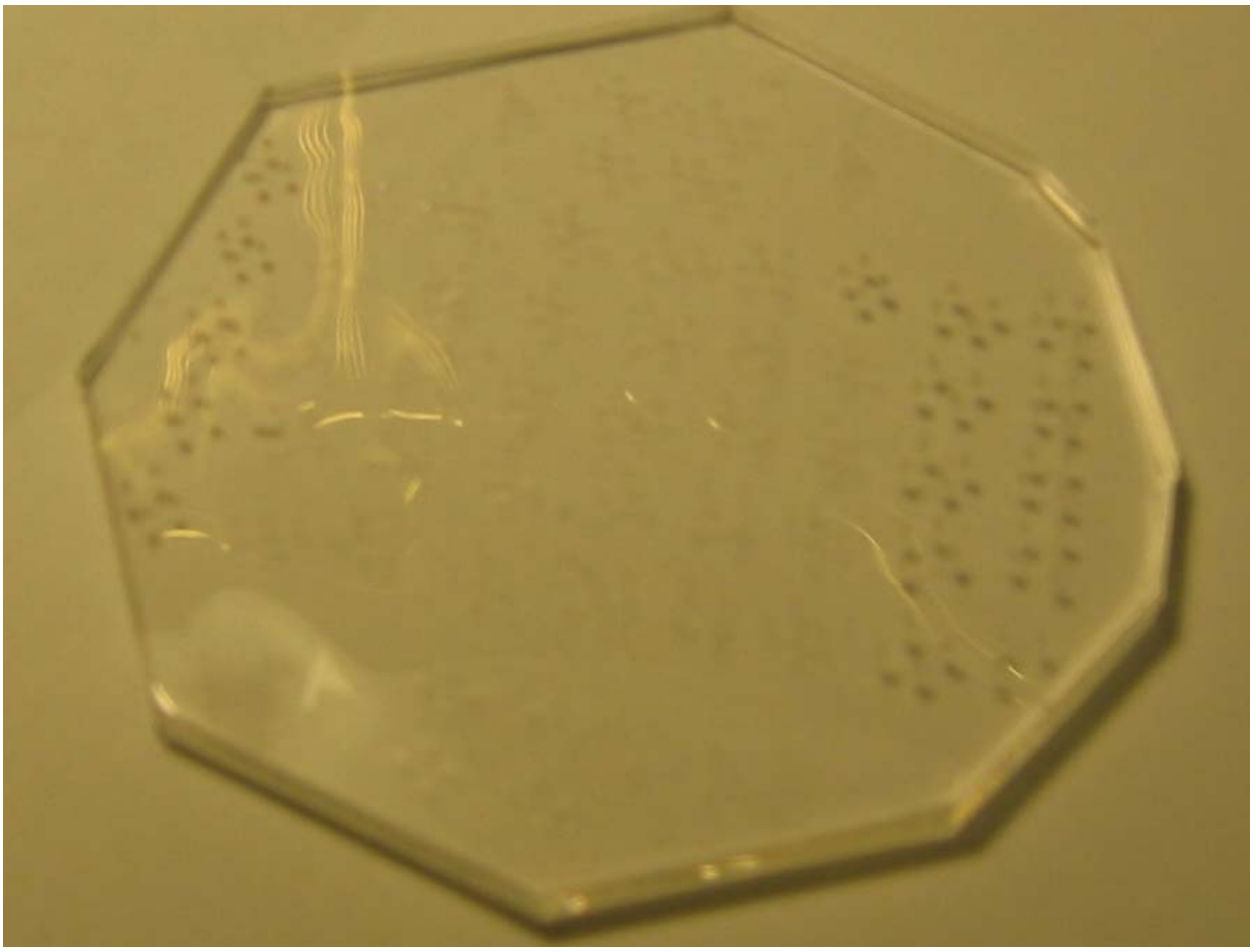

Figure 15: PDMS casted chip

Each microchannel is equipped with an inlet and exhaust port at each end of the channel, as well as pressure ports at key points along the channel. The ports appear as large circles which will be tapped at a later time. The pressure ports come off perpendicularly to the channel it self using a hydraulic diameter as small as possible, and then expanding to its respective large circle. The port is initially as minimal as possible so it will cause as little flow disturbance as can be

helped. It then opens up so that any fluid that must flow in or out to exchange pressure data will have as little impedance as possible.

Channel Diameter and Profile

There are two characteristics of a sweeping-bend that could be easily adjusted and tested for. First there is the radius of the sweeping-bend usually portrayed as a ratio of radius over channel width or diameter. Tighter radii would likely induce secondary flows causing greater pressure losses. Second there is the angle of the bend to explore. Nearly all tests previous to now studied only 90º channels, which is admittedly the most common form of channel bend used, but not the only one. Other features not specific to bends that could be tested include Reynolds number and hydraulic diameter. Trying to test a wide range of all these variables would require many hundreds of experiments, and that doesn't even include repeated testing. It was decided that a nominal diameter of 100μm would be used with 45°, 90° and 180° all at a bend radius of 125 to 625μm increasing by 125μm each time. This produced 3 bend angles and 5 radii for a total of 15 different combinations of channel types. Nearly all of these channels had a path distance between the pressure ports of 1mm. The larger 180° bend channels were large enough to require 2mm, so to be able to compare pressure loss coefficient of the bend channel versus a straight one a set of straight 1 and 2mm channels were included. Finally a set of practice channels were created in order to do check outs on a simpler easier to test channel and practice some of the piercing techniques that were developed.

With the channels manufactured there must be a way to test their profiles to ensure that the hydraulic diameter is known as closely as possible. The manufacturer's website stated that

the process would be accurate to with in 10μm. Though this may sound incredibly small it represents a 10% deviation in both height and width. In order to confirm more exact dimensions a digital microscope was employed with image resolution of 350x280 pixels and with optical zooming of 4X, 10X, 40X, and 100X magnification. In order to interpret what dimensions a pixel represented a marked slide was obtained from fisher scientific that was ruled to both 10 and 100 micron. The slide was captured at each magnification, and pixels between the ruled marks were counted. Figure 16 below is that marked slide at 4X magnification.

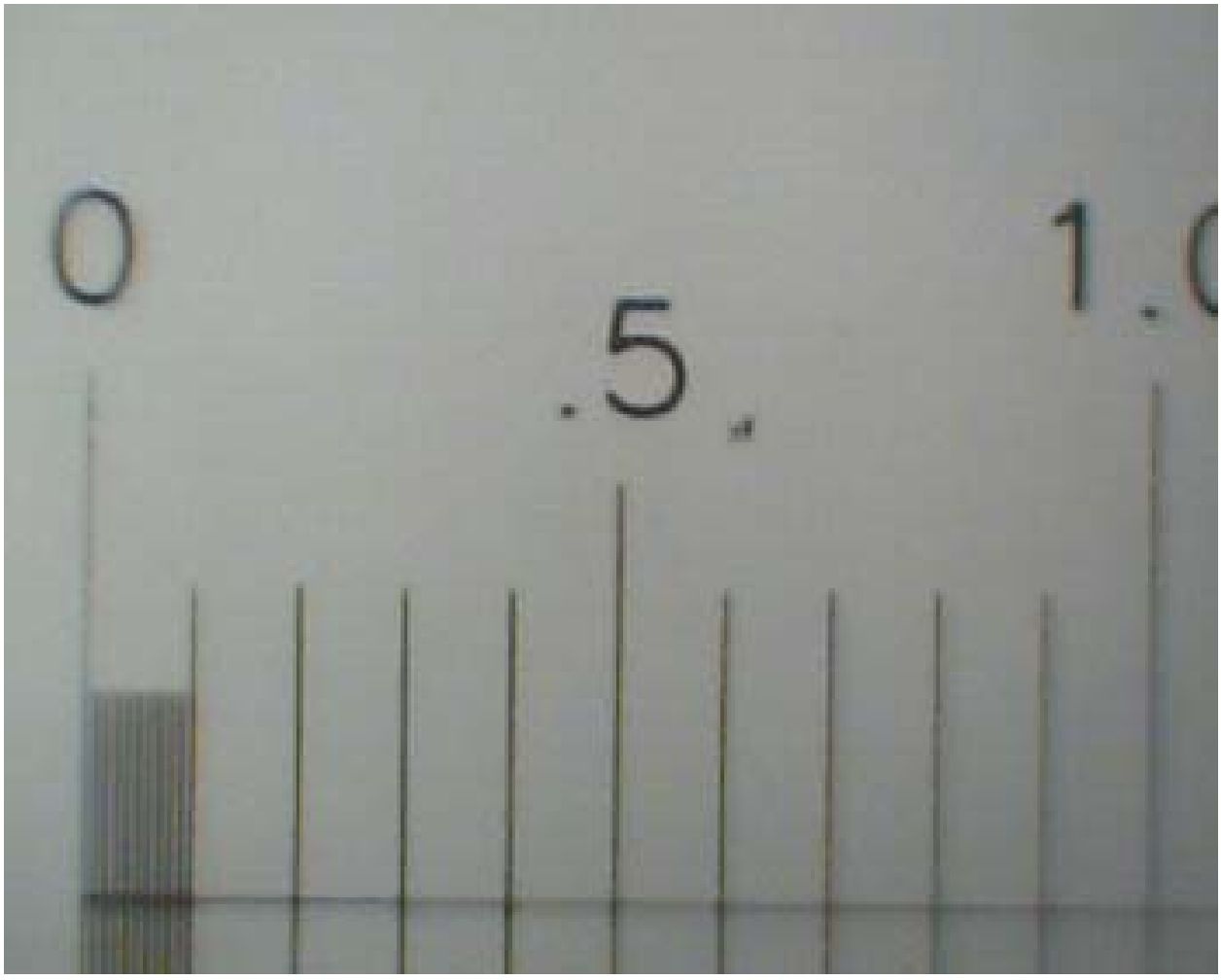

Figure 16: Calibrated Slide at 4X

The distance in between each major "tick" mark was known to be 1/10 of a mm or 100 micron, which corresponds to 30 pixels. Also, between the 0 mark and the first 1/10 was a 1/100 graduation. Correlation between pixels and distance was carried out through a range of magnifications and distances, and Table 1 shows the list of correlations.

Table 1: Microscope image calibration

Magnification	100 μm	10 μm
4X	28	NA
10X	70	7
40X	280	28
100X	NA	70

With a correlation setup between pixel size and distance, the various channels can be imaged and their true hydraulic diameters found. Blades were used to cut the channel from top to bottom forming slices that could be placed on their sides and viewed. Figure 17 shows one of the channels sliced in profile. In order to get as close of a hydraulic diameter as possible the area and perimeter will be measured to produce a hydraulic diameter. Calculations assumed the channel to be rectangular in profile, so width and height measurements had to be taken for each slice. Several slices for each channel were measured to ensure greater hydraulic diameter accuracy. Straight channels are easy to square up and slice with knives cleanly. Bent channels on the other hand provide a very difficult target, the bend make blade placement more critical, and turns mean that cutting perpendicular to the channel more difficult. All of this combined with variability from manufacturing lead to a majority of the error coming from uncertainty of the diameter measurements.

Figure 17: Profile cut of microchannel

Apparatus Schematic

With each individual cog in the mighty testing machine established they need to be placed together to form a cohesive testing apparatus. Figure 18 is a simplified diagram of the test equipment with equipment details listed in Table 2. Arrows indicate one way direction of flow. From the reservoir test fluid is pumped into the inlet port of the test chamber of a channel, and exhausted through the exit port. High and low pressure information is carried through the tubes to the differential pressure transducer. The transducer is powered by the power supply and voltage information is collected via the DAQ board. With this full understanding of how the equipment interacts and how data can be taken a detailed procedure of the finer points of prepping and testing channels will required.

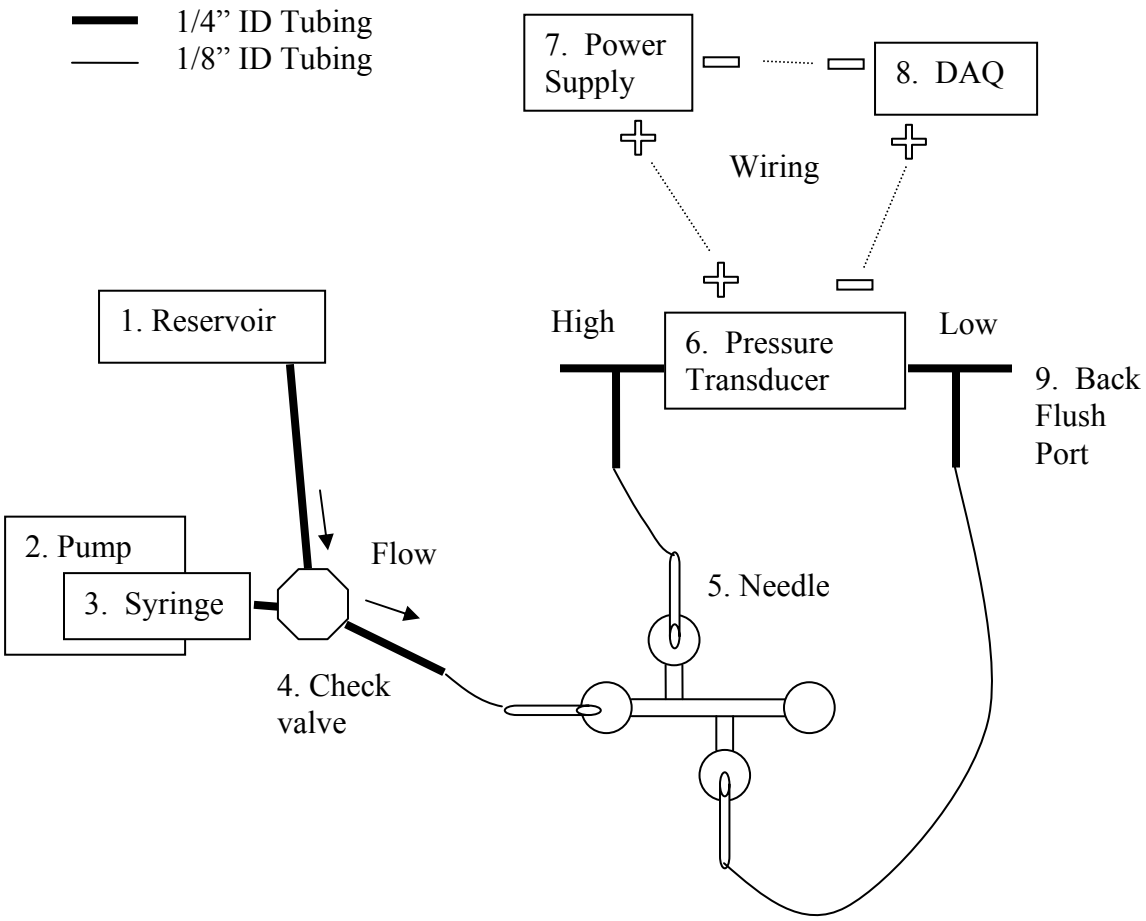

Figure 18: Experiment schematic

Table 2: Experiment schematic parts list

	Name	Description	Picture
1	Reservoir	Covered tank for holding test fluid	Figure 8
2	Syringe Pump	NE-1000 Single Syringe Pump	Figure 8
3	Syringe	6cc Monoject with leur lock	Figure 6
4	Check Valve	One way check valve	Figure 7
5	Needle	McMASTER-CARR: 75165A757	Figure 20
6	Transducer	Omega: PX2300-2DI	Figure 9
7	Power Supply	Omega: PSS-D12B	Figure 10
8	DAQ	Omega: OM-CP-QUADVOLT	Figure 12
9	Back Flush Port	Allows back flushing of pressure lines	Figure 19

Testing Procedure

With all the proper equipment chosen all that remains is the actual pressure testing. One testing problem still remains and that is how is the fluid going to get in and out of the channels along with the pressure data. By referring back to the mask figure, sets of large circles can be seen. These circles are all connected to the channel and allow for a needle to pierce the PDMS from above and couple with the microchannels. Having these pads off to the side away from the test channel means that the piercing process is not as critical and can be done quite clumsily and still not affect the test outcome. First a 21 gauge needle is pierced through the top layer of PDMS and down into the second one. Great care is taken not to go all the way through the second layer for this bottom piece would have to be resealed. Next the needle is carefully removed with a twisting motion such that the large circular port is left with a circular hole in the top layer that is the perfect size for a 21 gauge needle. Left in the piercing needle is a plug of PDMS that is discarded. Another 21 gauge needle is then placed in the now cleared hole and is thusly connected to the channel. This needle can be connected via tubing to either the syringe pump, the pressure transducers or to an exhaust dish which collects all the dispensed fluid. Many methods were tested for connecting equipment to the channels including direct hypodermic needle penetration, gluing tubes, drilling ports and a score of other methods. Every single one of them was tedious and highly prone to leakage. The method first described is the only one so far that appears to be almost 100% accurate easy and leak proof even after multiple insertions and removals of the needles.

Various tube diameters are required to fix the different pieces of equipment together, and great care is taken to reduce the over all volume and junctions as much as possible. Each junction is a possible leak point, and the more volume connected to each side of the pressure

transducer the more time it will take to reach steady state. Smaller tubing options also allowed the needle attachments to be lighter and more flexible making their placement easier.

Finally the channel is ready for testing. Unfortunately even with a simplified means of coupling to the microchannels there is still procedure required to keep small air bubbles from clogging the couplings and pressure ports. In between each pressure needle and the port on the transducer it self was a plug that could be removed so that a large 20cc syringe could be placed in line with the pressure port. The syringe is filled with the same test fluid as the reservoir and is used to back flush that port and grantee that no air is present in the needle before insertion. Also a set of needles were made and completely filled with glue to act as a plug. Assuming a channel has only one set of pressure ports the needle insertion procedure would be as follows. First the inlet needle from the pump would be placed in the channel and the pump would be set at a constant flow rate of about 500 μL per minute. This flushes the channel and all its ports with test fluid. To ensure that every port was completely flushed and cleaned of air and possible particles a plug is placed in both the exit and low pressure port. Once fluid can be visually seen coming out of the high pressure port on the PDMS test piece the high pressure needle is made ready for insertion. With the back flush syringe in place and the pump still exhausting through the high pressure port the high port needle is to be flushed so that fluid can be seen coming out of it. See Figure 19 for a close up of the plumbing with plug in place. The plug is removed and the flush syringe inserted.

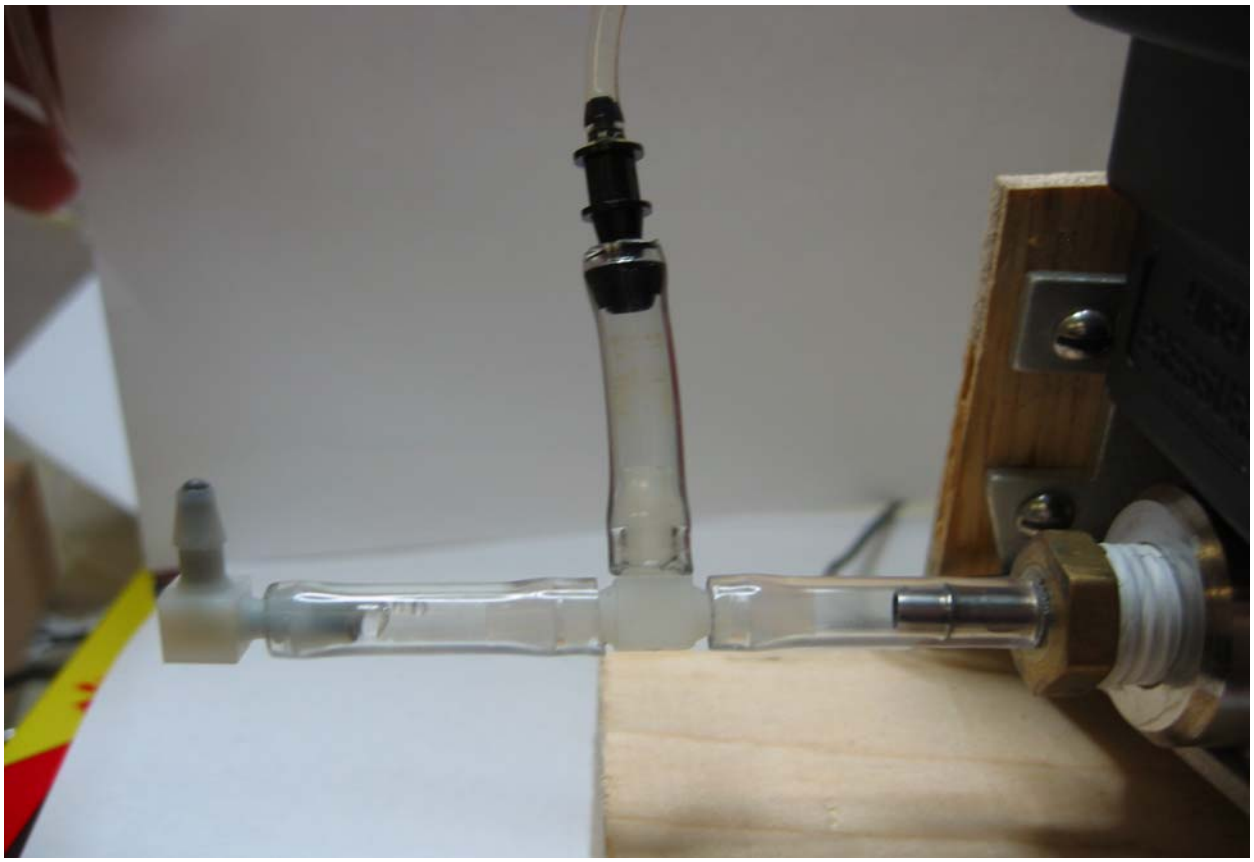

Figure 19: Flush plumbing for pressure port

Only when both the needle and PDMS port have fluid coming out are they to be joined with great care take so as not to place the needle passed the first layer of PDMS. This ensures that the high pressure needle is properly seated and contains no air. Next the low pressure plug should be removed from the low pressure port of the PDMS till fluid appears through it. The back flush procedure is then repeated and the low port installed. Finally the exhaust needle can be placed and should be watched till it flows with dispensed fluid. Early in testing this level of care was not taken and air was introduced in the system causing pressure ports to be blocked by the capillary effects resulting in sluggish pressure responses and incorrect readings. Any time a pressure or inlet needle leaves the test PDMS chip this procedure should be followed. Once the needles are inserted the back flush syringes can be removed and plugs put in their place; all the

while taking care not to introduce any air into the pressure system. Figure 20 is the chip fully plumbed and ready for testing.

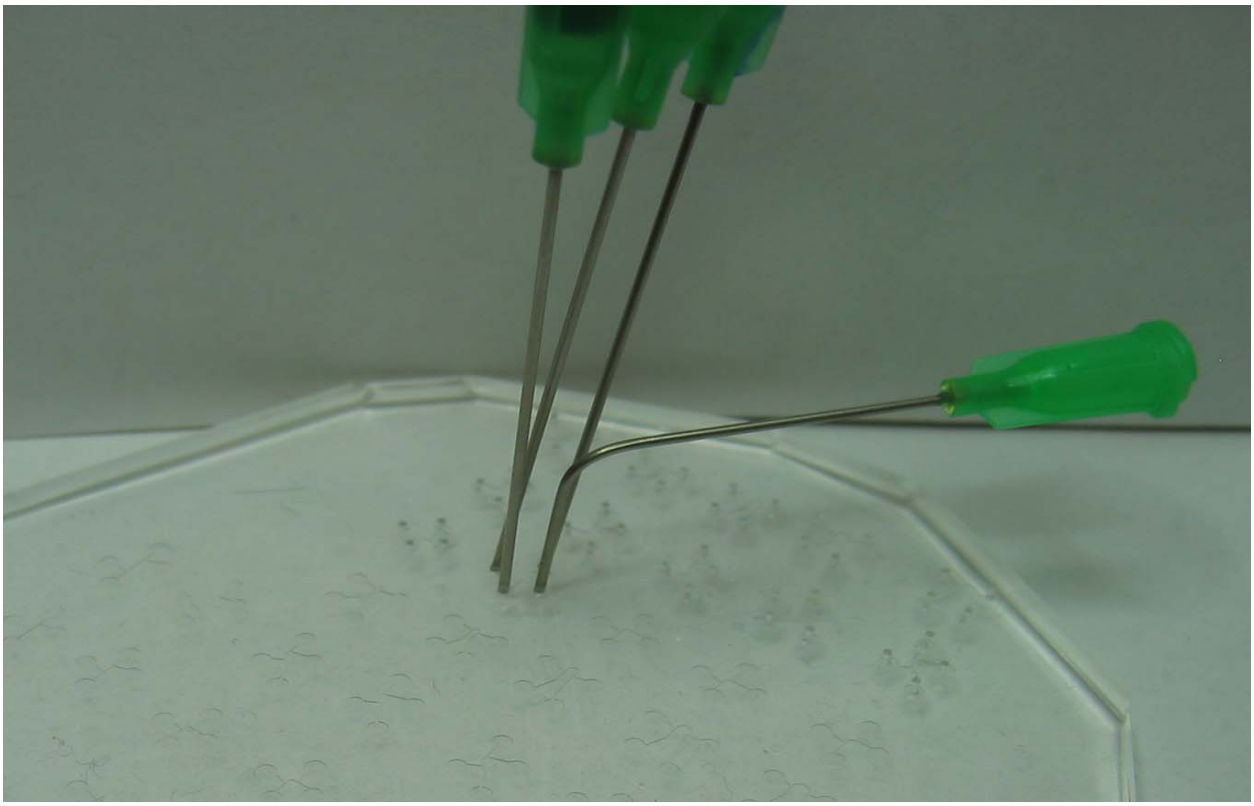

Figure 20: Channel pierced and ready for testing

With the plumbing procedure fully solved the final piece of the puzzle is what range of flow rates would be tested for their pressure losses. A wide range was desired going as low as possible while still being able to easily detect it with the transducer, and high enough to use most of the range of the pressure transducer. Because of the different types of bends it would have to range from a low flow rate in the straight 1mm length channels, and as high as the high flow rate in the 180° 2mm channels. Through a few trials it was decided that the extremes would be 50µL / min to 500µL / min. Between these extremes a number of flow rates were chosen to help fill in

the gaps. Table 3 is the chosen set of flow rates, their resulting velocities and Reynolds numbers assuming that the channel is perfectly 100μm square.

Table 3: Flow rates and Reynolds numbers for channels

Vol (μL/min)	50	100	150	200	250	300	350	400	450	500
Vel (m/s)	0.08	0.17	0.25	0.33	0.42	0.50	0.58	0.67	0.75	0.83
Re #	8.50	16.99	25.49	33.98	42.48	50.97	59.47	67.96	76.46	84.95

The experiment has been fully developed for testing the microchannels for pressure losses. These measures were created from trial and error of various testing procedures and test equipments. With the ability to easily gather repeatable data full data acquisition and analysis could begin. Next is a results section discussing how the acquired data was treated and analyzed.

CHAPTER FOUR: RESULTS

With a full test procedure in place it was time to begin a small validation stage. A literature review revealed a great amount of uncertainty in how simple straight-duct microchannels acted in relation to their larger macro cousins. As a result the first step was to test a number of these straight channels to see if "macro theory" held up or not. This also needed to be done regardless of the outcome to have a way to compare straight-duct findings with those same lengths containing a bend in them.

During testing great care was taken to remove air bubbles from the pressure lines, monitor ambient temperatures, prevent test fluid contamination and other such considerations to help produce quality results. A test channel would be pierced plumed and allowed to run through its prescribed pump routine. After completion the voltage data is saved for later analysis. Figure 21 is a good representation of what this properly captured pressure loss data would look like once a test set was completed.

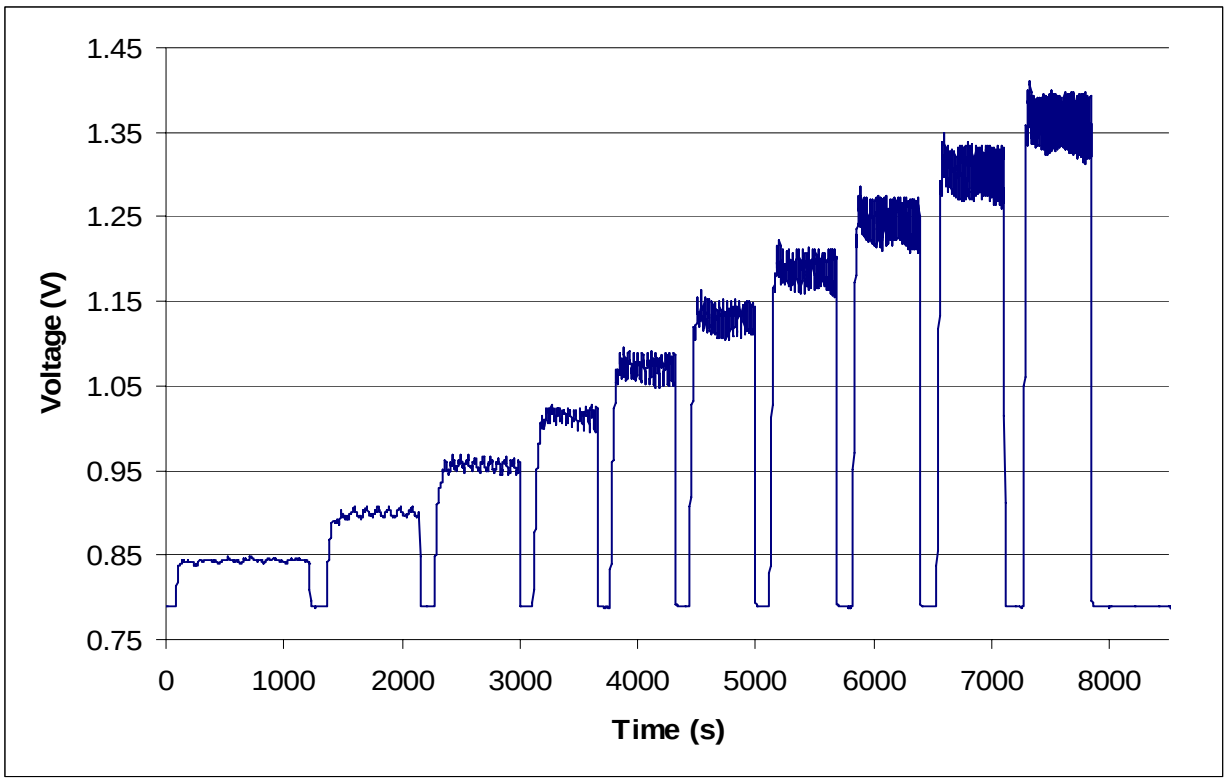

Figure 21: Raw voltage data

This figure appears very confusing and requires a bit of explanation. First note that the amplitude is in volts not a particular pressure. From the calibration however, a relation curve from volts to inches of water is known, so this can be changed into any form of pressure units that are desired. Secondly the data comes in odd plateaus and spikes. If the plateaus are counted there are ten of them. These represent the steady state flow of water through the channels at the ten different flow rates from lowest to highest. On the plateaus the data appears to oscillate in a sine wave. Extensive testing revealed that the main shaft on the syringe pump was slightly bent. It still gave correct flow rates, but the flow rates varied slightly as the pump shaft moves the pusher block up and down. In order to help cancel out any effects differing diameters changes in the syringe and oscillations in the shaft the pump program was setup to run the particular flow

rate for at least 10 minutes before withdrawing the syringe to fill the expended test fluid. This would provide a large number of periods that could later be averaged across to find a time averaged value. Because the slower flow rates would cause fewer periods of the varying flow rate the earlier flow rates were allowed to go for a longer time than the higher ones. A 6cc syringe was used so that even the highest flow rate, 500µL / min, would have 10 minutes of run time.

This periodic data caused a bit of an issue when it came to turning this raw data into individual pressure loss for each flow rate. To process the raw data a code was written in MathCAD to help isolate individual flow rates automatically. Appendix B contains the code and some example extraction. It works by manually setting a cutting line between the zero pressure voltage and the lowest pressure values for the first flow rate. With this cut off line set the program moves from left to right and every time the voltage goes above the line it is clipped out and placed into a new array until the voltage passes below the line. This produces 10 arrays; one array for each flow rate. A predetermined number of points were then clipped off of either end of these arrays. This would remove the non steady state portions of the pressure trends. All that is left is a straight sine wave that is then averaged and saved as the final pressure. For this final pressure to have meaning the zero voltage must be subtracted from it. So another portion of code adds up everything below the cut line and removes the first few set number of points from that array. This will clip the non-zero steady sate values from the flow pressure coming down. With steady state and zero pressures found the values were placed into an excel file used to collect and organize the pressure data that would zero the voltage data so that it can be directly converted to pressures via the calibrations curve slope.

Straight Microchannels

With empirical data collected for straight channels it must be compared to previously established text book values for square channels in the laminar flow region. From Belvins [34] the following set of equations are required to find head loss in a straight square laminar channel . Equation 1 is the head loss, or loss of useful pressure across a length of pipe L, traveling at average velocity U, with friction factor f, and hydraulic diameter D. According to Belvins hydraulic diameter for a noncircular channel is four times the area divided by the perimeter of the shape Equation 2. The average velocity was backed out from the area and volumetric flow rate of the test being known. Finally the friction factor f was suggested as being Equation 3. Because manufacturing might produce a channel that is not perfectly square the rectangular friction factor equation was used. Reynolds numbers were easily found for the temperature and volumetric flow rates of the test fluid through the testing.

Equation 1: Head loss

$$\Delta p = \frac{\rho \cdot U^2}{2} \cdot \frac{f \cdot L}{D}$$

Equation 2: Hydraulic diameter

$$D = \frac{4 \cdot (w \cdot h)}{2 \cdot h + 2 \cdot w}$$

Equation 3: Friction factor

$$f = \frac{64}{Re \cdot \left[\frac{2}{3} + \frac{11}{24} \cdot \frac{h}{w} \cdot \left(2 - \frac{h}{w} \right) \right]}$$

With basic theoretical pressure loss discovered it could be compared to the data taken in straight channels. Before, however, a bit of uncertainty had to be taken into account. Normally

it would be expected that the theoretical values be considered "perfect" and that experimental values have uncertainty attached to them. In this case the experimental data was a fairly direct measurement with only a small amount of uncertainty and bias possible. The theoretical pressure losses on the other hand were inferred and are highly dependent on temperature, height and width measurements of the test channel, and volumetric flow rate. Previous research and testing pointed towards a small temperature swing having huge effects on viscosity which, as low Reynolds numbers directly indicate, is extremely important. In addition the channel dimensions are difficult to take. The channel must first be cut perpendicular to its run in order to get a properly squared profile. Being off a few degrees from the cut can make the channel seem wider or taller than it really is. In addition off square cuts make focusing the whole profile at once impossible. Manufacturing also causes the channels not to always be perfect squares, but sometimes more of a trapezoidal shape. Lastly the resolution of the camera was such that each pixel represented roughly 1.4 micron in length. Lining up the pixel measurement tool to the exact pixel is nearly impossible because of image quality. As a result the if manual measurements of height and width are off by even a few pixels it translates to an area difference of as much as 10%.

To account for all these issues in tolerance and uncertainty a relative uncertainty analysis was done to all the governing equations used to develop the theoretical pressure loss. This analysis can be seen in Appendix C and determines an uncertainty value for a calculation by using the partial derivative and uncertainty of each component, adding the squares of each of these sets, and then taking the square root of the whole pile.

All the uncertainty analysis comes down to a final ± value that gives the median pressure value a range of uncertainty or error bar. These error bars represent the limits of the ability to

predict a pressure loss for a certain channel do to variability in channel size water temperature and a number of other factors. The final theoretical head loss uncertainty yielded varies between 9 and 9.4% of the total head loss a particular Reynolds number. As long as the data falls with in the lines prescribed as undetectable variability then the data can be considered to adhere to the governing equations used to generate the theoretical pressure loss curves.

An example of adherence to straight-duct pressure loss theory can be seen in Figure 22. Red lines indicate error bars on the theoretical pressure uncertainty at given Reynolds numbers. Blue "X"s are actual direct pressure measurements. This represents an ideal piece of data pointing heavily to there being no difference in micro and macro scale flow relations.

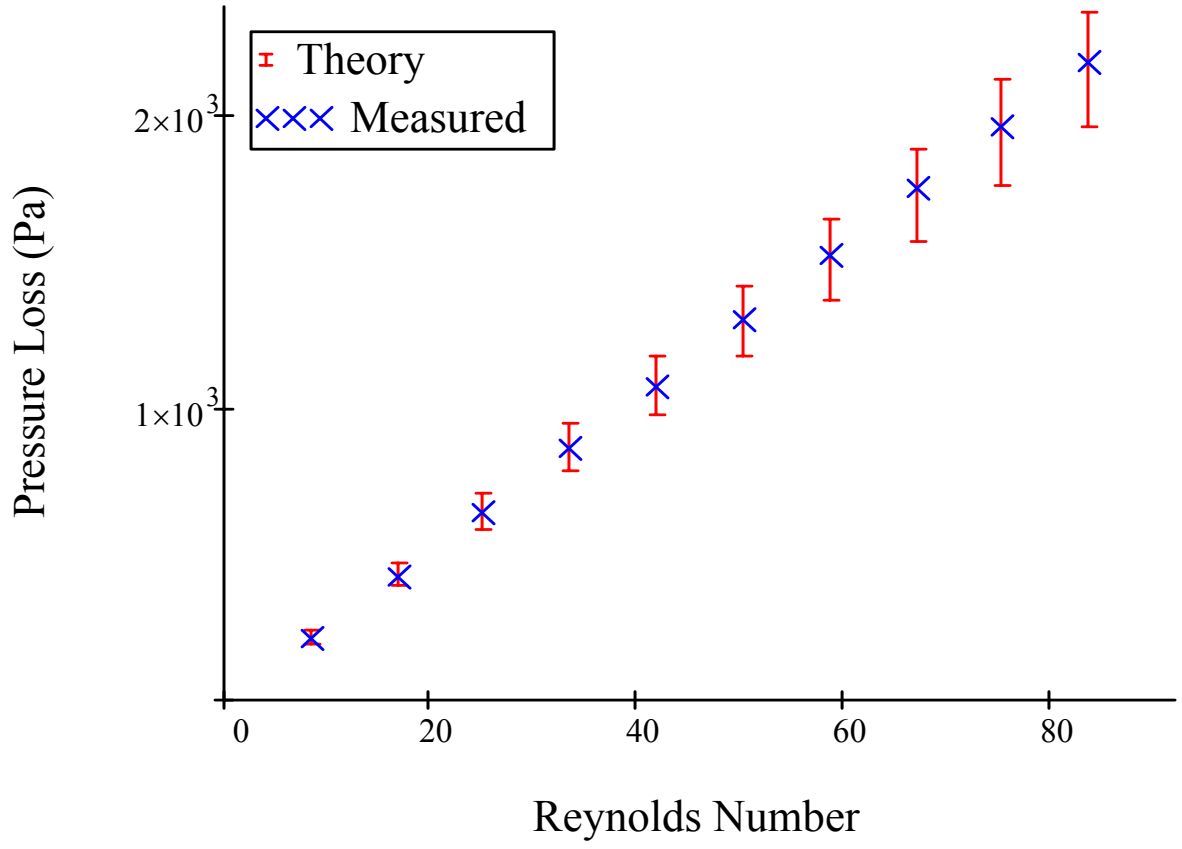

Figure 22: Straight-duct pressure losses

Many 1 and 2mm channels were tested and an interesting trend emerged. All of the 2mm straight channels tested fell with in their error bars, but not all the 1mm channels did. The 1mm channel data appeared to behave more sporadically both above and below the theoretical loss values. It could be that at the great length of the 2mm channels small hiccups like area changes due to manufacturing have less effect on the total pressure loss through a channel. Another source of error that the 1mm channels possessed over the 2mm ones is their shortened length offered fewer diameter measurements. The more times a channel can be cut and measured under the microscope the more likely a good reasonable average can be found of its over all diameter, but with fewer cuts this average is more likely to be off from the true diameter. More than likely though is the fact that the lower pressures to be detected in the 1mm channels were closer to the noise level of the pressure transducer. The transducer has a 0.25% of the full scale range that as its uncertainty. This is true across the whole range, which means a 0.1psi reading has a high percentage of uncertainty, while the same pressure uncertainty on a higher pressure measurement yields an over all lower percentage. The ultimate result being that low pressure measurements are going to be a lot nosier than high pressure measurements. The worst example of a channel over and under shooting the established pressure loss theory and error bars is available in Figure 23 and Figure 24. Graphs of all straight channel pressure loss data can be seen in Appendix D.

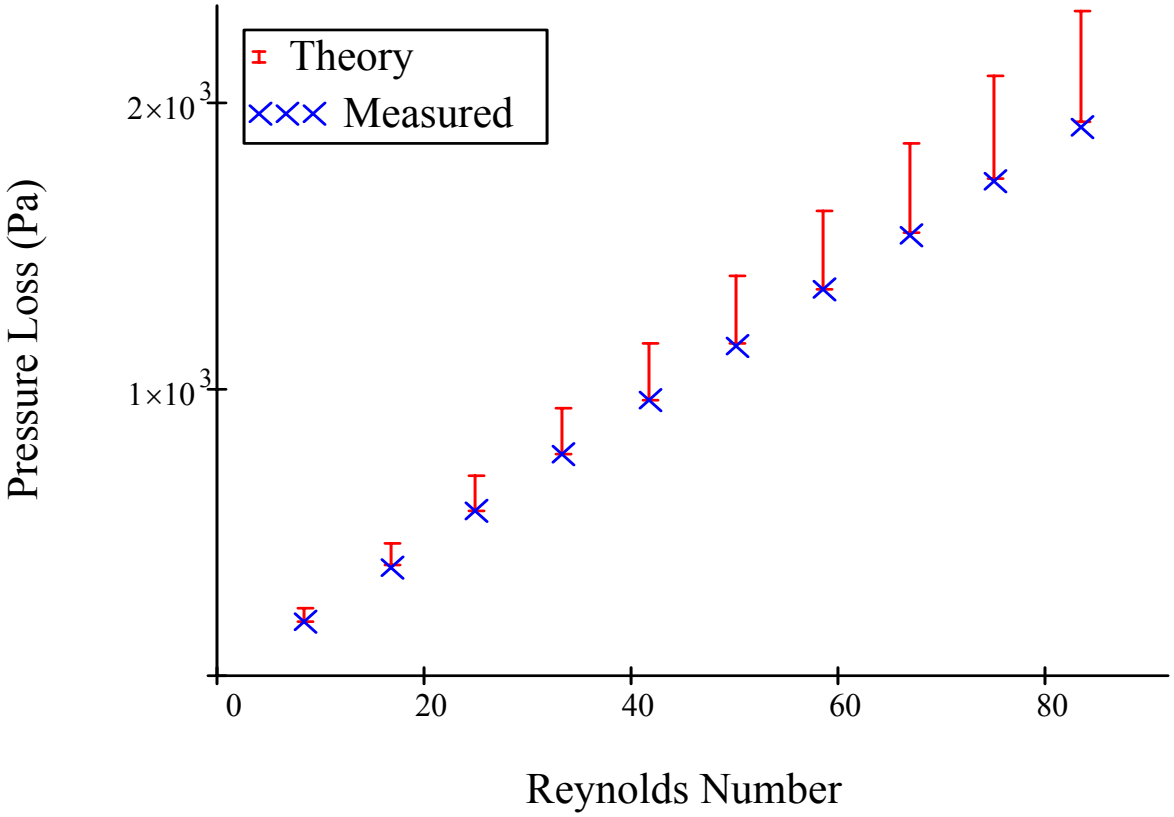

Figure 23: Outlier pressure data 1

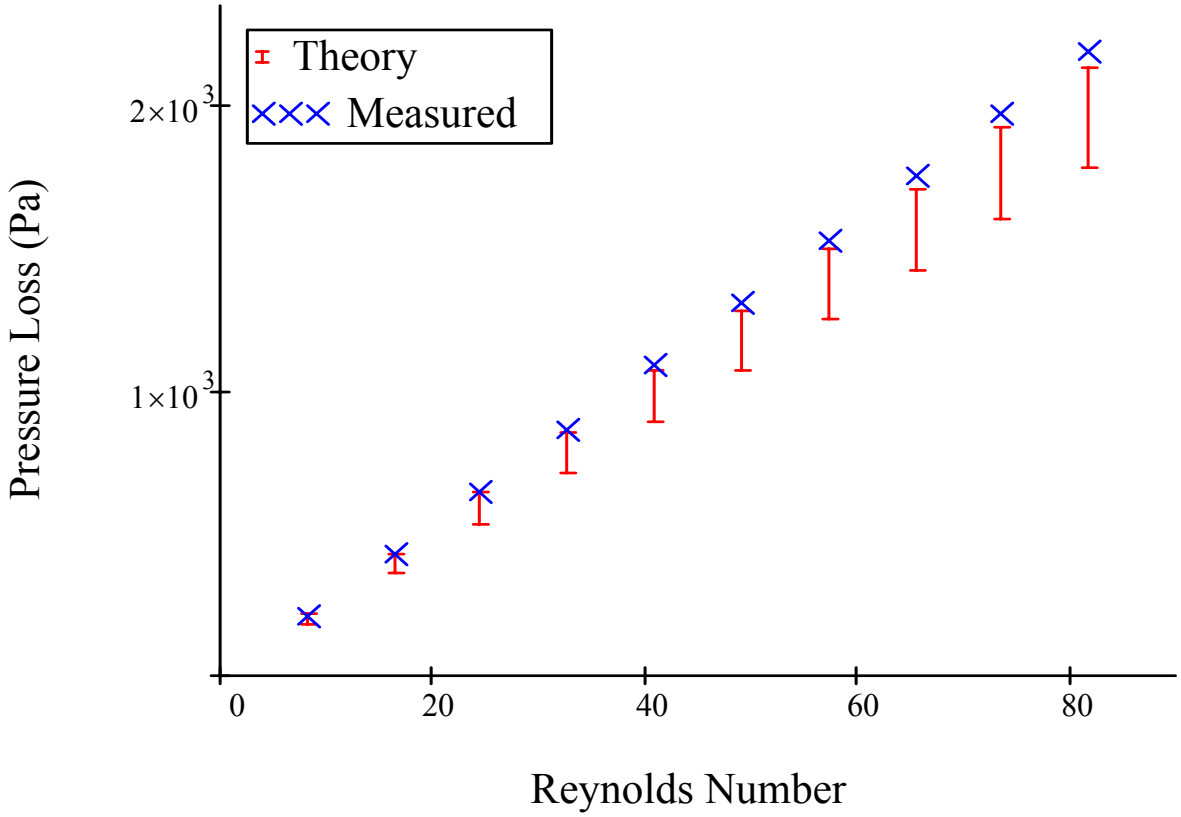

Figure 24: Outlier pressure data 2

In addition to viewing graphs, the direct measurement pressure losses were divided by their theoretical losses and then averaged to see if any trend emerged. This was done for both the 1 and 2mm channel sets resulting in a 1 to 2% average deviation above the theoretical pressure loss. This represents a bias in the channels towards a higher pressure loss, but a 1% bias is not seen as being in any way significant. A temperature detection bias of one degree Celsius would cause a greater shift than that. Between the averaged differences matching so accurately and most of the data falling with in the uncertainty tolerances it can be confidently assumed that pressure loss through a straight channel adheres exactly to standard theoretical practice.

Sweeping-Bend Microchannels

Standard practice for bends in macro theory has been to treat the entire bend like a black box and apply a loss value to it for use at a certain Reynolds number. This loss value is often referred to as "K" or the loss coefficient, and is used as a blanket loss for anything from fittings to valves to bends and much more in the world of hydraulics. K values are found via Equation 4, and once established can simply be multiplied by dynamic pressure and added to the pressure loss calculations for straight-ducting or any other kind of piping to establish a total head loss for a flow network. This is often easy for engineers to use because they can break up the loss calculations by its components by adding up their straight-ducts and putting all K values for any extra fittings needed together with dynamic pressure.

Equation 4: K loss coefficient

$$K = \frac{2 \cdot \Delta P}{\rho \cdot U^2}$$

In order to establish a range of K loss coefficients for sweeping pipe bends a series of bends of angle 45º, 90º and 180º were tested with bend radii ranging from 125μm in those increments until 625μm was reached. With 3 bend angles and 5 bend radii a set of 15 different channel types had to be tested at least 5 times to find a good average K value trend for that particular bend type. In the case of many tested channels the pressure ports were some distance away from the bend on both ends to make sure that no disturbances from the side offshoot pressure ports would affect the bends or vise versa. Meaning a certain length of straight-duct losses had to be removed from each pressure measurement to establish the pressure losses for the isolated bend.

Ideally previous work with sweeping-bend channels on the macro scale would be available to compare to the data taken here. Because of the very low Reynolds numbers macro scale data would have to be highly laminar for a comparison to take place. The only laminar sweeping-bend loss coefficient data that could be found was for round tube macro channels. Work has been done on square and rectangular duct channels, but all the established data was found to be for higher Reynolds numbers well into the turbulent zone. With no square duct K values to directly compare it was decided that the circular profile channels would be viewed for a similarity comparison. Exact loss coefficients are not expected to match, but performance should be similar. Figure 25 displays accumulated data Blevins [34] collected on round tube sweeping-bend channels in laminar flow. The handbook goes on to say that these values are valid for bend radius over diameter ratios of 0.5 to 11.7. In addition, this range of values is applicable for both 45º and 90º degree channels. It is suggested that the values of K be doubled for bends of 180º. The ranges provided are quite wide, and lumping both 45 and 90 degree channels together seems counter intuitive, it would be expected that the one posses twice the losses of the other. A set of straight lines like this indicates that losses are a direct relation to Reynolds number. This is the exact type of behavior expected from straight-ducts meaning that no secondary flow is occurring. Regardless, this shows the near complete lack of experimental data for laminar pipe bends of any type scale or profile shape thus further highlighting the need for this type of fundamental research.

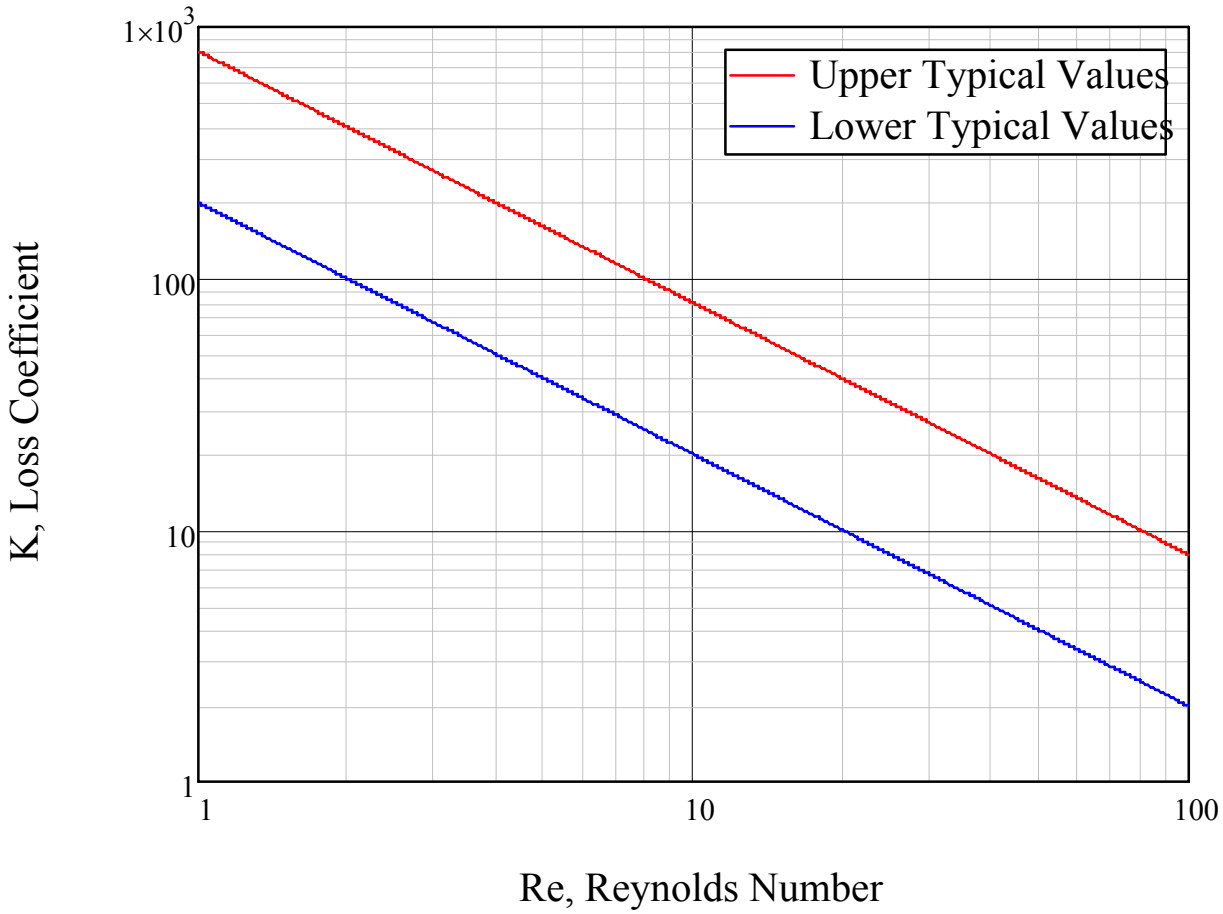

Figure 25: Typical K values for 45º or 90º round tube bends

Some nomenclature needs to be established when describing specific geometry used in rectangular sweeping-bend microchannels. Figure 26 is a diagram of any given rectangular micro channel. Assuming the channel height is constant and into the paper the main features of importance are given in the figure. A centerline runs through the channel half way between the inner and outer wall. The curve of this centerline is determined by the bend radius. To form the inner and outer walls an offset on either side of w/2 is done to form the full channel. Bend angle is the angle between the start and end of the sweeping section from the curve center point. Bend angle is a universal trait of all sweeping-bends regardless of their size, but radius is very different from one situation to the next. In order to nondimensionalize this and make it more applicable to

a wider variety of channel types the radius will be divided by the width and referred to as the radius ratio, or simply lower case "r". Given that the channels are on the width order of 100μm the five different radii are converted to their ratio by reducing the order of magnitude by two. For example the channels with a bend radius of 125μm will now be known as a 1.25r channel. This practice of dividing square channel's widths by the path radius to form a radius ratio has been established in many previous works, and will be continued here to provide easy comparison.

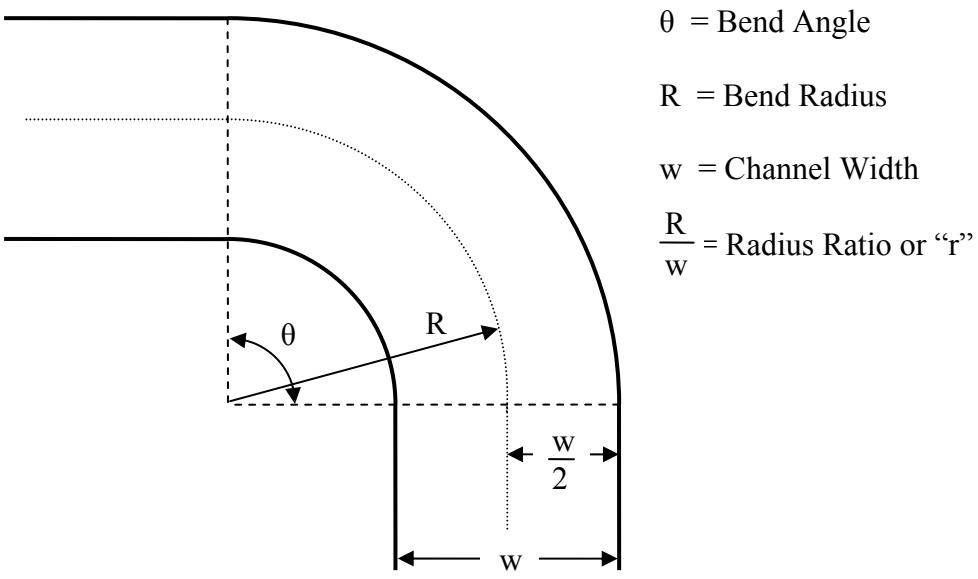

Figure 26: Sweeping-bend channel nomenclature

Large amounts of data were collected for each channel type; up to 10 data sets in some situations. In order to reduce complexity and allow for easier comparison a curve fit will be used to collapse the data into a more manageable form. A power curve fit algorithm was selected from MathCAD to turn raw pressure loss trends from multiple channels of the same type into a single easily defined function. This algorithm takes a set of guess values and works out the best

values to fill Equation 5. The curve fitting process creates proper values for the a, b, and c terms in the equation. When the equation is plotted the x term will be Reynolds number, and the total equation will produce a K loss coefficient curve.

Equation 5: Curve fit equation

$$\text{CurveFit} = a \cdot x^{b} + c$$

Figure 27 is an excellent example of how this curve fit solution works to idealize the raw data taken. It can be seen that the data points form a band, and the curve fitting program shoots the band in such a way as to best represent that data set. Raw data can then be left behind and a smaller simpler more compact curve equation can be used in its stead. Finally, the same curve fit equation was used for every channel type, and only a set of three values were modified to make each curve special tailored to that data set. This means that once all the data has been curve fit, not even the graphs are really needed, but simply a curve fit equation with three variables special to each channel type, and a table of those variables. Every curve fits used for all 15 sets can be seen in Appendix E.

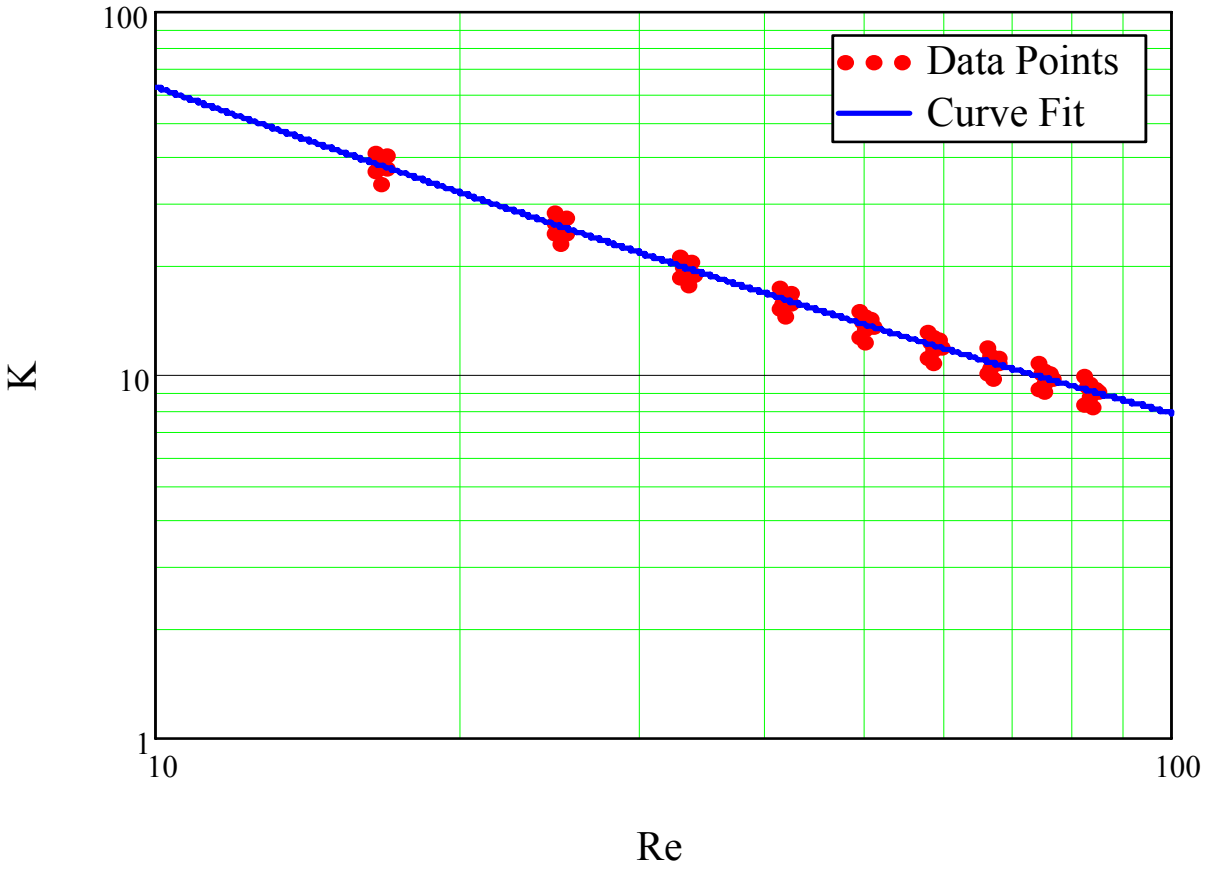

Figure 27: Example of good curve fit

Some of the data bands acquired appear clean and crisp like the one in Figure 27, but not all do. For the sake of completeness an example of a less than ideal curve fit can be seen in Figure 28. This is the 45º bend with the tightest radius of 125µm. Keeping in mind that K values sum up the entire loss across the whole feature it is apparent that duct length is the greatest contributor as will be seen in later charts. Because this bend has the smallest angle and radius of any of those tested meaning it has the shortest distance to travel; which results in a K value that is the smallest, and in this case falls at the edge of the noise level.

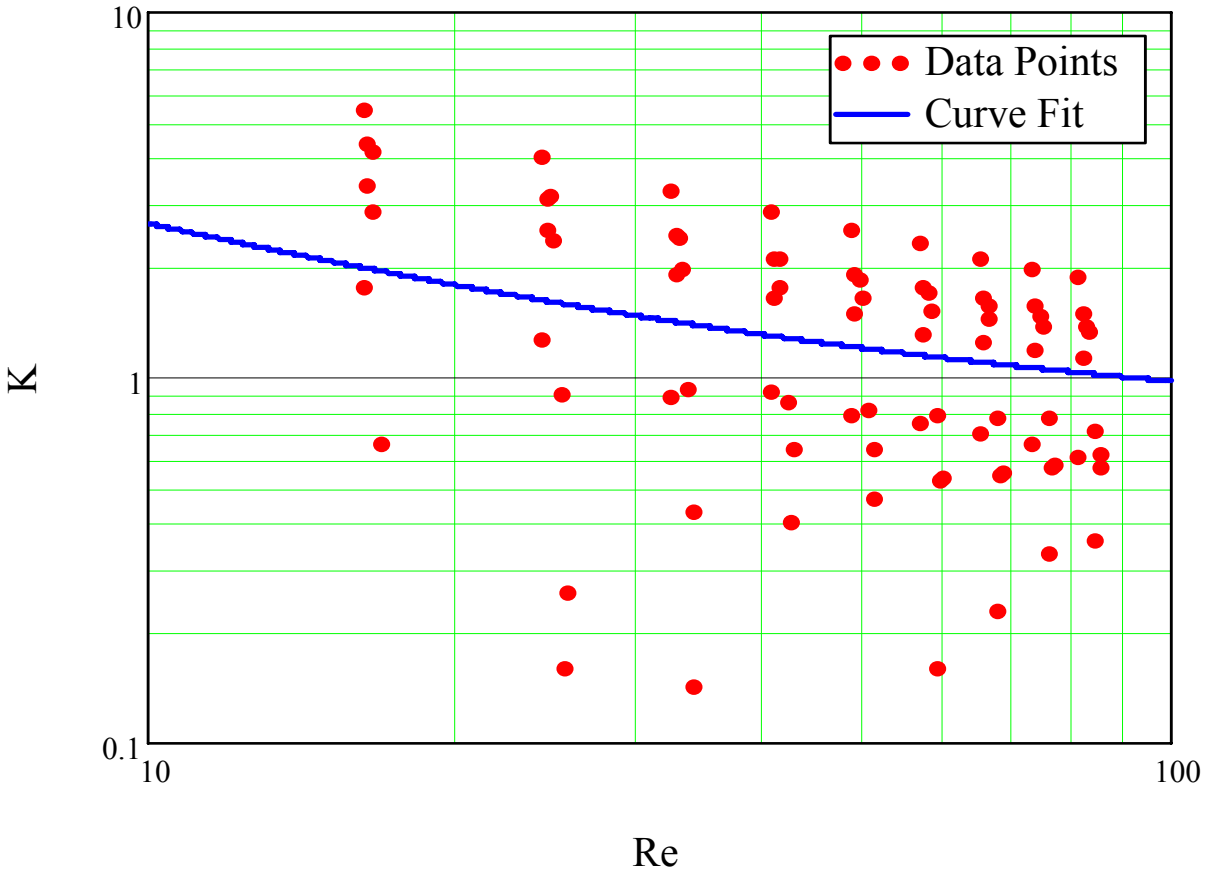

Figure 28: Example of bad curve fit

It should be noted that no successful tests were removed from the pool of data. By successful it is meant that the test ran through to completion with out obvious incident. On occasion air bubbles would find their way into the pressure lines and cause the pressure profiles to be highly erroneous. This would be obvious because during periods of zero pressure the voltage would vary greatly from one withdraw session to another. During a given flow rate the pressure could vary by a large factor or drop out completely. This type of performance was usually coupled with a visible air bubble in the pressure lines. Data of this type was usually not allowed to complete a test cycle, and at any rate was thrown out. If, however, the test finished and there were no obvious signs of error like these then it would be kept permanently. It will be

seen later that the use of a high number of samples and the excellent testing procedure has circumvented any need to exclude any data for any reason.

With curve fitting fully established and an understanding reached about how data has been cared for at this point the final charts of loss coefficient curves can be observed. Starting with the 45º bend channels, Figure 29 shows a set of definitive curves for all 5 end radii. The loss coefficient chart is counterintuitive at first; the smallest radius ratio bends offer the smallest K values for any given flow rate. This does not mean that a smaller radius is always desired. Larger radius ratio bends may cause a higher K value, but this is because they cover a greater distance. The three largest bend ratio channels appear "straight" on the log-log curve and vary in a clean manner with Reynolds number. The two smallest radius ratios, however, have a distinct curve to them; they flatten out as the Reynolds numbers increase and shoot up towards the lower end. A performance difference such as this indicates that the status quo has been disturbed and something additional is occurring. It is probably likely that the tight bend of the smaller radius ratios is causing some sort of secondary flows to occur. One final note should be made, though data was taken on Reynolds numbers as low as 8.5, on the log scale display of this portion of the curve is difficult and could be confusing. So though the data was used to produce the curve fits that range will not be shown on any of the following graphs.

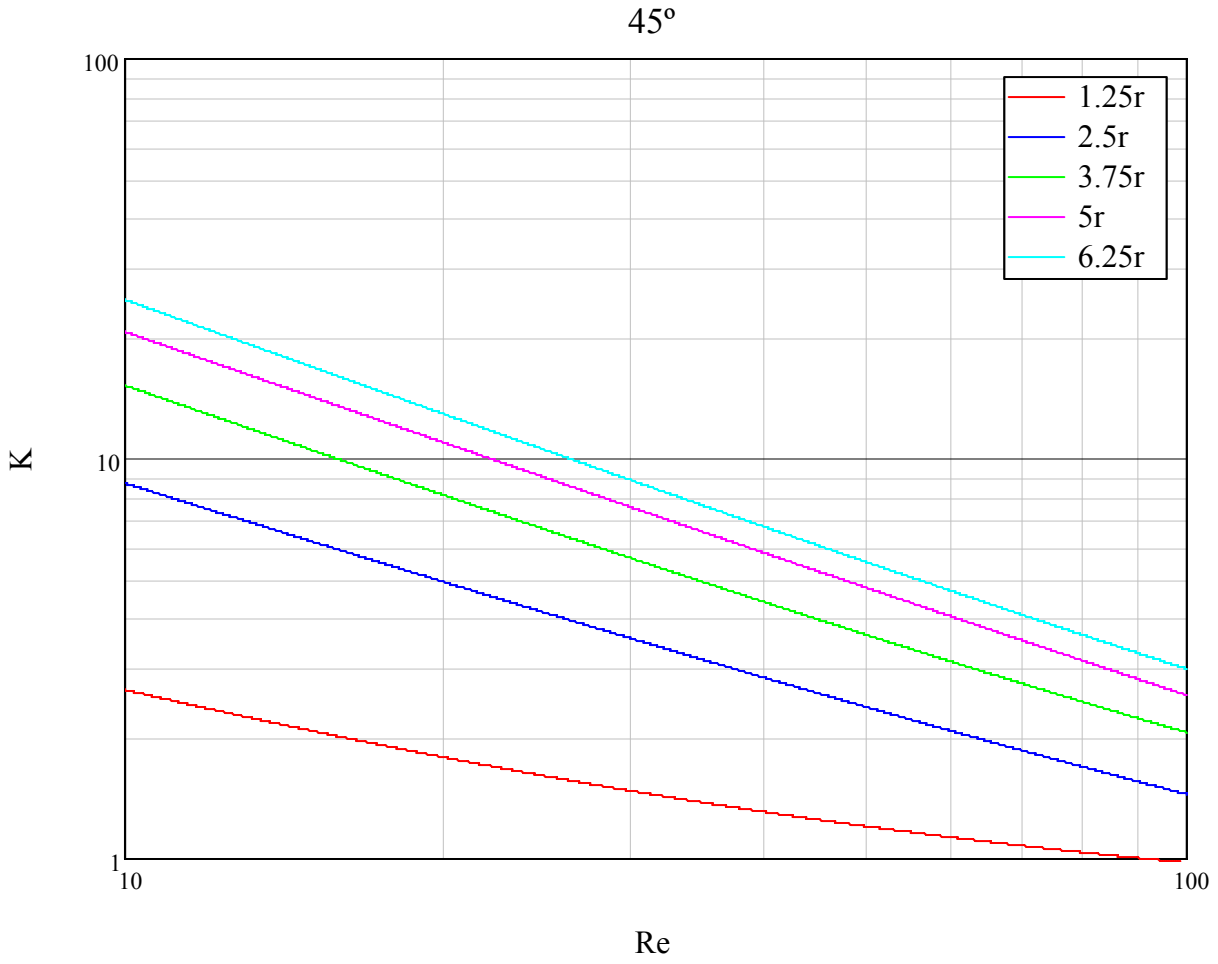

Figure 29: Loss coefficient vs. Reynolds number, 45°

A look at the 90 degree channel line up reveals a similar result only with higher K values. Figure 30 is the 90 degree equivalent of the plot from before. Again notice how the three highest radius ratios are all very straight with respect to the log scale. Similarly the 2.5r curve is slightly bent towards the higher Reynolds numbers, and the tightest ratio is heavily curved compared to the others. Though the K values are different the gaps between the curves appear the same, and the slopes appear similar also. As the 180 degree duct network is revealed in Figure 31 the exact same trends are seen again.

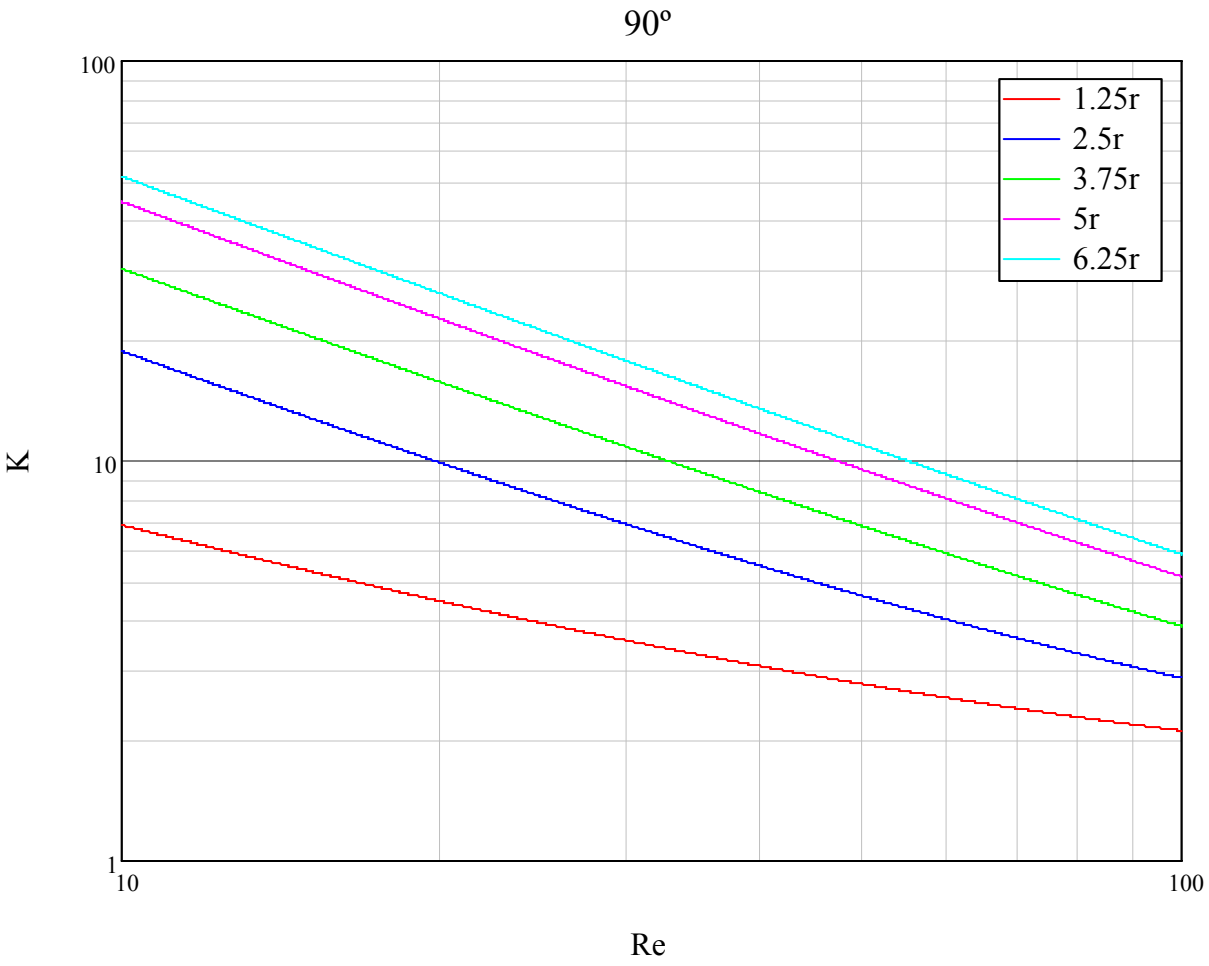

Figure 30: Loss coefficient vs. Reynolds number, 90º

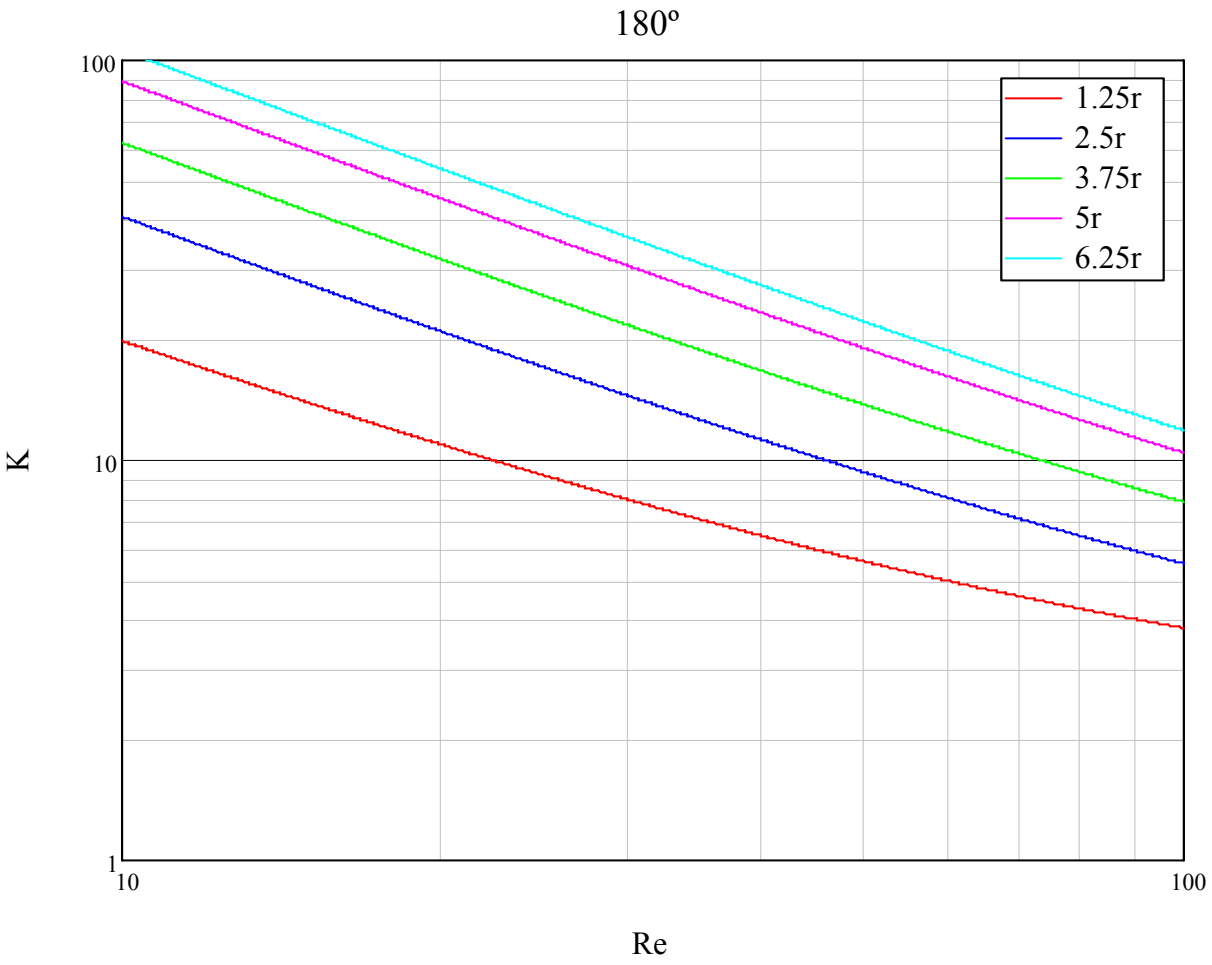

Figure 31: Loss coefficient vs. Reynolds number, 180º

At this point it is again noticed that the only apparent difference is a shift of the values up in the K direction. So, in order to fully explore this; the individual radius ratios must be graphed with each other and scaled to see if they match. Using the idea that loss is fully a function of length, the 90º loss curves will be divided by 2 so as to possibly equal the 45º channels, and likewise the 180º curves are divided by 4. If the loss coefficients are purely based on bend channel length, then these adjustments should cause the curves to fit right on top of each other. Another possibility is that some form of additional losses created by the bend is a direct function

of time spent time spent in the bend. This would cause the adjustments made to line up the curves on top of each other. To account for this a theoretical loss curve is also mapped to see if it matches. If all three loss curves match, and fall under the theoretical straight-duct curve then for that particular bend there is no difference between the bent channel and the same length of straight channel. The result of these adjustments for the longest bend ratio (6.25r) is Figure 32.

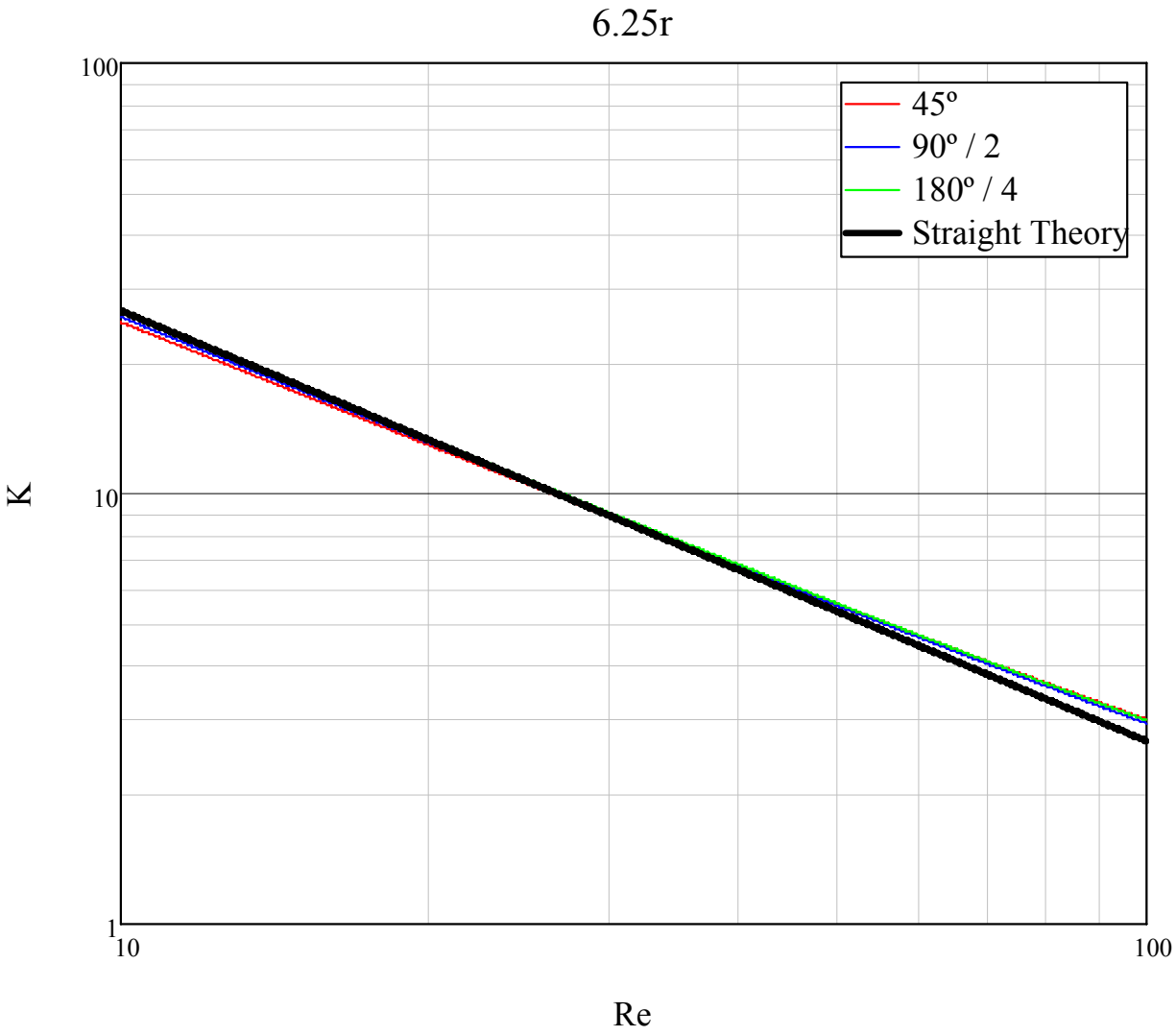

Figure 32: Adjusted 6.25r loss curves

This is not entirely unexpected, and shows a number of interesting things. First, the curves match each other so heavily it is difficult to tell them apart, indicating that their

performance with respect to Reynolds number is the same, and once adjusted for path distance is independent of the bend angle. The thick black line represents losses for a straight-duct of 105μm nominal hydraulic diameter. Though diameters varied form channel to channel this best represented the average size tested and would form a good basis of comparison to indicate secondary flow losses. The theoretical loss curve follows closely the other adjusted curves indicating that there are no significant losses due to secondary flow from bends. This would suggest that at this particular radius ratio the sweeping-bend acts almost exactly like a straight-duct. With Reynolds numbers being as small as they are viscous forces are extremely high, so any swirl that tries to take place from centrifuge forces during the bend are dampened out and do not show any noticeable effects. In this case it is as if the fluid doesn't "know" that it is going through any sort of a bend. Another useful attribute of having these flow curves graphed this way is that their excellent matching indicates that the data was collected carefully and properly. It was expected that given the low Reynolds number, and gentleness of the sweeping-bend that these channels would perform very similarly to straight-ducts. If, however, there was some sort of added losses due to the bend it should be noticeable by the 180 degree curve having higher losses than the 90, and that one with higher losses than the 45 channel, once adjusted for distance. Next, the 5, 3.75, and 2.5 bend ratios are displayed in the same chart in Figure 33.

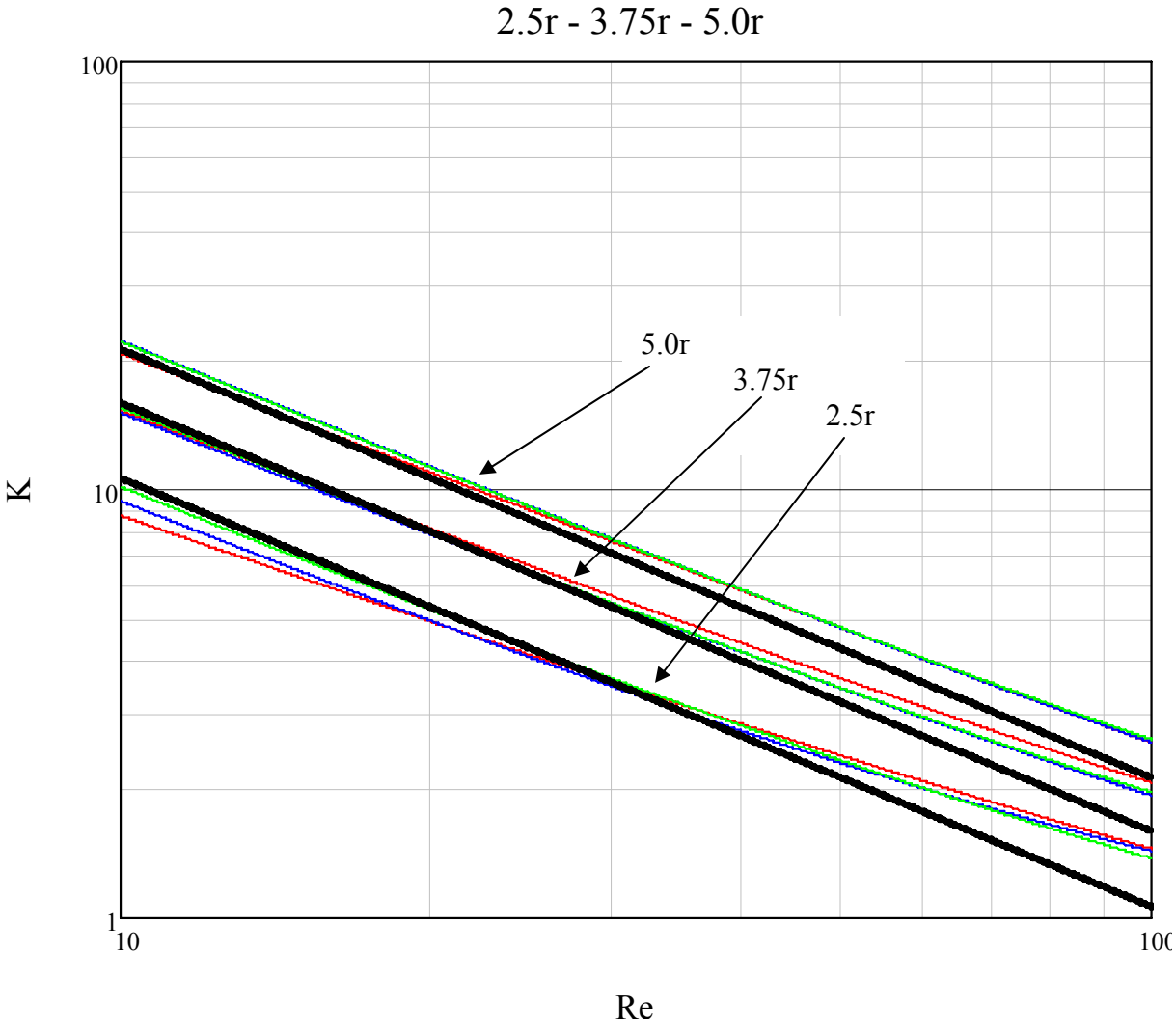

Figure 33: Adjusted 2.5r, 3.75r and 5.0r loss curves

All three curves tell a similar story to those of 6.25. All three bend angles fit nicely on top of each other with a slight increase in difference between the curves as bend ratio decreases. This higher volatility is probably because the K loss coefficients are getting smaller with the tighter radius ratios. The smaller the losses that are being detected get closer to the noise level them become and the more difficult it is to capture them accurately. With respect to the straight-duct theory a trend emerges that as the tighter the radius ratio the more the losses increase over straight theory at the higher Reynolds numbers. It could be that below a Reynolds number of

roughly 50 the bend makes no deviation from straight-duct theory, but once past that Reynolds number losses increase dramatically. A look at a tighter bend ratio would be helpful in indicating if this really was a trend worth noting. Finally, the smallest radius ratio of 1.25r is plotted in Figure 34 and creates many questions to be answered.

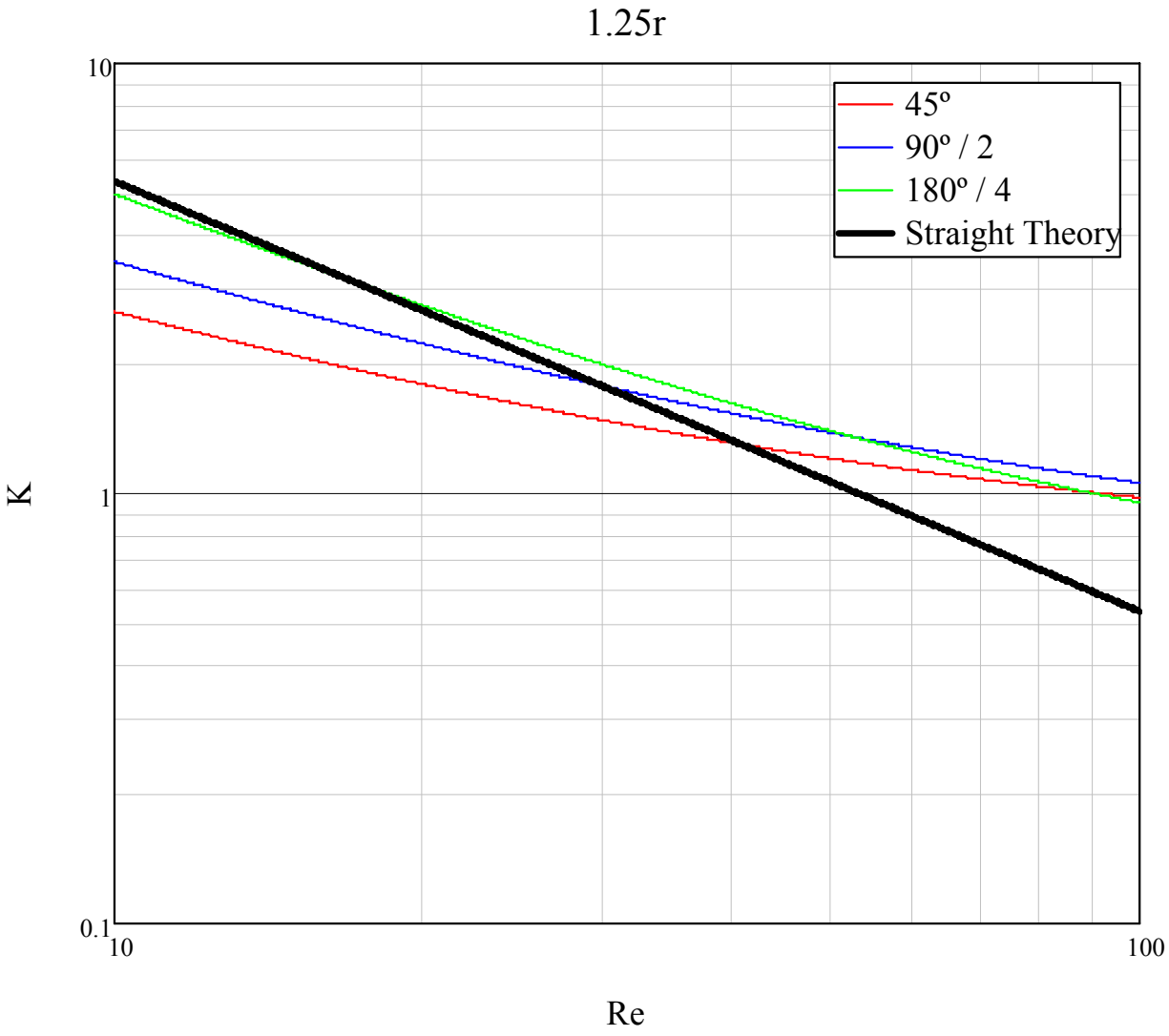

Figure 34: Adjusted 1.25r loss curves

Keeping in mind that these loss curves are adjusted the first two bend angles appear to behave similarly, but an offset still exists between them. The 180 degree channel seems to act like the previous channels; starting off very close to straight-duct loss at the lower Reynolds

number and the deviating higher as Reynolds number increases. The other two bend angles perform very differently from any previously established curves. Comparing the pressure losses through these small bends and the transducer uncertainty reveals that the uncertainty surpasses the supposed detection in some places. This means some of the smaller channel K losses could be over 100% off at the lowest Reynolds numbers; though at the faster flow rates uncertainty quickly reduces to just a few percent. Keeping in mind that the lower Reynolds number ranges of the 45º and 90º are not to be trusted, the higher flow rate patter reemerges. The 180º channel tracks nicely with straight-duct at lower Reynolds number, and begin to diverge around Re 20-30. At the high end the two smaller bend angles perk up and all three curves converge to loss coefficients much higher than the straight-duct theory would predict.

It appears that as the radius ratio decreases it begins to stop acting like a straight-duct and incurs extra losses, more specifically at some of the higher Reynolds numbers tested. Between the clearly increasing trend of loss deviation at higher Reynolds numbers in Figure 33 and the continuation of this in the 1.25r 180º channel in Figure 34 there is clearly some sort of minor losses beginning to occur in these regions. An attempt was made to find an empirical relation that predicts these added flow losses but the additional losses were small and only represented a small portion of the data. A more directed data set would be required to provide a proper relation.

In light of no proper empirical relation existing all the curve fit values used can be found in Table 4. These curve fit values are to be placed in Equation 5 and used only across a certain tested range. It should be considered that the curves provided only hold true from Reynolds numbers of 10 to 100, between radius ratios of 1.25r and 6.25, and between bend angles 45º and

180º. The shortest two bend angles for the 1.25r curves should probably be ignored and a division of 180º by the desired bend angle would be substituted.

Table 4: Curve fit coefficients

	a			b			c		
	45º	90º	180º	45º	90º	180º	45º	90º	180º
1.25r	13.023	37.701	179.571	-0.821	-0.824	-1.002	0.682	1.271	2.034
2.5r	61.174	184.688	406.069	-0.862	-1.020	-1.019	0.297	1.181	1.795
3.75r	132.492	280.190	628.863	-0.949	-0.978	-1.019	0.400	0.761	2.118
5.0r	176.342	437.710	882.060	-0.931	-1.000	-1.007	0.149	0.774	1.908
6.25r	230.921	498.219	1.07E+03	-0.971	-0.992	-1.011	0.350	0.668	1.718

With this set of curve fit correlation values a number of trends can be noticed. For example all the "b" values are very close to negative one. These trends along with a number of other relations were used to create a new empirical loss equation. This new loss coefficient generation equation can be seen in **Error! Reference source not found.**. This new relation was generated from noticed trends and performances of the previously established curve fits.

Equation 6: New bend loss equation

$$K_{bend} = \frac{\theta}{90^{\circ}} \cdot \left[\frac{3}{2} \cdot \left(\frac{R}{w} \right) \cdot \frac{f}{Re} + 1 \right]$$

Assuming that the macro laminar straight-duct loss equation can be used to predict flow losses at "low" Reynolds numbers, and this new equation should be used to predict higher Re losses, then the two should meet somewhere in the middle. With this concept in mind a deviation assumption of 5% was assumed to be the tolerance of acceptable threshold. All curve fits were compared to the straight duct theory and the point of their deviation beyond the threshold was noticed. Figure 35 shows the result of this threshold analysis.

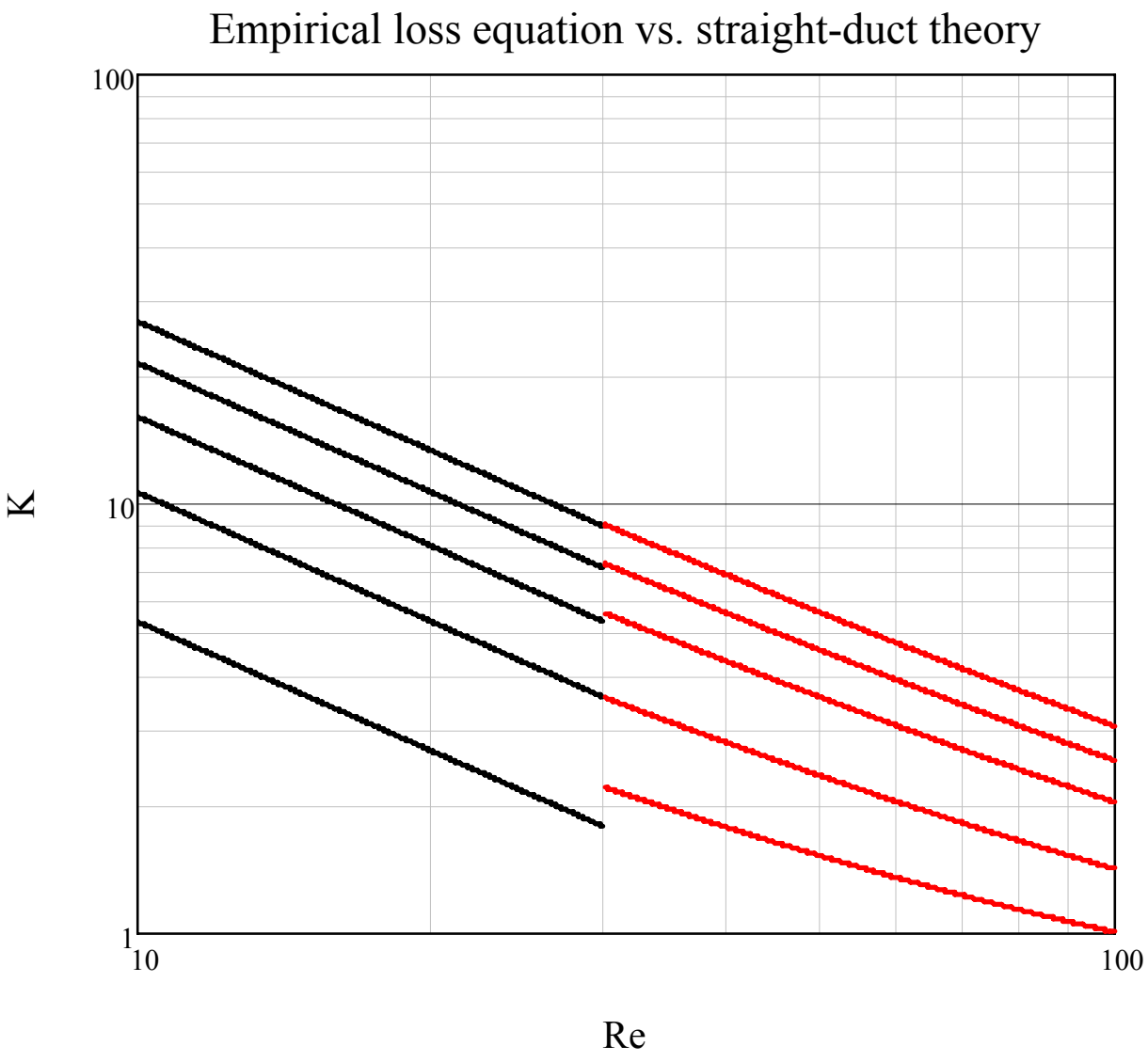

Figure 35: New bend loss equation vs. straight-duct theory

The average channel type deviated above straight duct theory at a Reynolds number of 30. The figure shows what the performance of each prediction method looks like across the whole Reynolds number range tested. The 30 Re matching isn't perfect but represents a meeting of the two theories where one begins to drop off and the other takes over.

CHAPTER FIVE: CONCLUSIONS

The field of microfluidcs though widely explored still contains many uncharted regions. Previous to now whole systems testing has resulted in novel designs, but little understanding, or at least charting of desirable features has been accomplished. Straight-duct microchannel flow has received attention, but the few domains and situations tested leave more areas to be discovered. Many pipe features such as bends and sudden and gradual area changes have yet to be tested rigorously in the laminar microscale domain. Because of this grievous gap of understanding sweeping-bend microchannels were tested for pressure losses over a range of Reynolds numbers, bend radii, and bend angles. This pressure loss mapping will require a new kind of test bed that can give accurate repeatable pressure data on a range of channel types. In addition a set of straight-duct microchannels were tested in order to validate the new test bed and help prove or disprove their adherence to macro scale laminar straight-duct theory.

Square-profile 100μm channels containing bends were cast in PDMS along with static pressure ports at key locations up and downstream of the feature to be tested. Bend channels were of angles 45º, 90º and 180º with five radii ranging from 125 to 625μm. Additionally a set of 1 and 2mm straight channels were included for testing and verification of laminar macro flow theory. A programmable syringe pump was used to deliver distilled water at set volumetric flow rates ranging from 50μL/min to 500μL/min resulting in Reynolds numbers between 8.5 and 85. Pressure losses were detected through the static pressure port using a differential pressure transducer which was captured via a data acquisition board for full automation. Channels were plumbed to the pump and transducer via needles and small diameter tubing that was to remain

filled with water at all times. Special procedure had to be used to ensure that during the plumbing phase no air bubbles were present in either the channel or the pressure lines. Capillary effects of a bubble blocking any portion of the flow network would result in extreme errors in pressure loss data. Once a channel was plumbed and tested, cross section slices were imaged under a microscope to verify exact dimensions of the manufactured channels.

With test bed and procedures set a large quantity of straight and bend microchannels were tested for average pressure losses. First the straight-duct channels were tested against macro theory, and to help act as validation for the new test bed. Ten trials of each length of straight-duct channel were tested with excellent results. All of the 2mm channels fell with in the bounds of the uncertainty analysis, and only minor deviations beyond expected uncertainty were recorded in the 1mm channels. Over all the 1mm channels deviated an average 1.1% above the exact theoretical values of pressure loss for that channel type. Similarly the 2mm channels were again averaged to be above theory by 1.8%. This small deviation above theoretical pressure loss noticed across all the tests could come from a small bias in any piece of equipment. The deviation was not viewed as being significant and it was concluded that 100μm square-profile microchannels strictly adhere to laminar macro head loss theory.

Straight-duct pressure loss testing had proven the test bed of being capable of producing acceptably reproducible and accurate data for microchannels. Sweeping-bend microchannels were then tested for their pressure loss characteristics. Very little previously established macro scale theory or experimental data exists, but according to what was available the sweeping bend channels should behave like straight channels of the same length across the Reynolds numbers in question. Essentially the theoretical work before now made no reference to any sort of additional losses due to secondary flow which is commonly observed in turbulent flows. The data collected

seems to point to an entirely different conclusion. When compared to straight duct theory for channels of the same path length the sweeping-bends followed closely at low Reynolds numbers. As the flow rate increased, however, the losses were seen to increase above and beyond what straight-duct theory had predicted. Tighter channel's deviations were more greatly exaggerated, and the effect was a definite function of Reynolds number. The combined pressure losses were rendered into a general equation that would predict a loss coefficient for sweeping bends shown again in Equation 7. This equation has only been tested on 100μm square-profile channels with radii from 125 to 625μm and bend angles of 45, 90, and 180º. It is applicable in a Reynolds number range of 30 to 90. Below 30 macro laminar head loss theory for straight ducts should be used. The transition, of Re being 30, was decided upon by a 5% error between real measurements and straight-duct prediction.

Equation 7: Loss coefficient equation for bends

$$K_{bend} = \frac{\theta}{90^{o}} \cdot \left[\frac{3}{2} \cdot \left(\frac{R}{w} \right) \cdot \frac{f}{Re} + 1 \right]$$

All initial goals were well met on the project. First a new method of detecting head loss in microchannels was created and heavily tested proving its accuracy and repeatability. Then straight-duct losses in 100μm square-profile microchannels were found to adhere to macro scale laminar head loss predictions. Finally, a new loss equation was found that predicts head loss though sweeping-bend microchannels of across a range of radii, bend angles, and Reynolds numbers.

APPENDIX A: MICROCHANNEL CALCULATIONS

A "standard" microchannel is considered to have common characteristics as seen below.

MicroLiter	$\mu L := 10^{-6} L$
Diameter	$100 \mu m$
Length	$1 cm$
Flow Rate	$100 \frac{\mu L}{min}$
Density	$1000 \frac{kg}{m^3}$
Viscosity	$8 \cdot 10^{-4} \cdot \frac{N \cdot s}{m^2}$

Reynolds number calculation for standard microchannel.

$A := \pi \cdot (50 \mu m)^2$ $Q := 100 \cdot 10^{-6} \frac{L}{min}$ $V := \frac{Q}{A}$ $V = 0.212 \frac{m}{s}$

$\rho := 1000 \frac{kg}{m^3}$ $D := 100 \mu m$ $\mu := 8 \cdot 10^{-4} \cdot \frac{N \cdot s}{m^2}$

$Re := \frac{\rho \cdot V \cdot D}{\mu}$ $Re = 26.526$

Knudesn number calculation for standard microchannel

$k_B := 1.38 \cdot 10^{-23} \cdot \frac{J}{K}$ $T := 298 K$ $P := 1 atm$ $L := 1 cm$ $\sigma := 2.75 \cdot 10^{-10} m$

$Kn := \frac{k_B \cdot T}{\sqrt{2} \cdot \pi \cdot \sigma^2 \cdot P \cdot L}$ $Kn = 1.208 \times 10^{-5}$

APPENDIX B: DATA EXTRACTION CODE

Data is read in from an excel file and graphed to make sure everything came out properly

input :=

extractor.xls

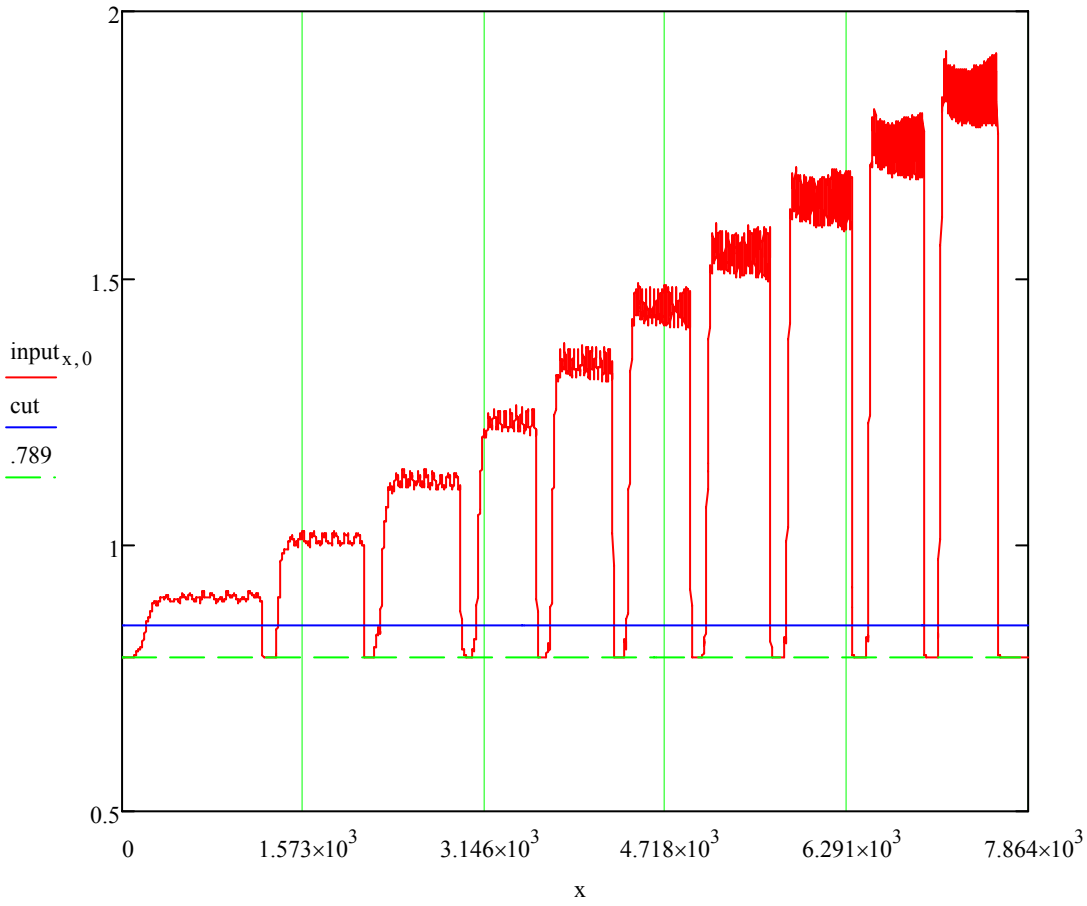

Data is chopped above the blue cut lines and cuts are placed into a matrix. The front and backs of the arrays are chopped to remove the zeroed portion of the flow.

```
ext(M, cut) := | n ← rows(M)
               | rt ← 0
               | for i ∈ 1.. n − 2
               |     start_rt ← i + F_cut  if M_{i,0} < cut ∧ M_{i+1,0} > cut
               |     if M_{i,0} > cut ∧ M_{i+1,0} < cut
               |         end_rt ← i − E_cut
               |         run ← 1
               |     while run = 1
               |         for j ∈ 0.. end_rt − start_rt
               |             flow_{j,rt} ← M_{(start_rt)+j,0}
               |         run ← 0
               |         trace(rt)
               |         rt ← rt + 1
               | flow

flow := ext(input, cut)
```

Matrix is passed to an averaging code that turns the middle flow rates to a time averaged value

```
average(flow) := | n ← cols(flow)
                 | flow_{rows(flow),0} ← 0
                 | for i ∈ 0.. n − 1
                 |     avg_i ← 0
                 |     for j ∈ 0.. rows(flow) − 1
                 |         avg_i ← avg_i + flow_{j,i}
                 |         (break)  if flow_{j,i} = 0
                 |     avg_i ← avg_i / (j + 1)
                 | avg
```

The last portion of the flow is averaged as a zero voltage.

```
ZeroFind(M, cut) := | n ← rows(M)
                    | for i ∈ 0.. n − 1
                    |     count ← count + 1  if M_{i, 0} < cut
                    |     count ← 0  otherwise
                    |     if count > 100 ∧ i > 5000
                    |         val ← val + M_{i, 0}
                    |         j ← j + 1
                    | val ← val / j
```

zero := ZeroFind(input, cut)

The 10 flow rates and zeroed voltage values are finally outputted. The cut values and lines can be adjusted as needed at this point to ensure that flow averages are found.

$F_{cut} \equiv 60$

est := average(flow)

est =

	0
0	0.899
1	1.007
2	1.116
3	1.226
4	1.335
5	1.441
6	1.542
7	1.642
8	1.743
9	1.842

zero = 0.794

Finally the chopped flow sections are displayed along side their averages. This ensures that no error occurred in the code or averaging.

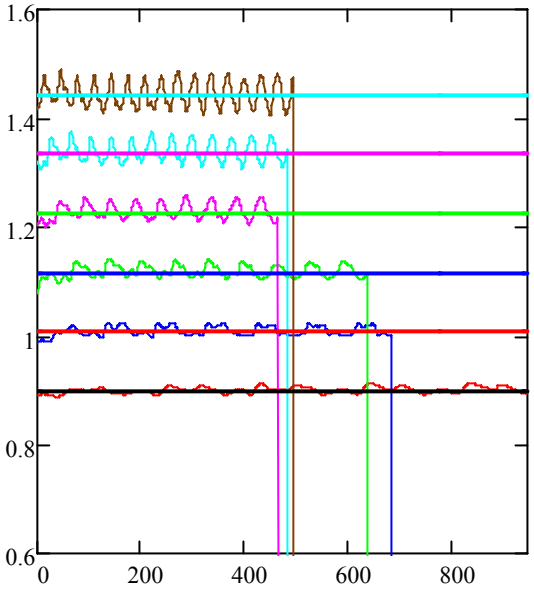

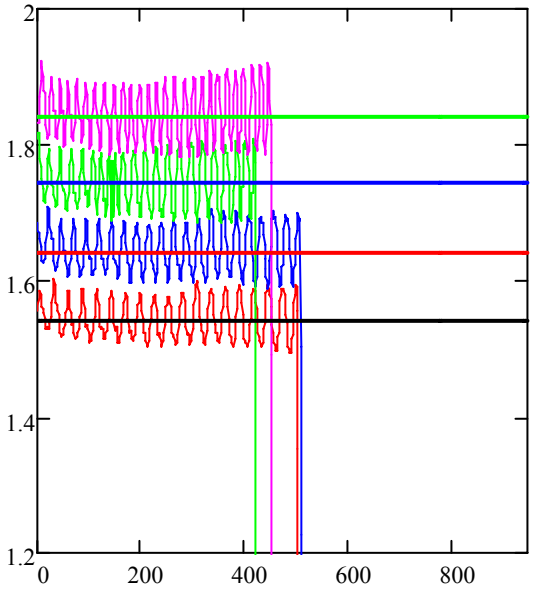

APPENDIX C: SYSTEMATIC UNCERTAINTY ANALYSIS

These defined constants and values are common to all analysis done

$\mu L := 10^{-6} L$ MathCAD does not have a standard measure for microliters, so one must be defined

$$Vol := \begin{pmatrix} 50 \\ 100 \\ 150 \\ 200 \\ 250 \\ 300 \\ 350 \\ 400 \\ 450 \\ 500 \end{pmatrix} \frac{\mu L}{min}$$ This array sets up the flow rates in microliters per minute as delivered by the syringe pump

$j := 0..9$ Range used to index the Volumetric flow rate

$\rho := 998 \frac{kg}{m^3}$ Density of water at 21°C

$\mu := 979 \cdot 10^{-6} \frac{kg}{m \cdot s}$ Viscosity of water at 21°C

$u_d := 4\mu m$ Uncertainty of width and height of channels from microscope

$u_\rho := .2 \frac{kg}{m^3}$ Uncertainty of density based off ±1°C

$u_\mu := 24 \times 10^{-6} \frac{kg}{m \cdot s}$ Uncertainty of viscosity based off ±1°C

input :=

Channel widths and heights are set and organized from observations made via microscope

input =

	0	1	2	3
0	"Mask Name"	"2a 1"	"2a 2"	"2a 3"
1	50	0.051	0.054	0.051
2	100	0.104	0.109	0.104
3	150	0.158	0.166	0.157
4	200	0.211	0.221	0.211
5	250	0.265	0.281	0.265
6	300	0.319	0.339	0.32
7	350	0.373	0.398	0.374
8	400	0.427	0.455	0.429
9	450	0.48	0.514	0.483
10	500	0.532	0.571	0.53
11	"Width"	109	106	105
12	"Height"	94	96	…

$i := 0, 1 .. \text{cols}(\text{input}) - 2$ Dynamic range for indexing dimensional arrays

$\text{len} := 1\text{mm} - 20\mu\text{m}$ Length between pressure ports must be slightly corrected because it was centered at 1mm, not started and stopped at this length.

Widths and heights are read in from the input excel file and turned into two vectors.

$$\begin{pmatrix} w \\ h \end{pmatrix} := \left| \begin{array}{l} \text{for } i \in 1 .. \text{cols}(\text{input}) - 1 \\ \quad \left| \begin{array}{l} w_{i-1} \leftarrow \text{input}_{11,i} \cdot \mu\text{m} \\ h_{i-1} \leftarrow \text{input}_{12,i} \cdot \mu\text{m} \end{array} \right. \\ \begin{pmatrix} w \\ h \end{pmatrix} \end{array} \right.$$

Analysis Calculations, each term is first labeled, calculated, then applied an uncertainty value

HYDRAULIC DIAMETER

$$D_{h_i} := \frac{4 \cdot w_i \left(h_i \right)}{2 \cdot \left(w_i + h_i \right)}$$

$$UD_i := \sqrt{\left[\left[\frac{4 \cdot w_i}{2 \cdot h_i + 2 \cdot w_i} - \frac{8 \cdot h_i \cdot w_i}{\left(2 \cdot h_i + 2 \cdot w_i \right)^2} \right] \cdot u_d \right]^2 + \left[\left[\frac{4 \cdot h_i}{2 \cdot h_i + 2 \cdot w_i} - \frac{8 \cdot h_i \cdot w_i}{\left(2 \cdot h_i + 2 \cdot w_i \right)^2} \right] \cdot u_d \right]^2}$$

VELOCITY

$$V_{i,j} := \frac{Vol_j}{w_i \cdot h_i}$$

$$UV_{i,j} := \sqrt{\left(\frac{Vol_j \cdot .01}{w_i \cdot h_i} \right)^2 + \left[\frac{Vol_j \cdot u_d}{\left(w_i \right)^2 \cdot h_i} \right]^2 + \left[\frac{Vol_j \cdot u_d}{w_i \cdot \left(h_i \right)^2} \right]^2}$$

REYNOLDS NUMBER

$$Re_{i,j} := \frac{\rho \cdot V_{i,j} \cdot D_{h_i}}{\mu}$$

$$URe_{i,j} := \sqrt{\left(\frac{u_\rho \cdot V_{i,j} \cdot D_{h_i}}{\mu} \right)^2 + \left(\frac{\rho \cdot UV_{i,j} \cdot D_{h_i}}{\mu} \right)^2 + \left(\frac{\rho \cdot V_{i,j} \cdot UD_i}{\mu} \right)^2 + \left(\frac{\rho \cdot V_{i,j} \cdot D_{h_i} \cdot u_\mu}{\mu^2} \right)^2}$$

HEIGHT TO WIDTH RATIO

$$r_i := \frac{h_i}{w_i}$$

$$Ur_i := \sqrt{\left(\frac{1}{w_i} \cdot u_d \right)^2 + \left[\frac{h_i}{\left(w_i \right)^2} \cdot u_d \right]^2}$$

THEORETICAL LAMINAR FRICTION FACTOR

$$f_{i,j} := \frac{64}{Re_{i,j} \cdot \left[\frac{2}{3} + \frac{11}{24} \cdot r_i \cdot \left(2 - r_i\right)\right]}$$

$$Uf_{i,j} := \sqrt{\left[\frac{64 \cdot \left(\frac{11 \cdot r_i}{12} - \frac{11}{12}\right) \cdot Ur_i}{Re_{i,j} \cdot \left[\frac{11 \cdot r_i \cdot \left(r_i - 2\right)}{24} - \frac{2}{3}\right]^2}\right]^2 + \left[\frac{64 \cdot URe_{i,j}}{\left(Re_{i,j}\right)^2 \cdot \left[\frac{11 \cdot r_i \cdot \left(r_i - 2\right)}{24} - \frac{2}{3}\right]}\right]^2}$$

STRAIGHT DUCT HEAD LOSS

$$Hloss_{i,j} := f_{i,j} \cdot \rho \cdot \frac{len}{D_{h_i}} \cdot \frac{\left(V_{i,j}\right)^2}{2}$$

$$a_{i,j} := \left[\left(\frac{f_{i,j} \cdot \rho \cdot len \cdot V_{i,j} \cdot UV_{i,j}}{D_{h_i} \cdot 2}\right)^2 + \left[\frac{f_{i,j} \cdot \rho \cdot len \cdot \left(V_{i,j}\right)^2 \cdot UD_i}{\left(D_{h_i}\right)^2 \cdot 2}\right]^2\right]$$

$$b_{i,j} := \left[\left[\frac{Uf_{i,j} \cdot \rho \cdot len \cdot \left(V_{i,j}\right)^2}{2 \cdot D_{h_i}}\right]^2 + \left[\frac{f_{i,j} \cdot u_\rho \cdot len \cdot \left(V_{i,j}\right)^2}{D_{h_i} \cdot 2}\right]^2\right]$$

$$UH_{i,j} := \sqrt{a_{i,j} + b_{i,j}}$$

APPENDIX D: STRAIGHT-DUCT THEORETICAL LOSSES

Each channel's pressure loss curves (blue X's) are compared to their theoretical values (red bars indicate error region).

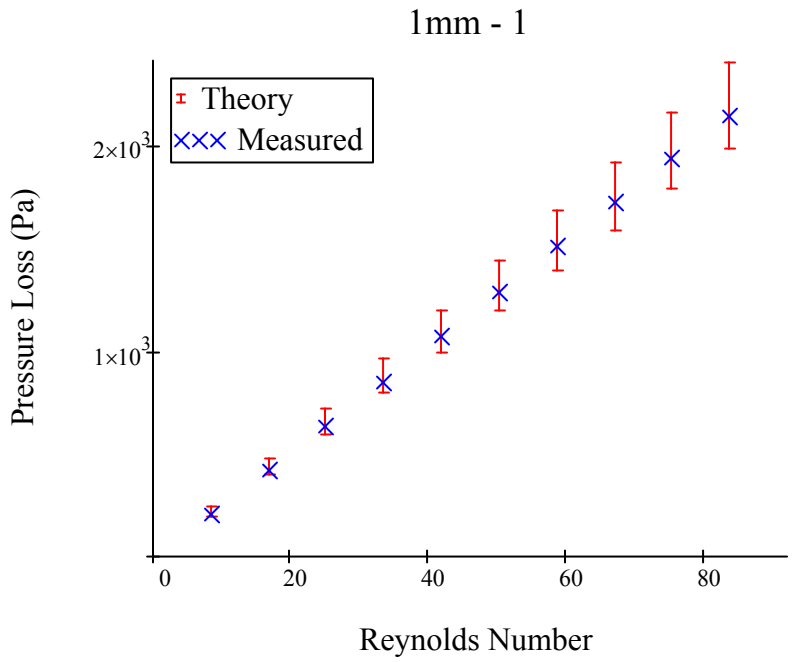

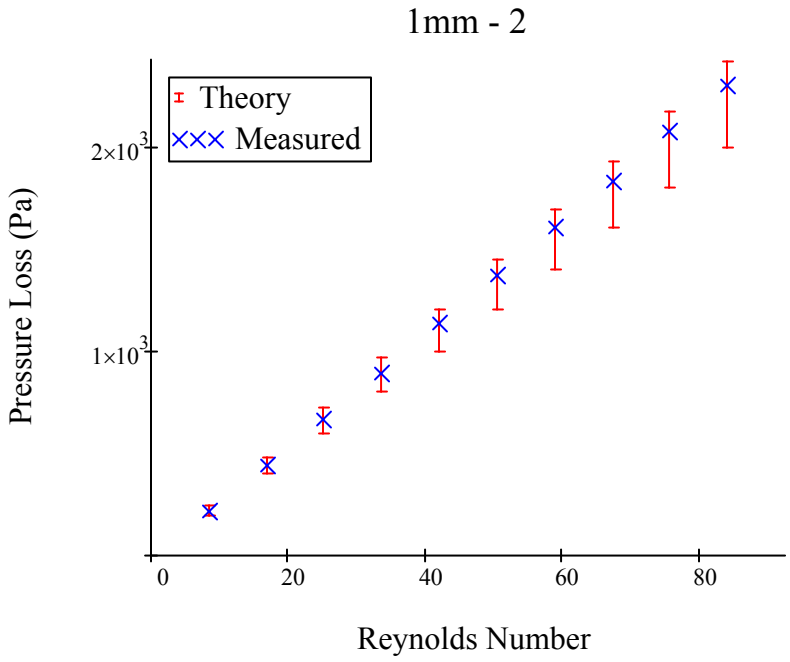

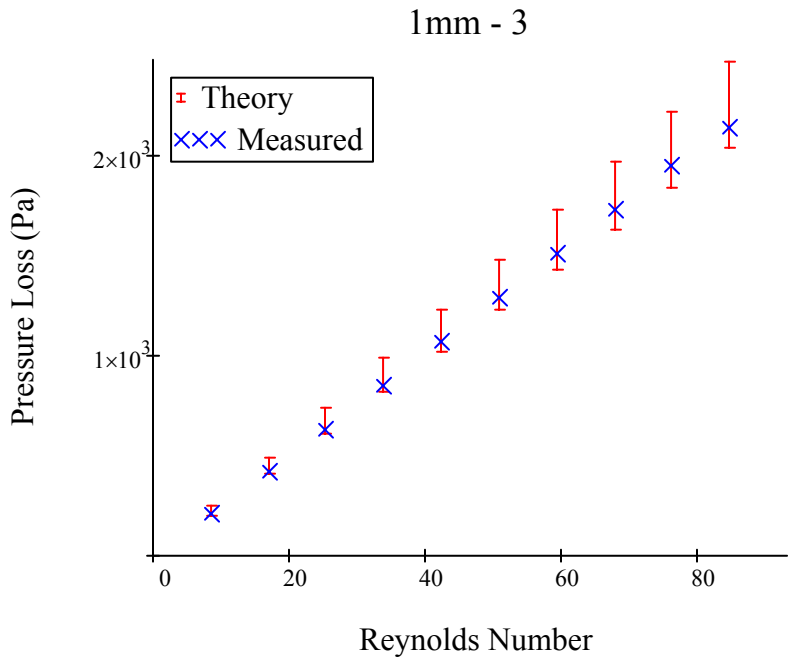
1mm - 3
Theory
Measured
2×10^3
1×10^3
Pressure Loss (Pa)
0
20
40
60
80
Reynolds Number

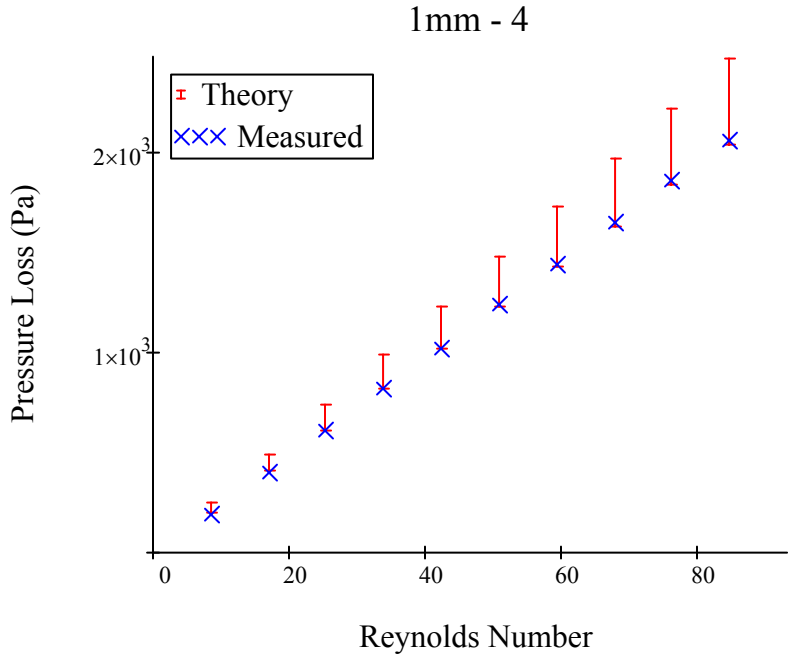
1mm - 4
Theory
Measured
2×10^3
1×10^3
Pressure Loss (Pa)
0
20
40
60
80
Reynolds Number

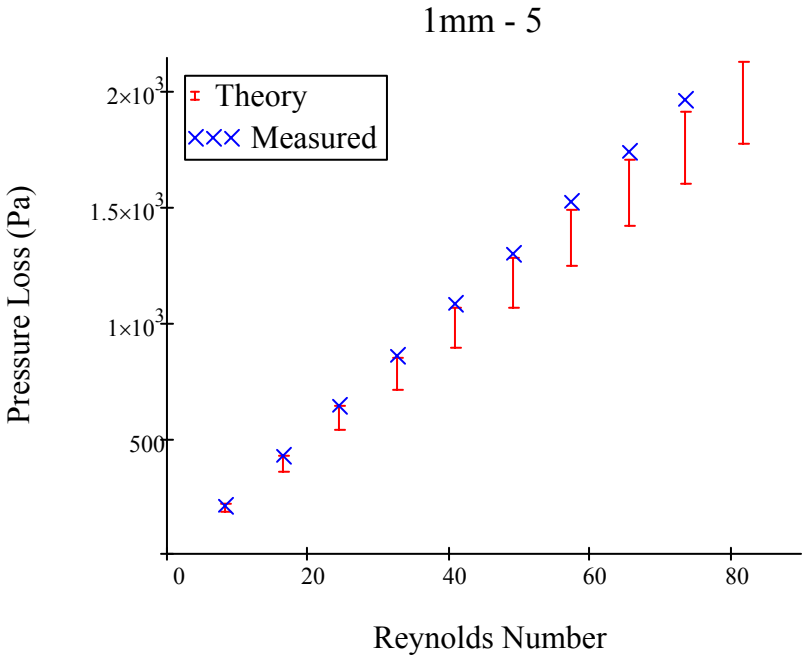
1mm - 5
Theory
Measured
2×10^3
1.5×10^3
1×10^3
500
Pressure Loss (Pa)
0
20
40
60
80
Reynolds Number

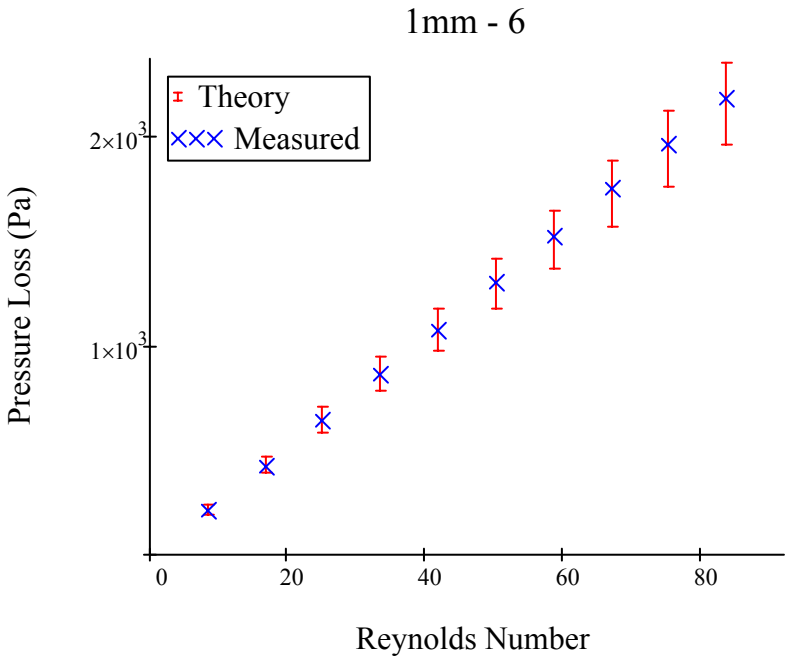
1mm - 6
Theory
Measured
2×10^3
1×10^3
Pressure Loss (Pa)
0
20
40
60
80
Reynolds Number

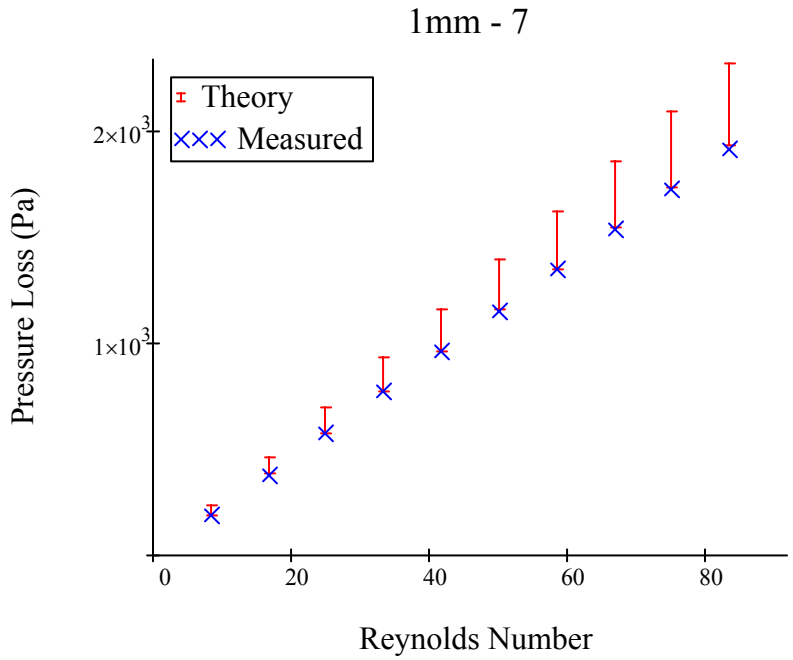
1mm - 7
Theory
Measured
2×10^3
1×10^3
Pressure Loss (Pa)
0
20
40
60
80
Reynolds Number

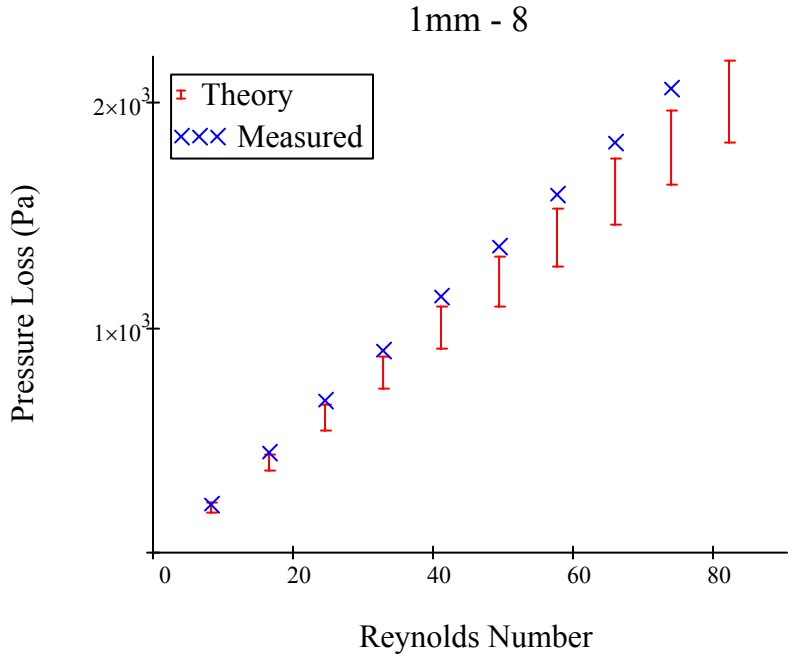
1mm - 8
Theory
Measured
2×10^3
1×10^3
Pressure Loss (Pa)
0
20
40
60
80
Reynolds Number

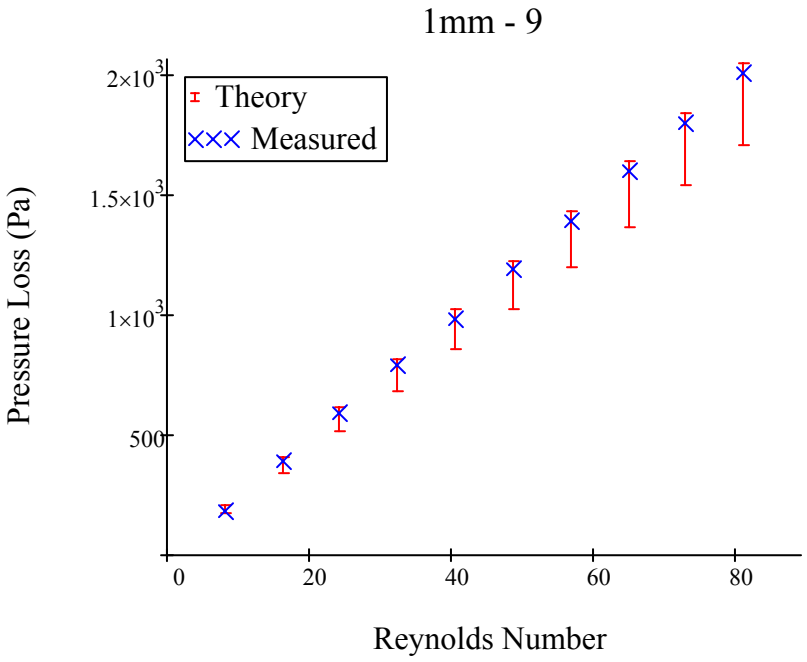
1mm - 9
Theory
Measured
Pressure Loss (Pa)
2×10^3
1.5×10^3
1×10^3
500
0
20
40
60
80
Reynolds Number

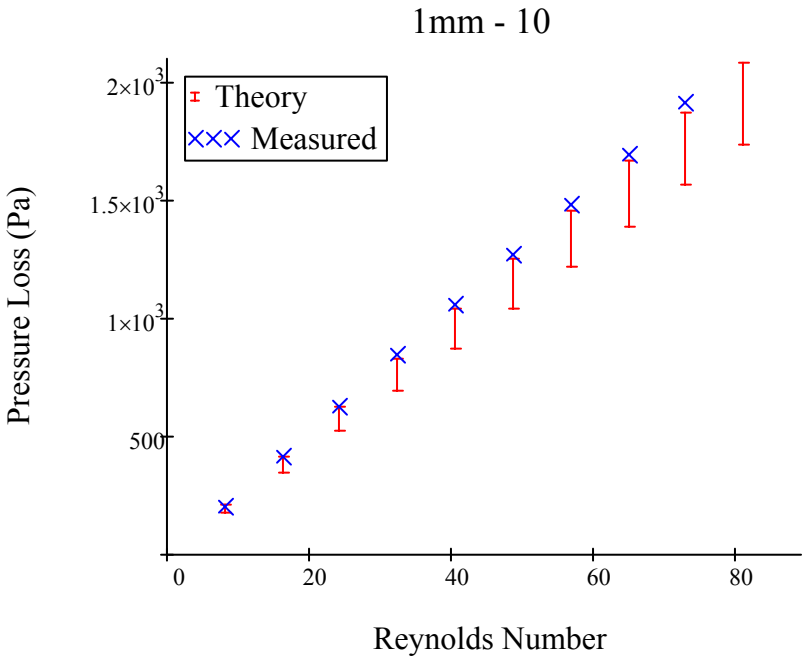
1mm - 10
Theory
Measured
Pressure Loss (Pa)
2×10^3
1.5×10^3
1×10^3
500
0
20
40
60
80
Reynolds Number

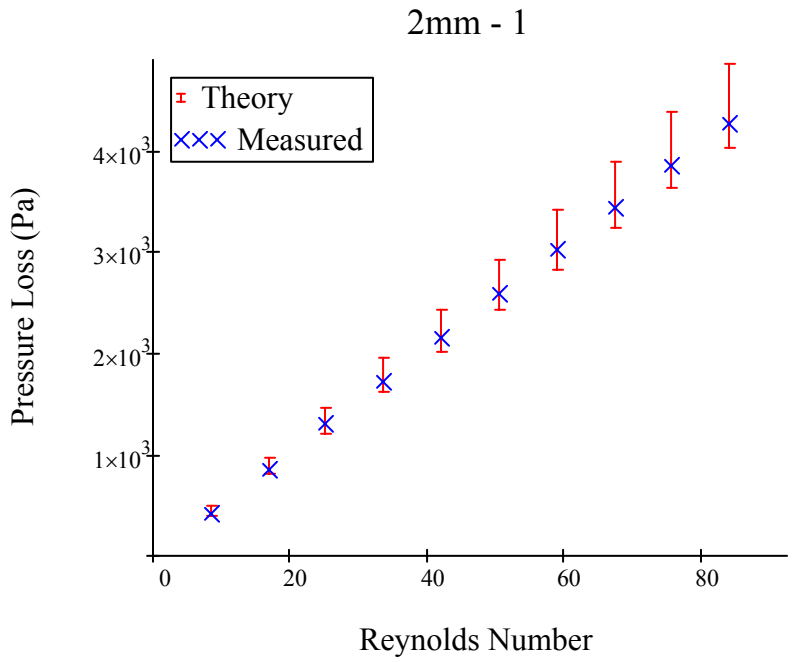
2mm - 1
Theory
Measured
Pressure Loss (Pa)
4×10^3
3×10^3
2×10^3
1×10^3
0
20
40
60
80
Reynolds Number

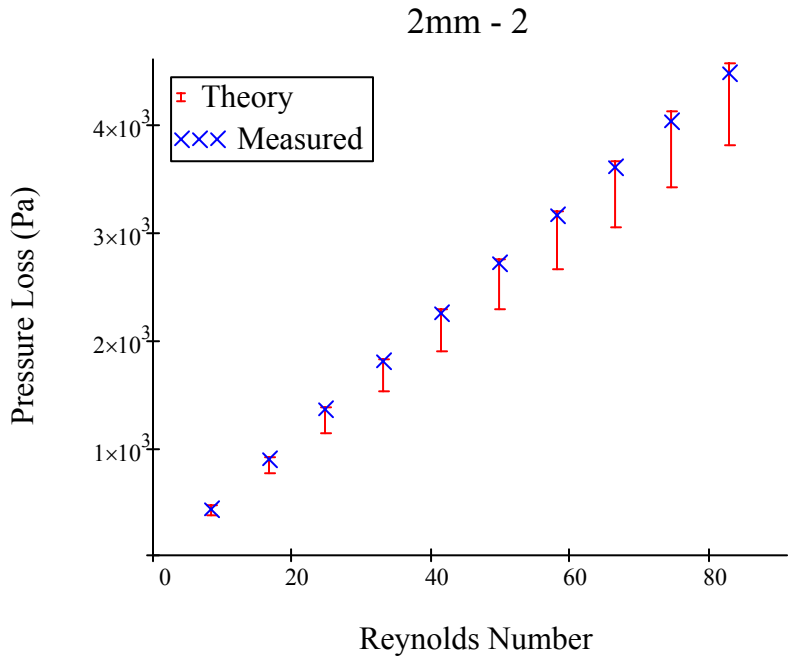
2mm - 2
Theory
Measured
Pressure Loss (Pa)
4×10^3
3×10^3
2×10^3
1×10^3
0
20
40
60
80
Reynolds Number

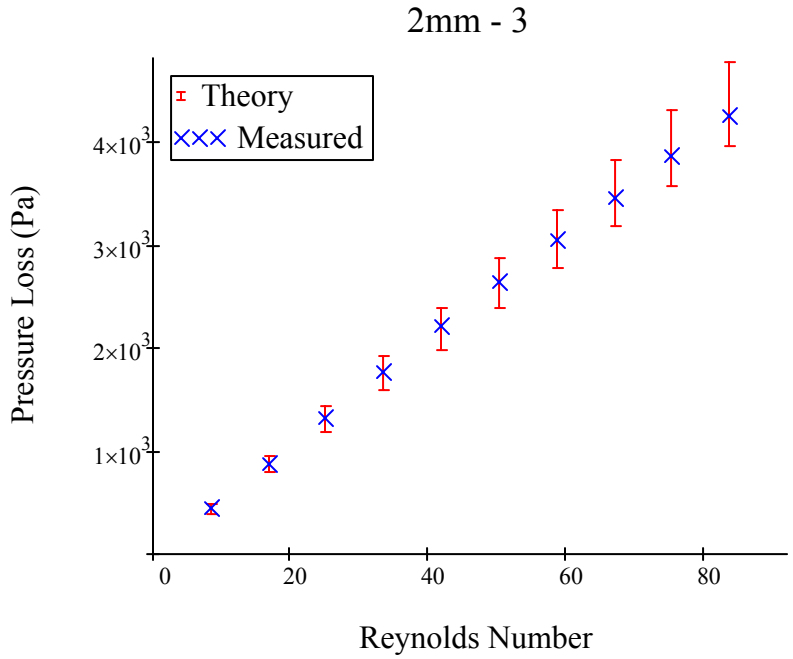
2mm - 3
Theory
Measured
Pressure Loss (Pa)
4×10^3
3×10^3
2×10^3
1×10^3
0
20
40
60
80
Reynolds Number

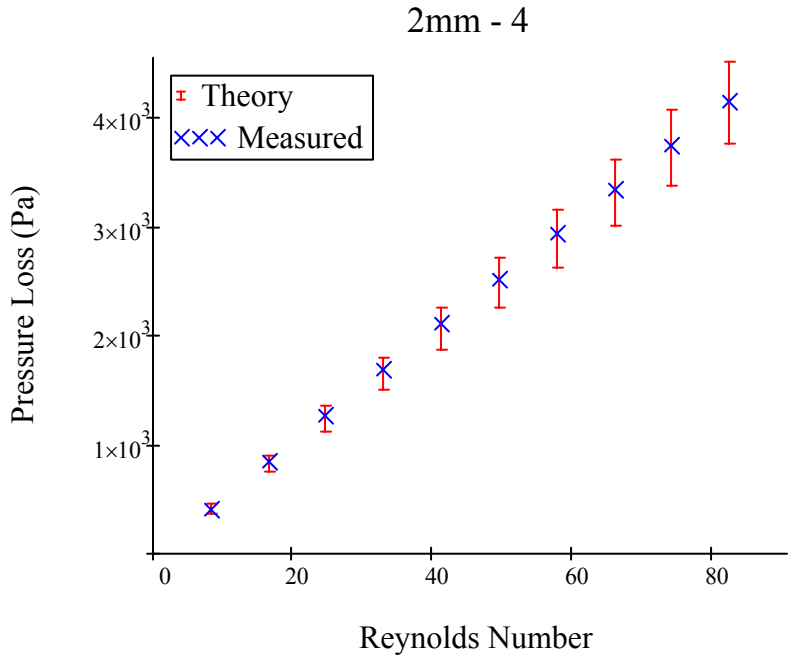
2mm - 4
Theory
Measured
Pressure Loss (Pa)
4×10^3
3×10^3
2×10^3
1×10^3
0
20
40
60
80
Reynolds Number

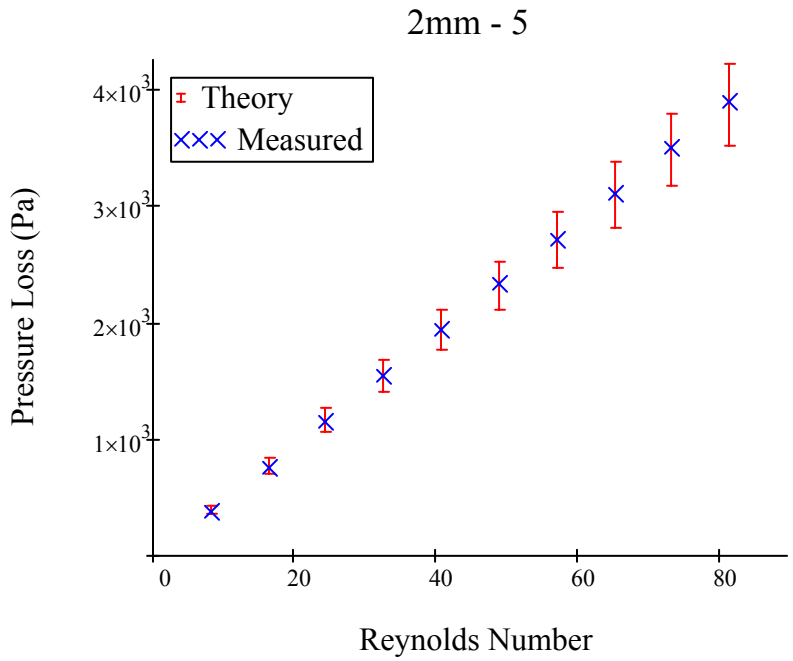
2mm - 5
Theory
Measured
Pressure Loss (Pa)
4×10^3
3×10^3
2×10^3
1×10^3
0
20
40
60
80
Reynolds Number

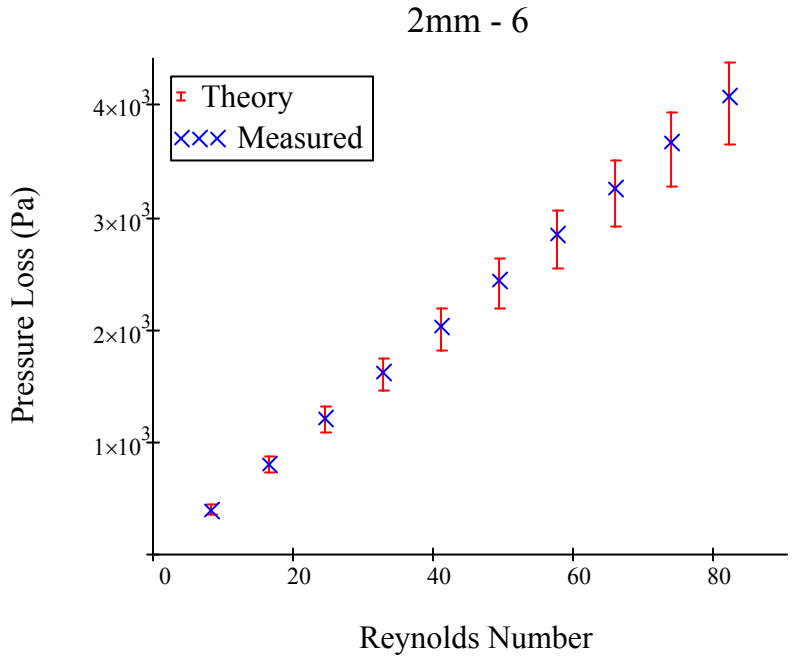
2mm - 6
Theory
Measured
Pressure Loss (Pa)
4×10^3
3×10^3
2×10^3
1×10^3
0
20
40
60
80
Reynolds Number

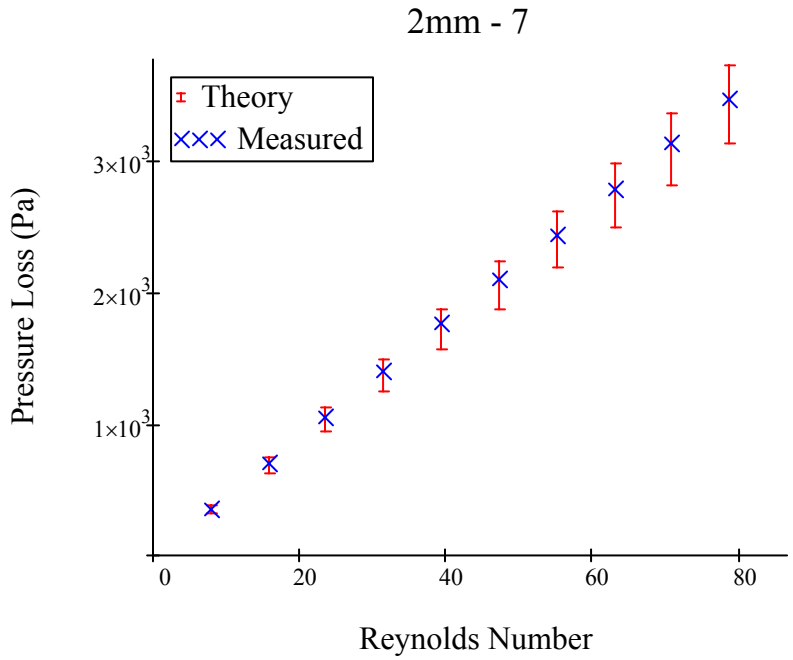
2mm - 7
Theory
Measured
Pressure Loss (Pa)
3×10^3
2×10^3
1×10^3
0
20
40
60
80
Reynolds Number

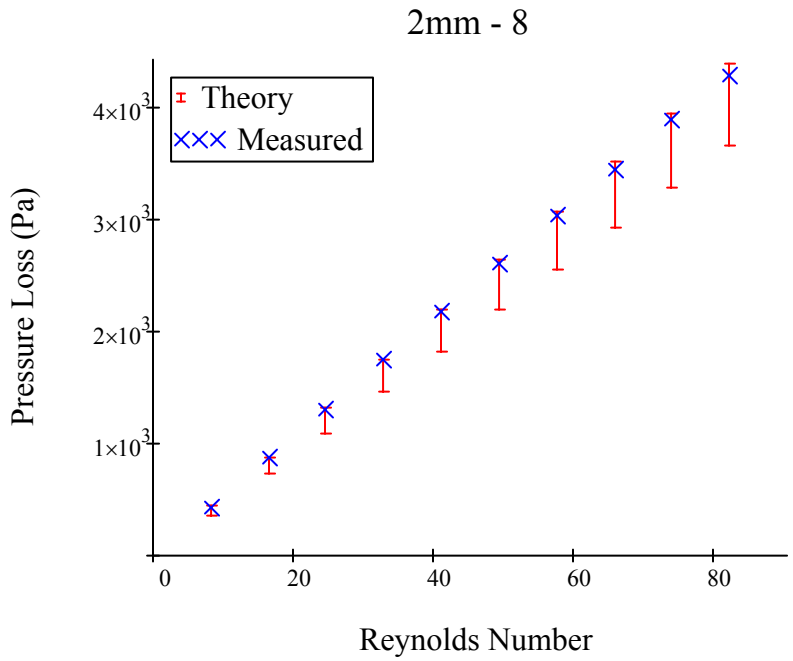
2mm - 8
Theory
Measured
Pressure Loss (Pa)
4×10^3
3×10^3
2×10^3
1×10^3
0
20
40
60
80
Reynolds Number

APPENDIX E: SWEEPING-BEND CURVE FITS

45º - 1.25r

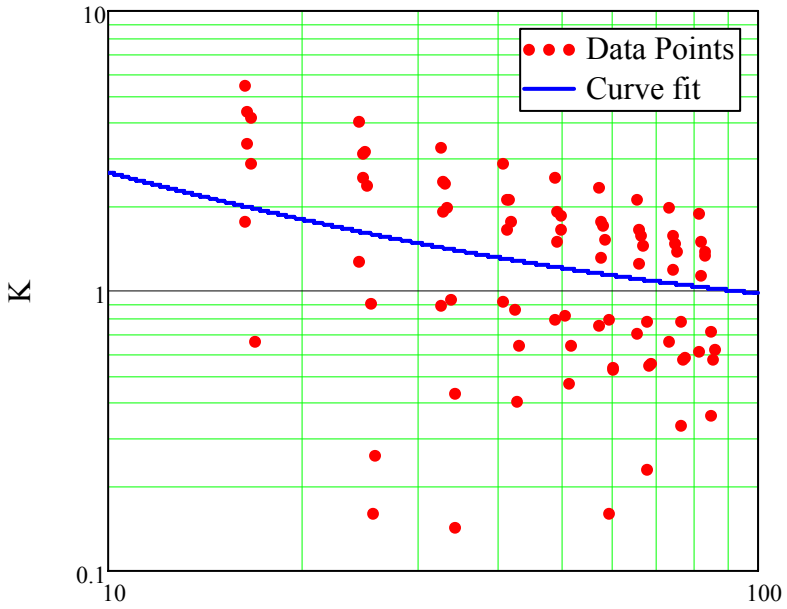

45º - 2.5r

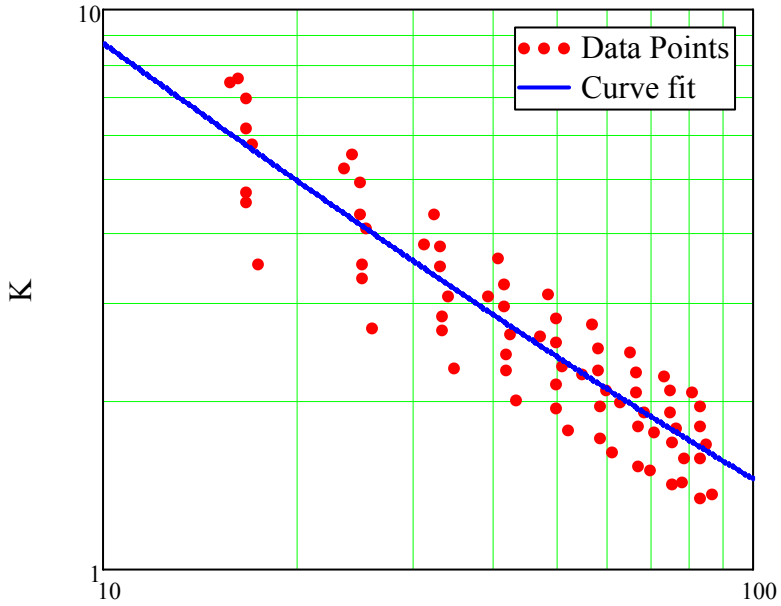

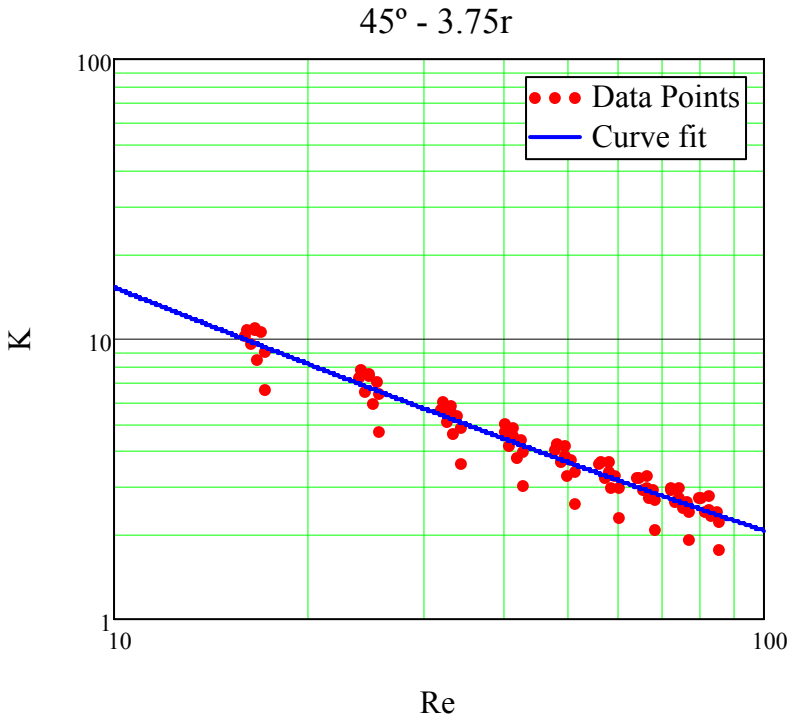
45º - 3.75r
100
10
1
K
10
100
Re
Data Points
Curve fit

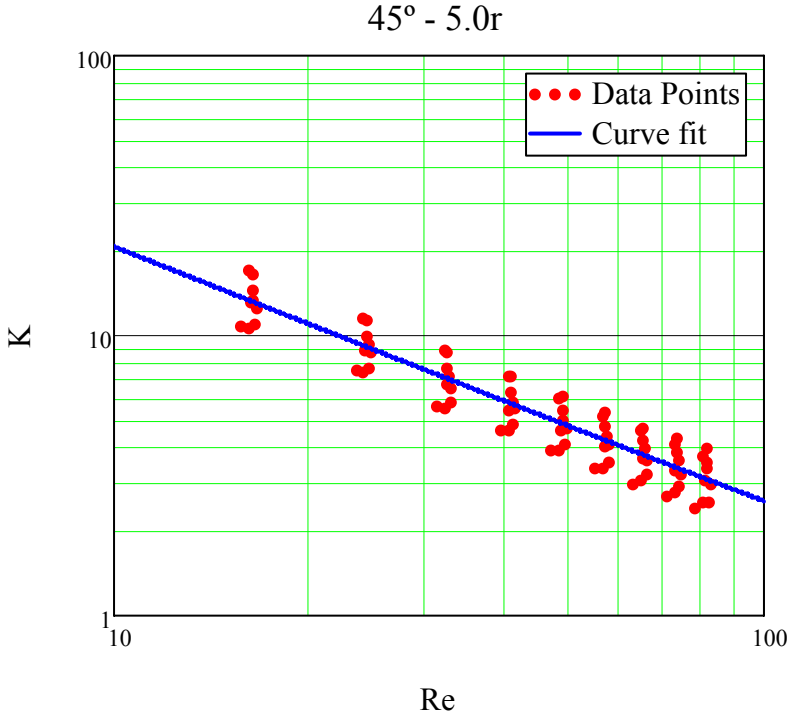
45º - 5.0r
100
10
1
K
10
100
Re
Data Points
Curve fit

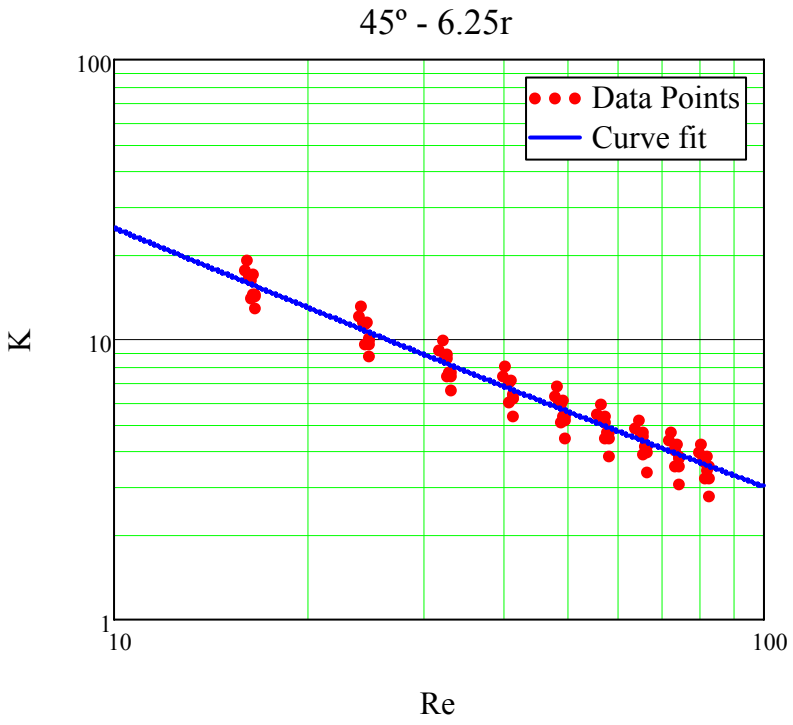
45º - 6.25r
100
10
1
K
10
100
Re
Data Points
Curve fit

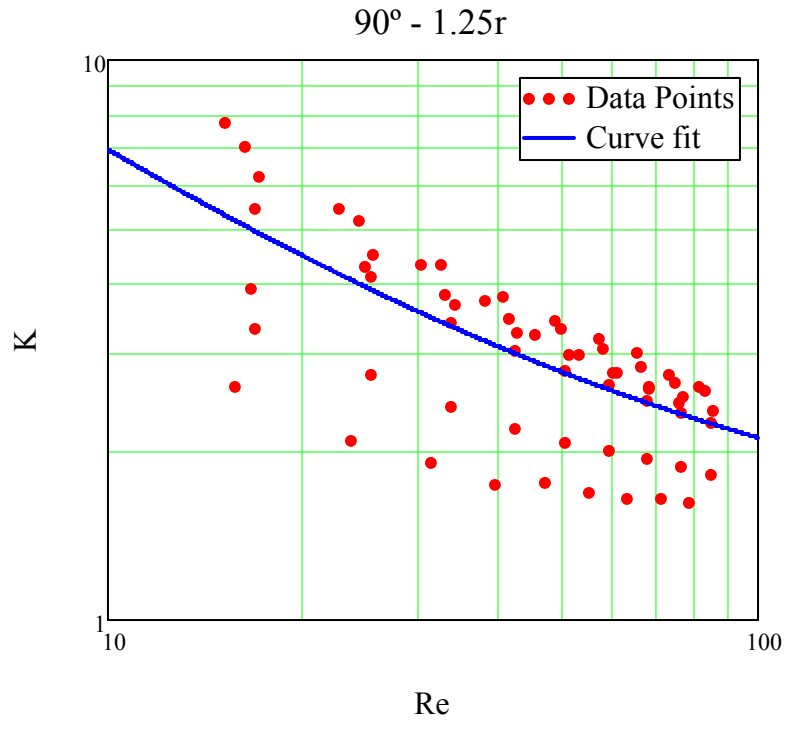
90º - 1.25r
10
1
K
10
100
Re
Data Points
Curve fit

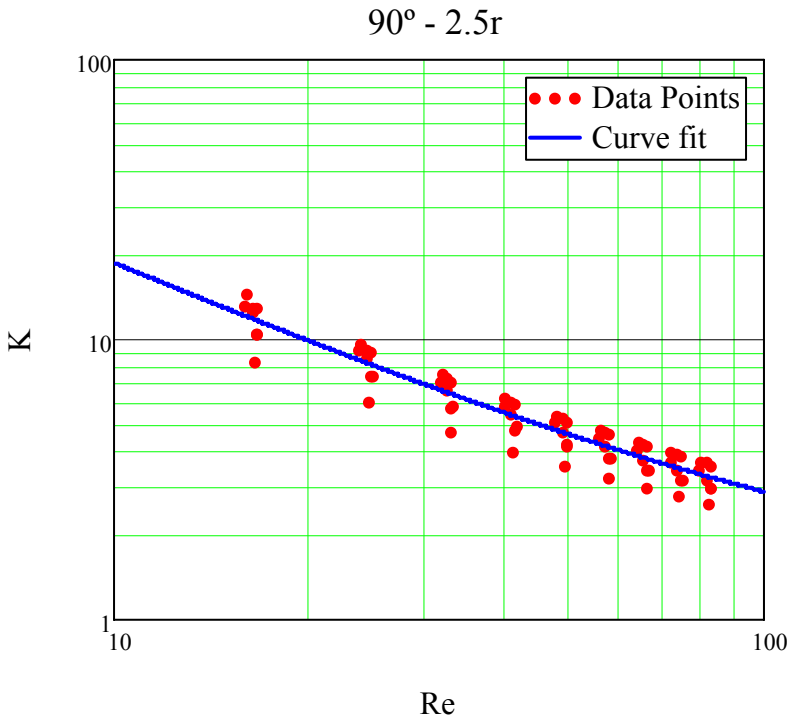
90º - 2.5r
100
10
1
K
Data Points
Curve fit
10
100
Re

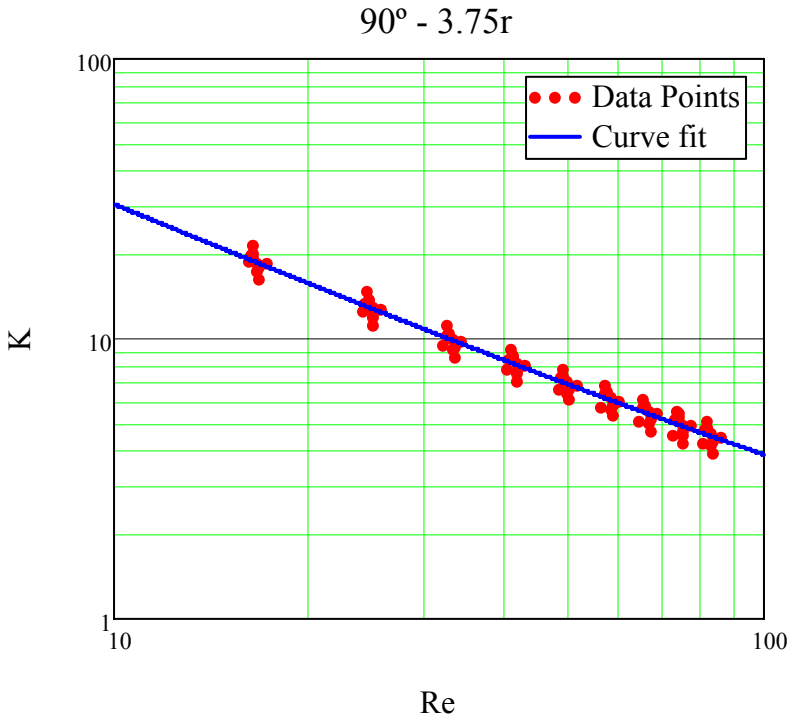
90º - 3.75r
100
10
1
K
Data Points
Curve fit
10
100
Re

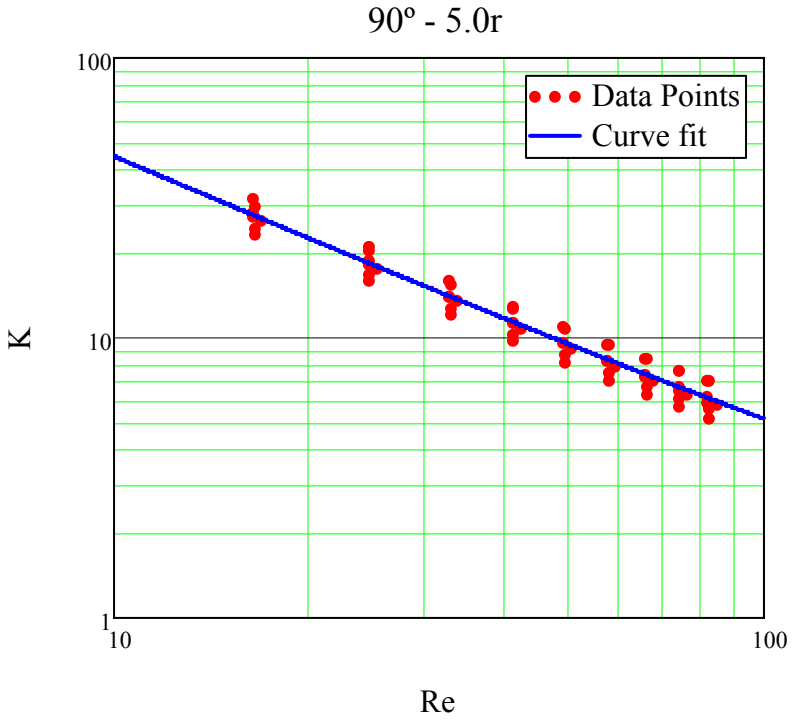
90º - 5.0r
100
10
1
K
10
100
Re
Data Points
Curve fit

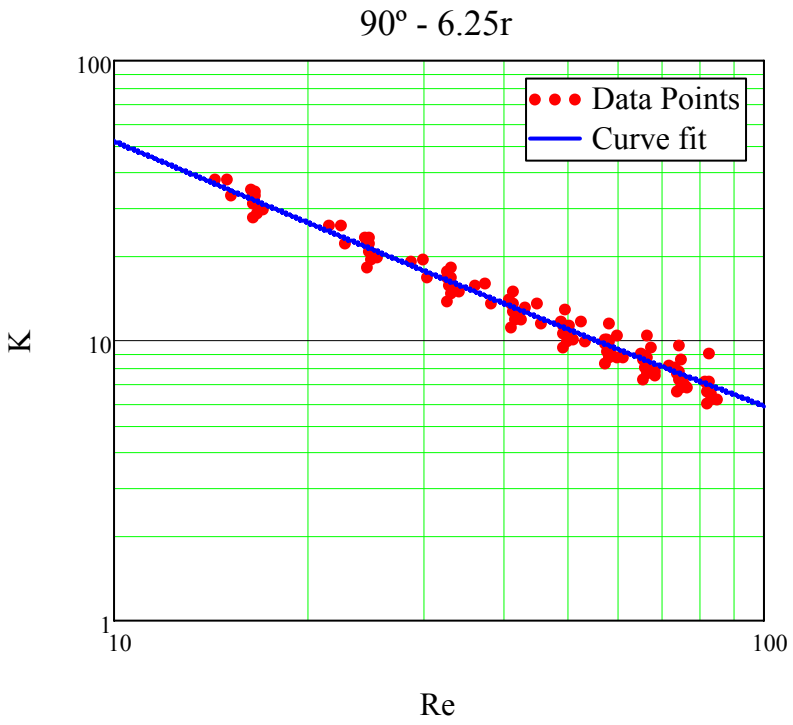
90º - 6.25r
100
10
1
K
10
100
Re
Data Points
Curve fit

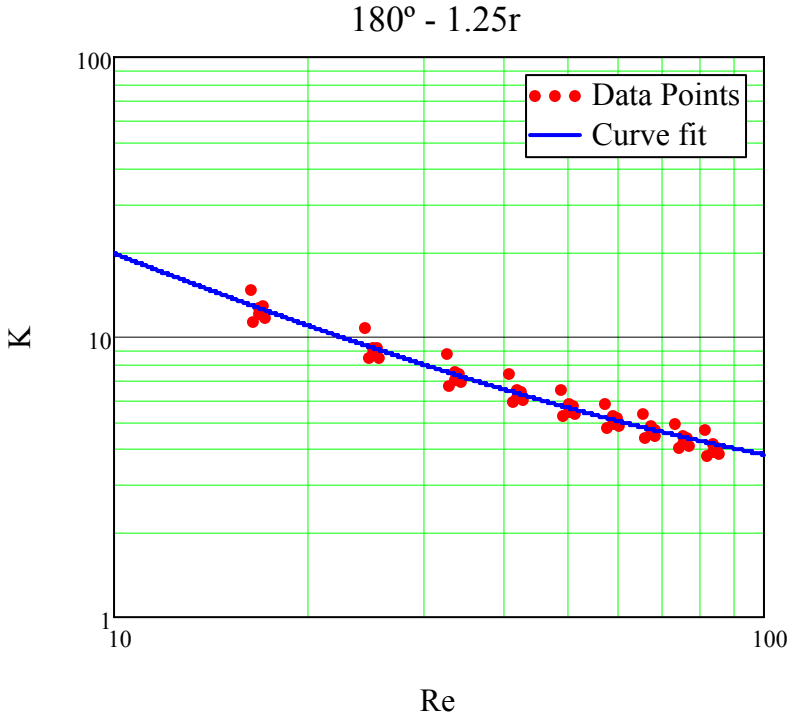
180º - 1.25r
Data Points
Curve fit
100
10
1
K
10
100
Re

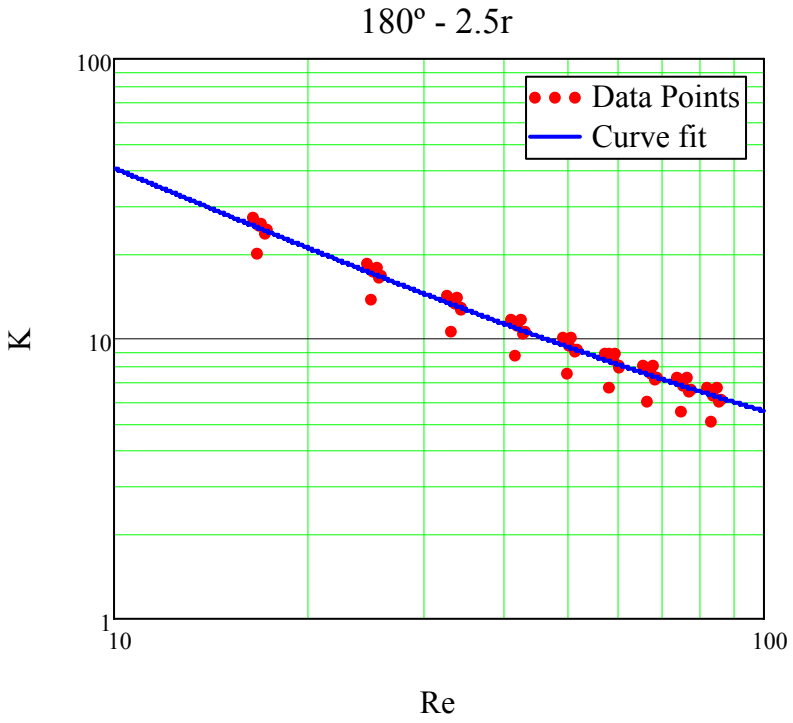
180º - 2.5r
Data Points
Curve fit
100
10
1
K
10
100
Re

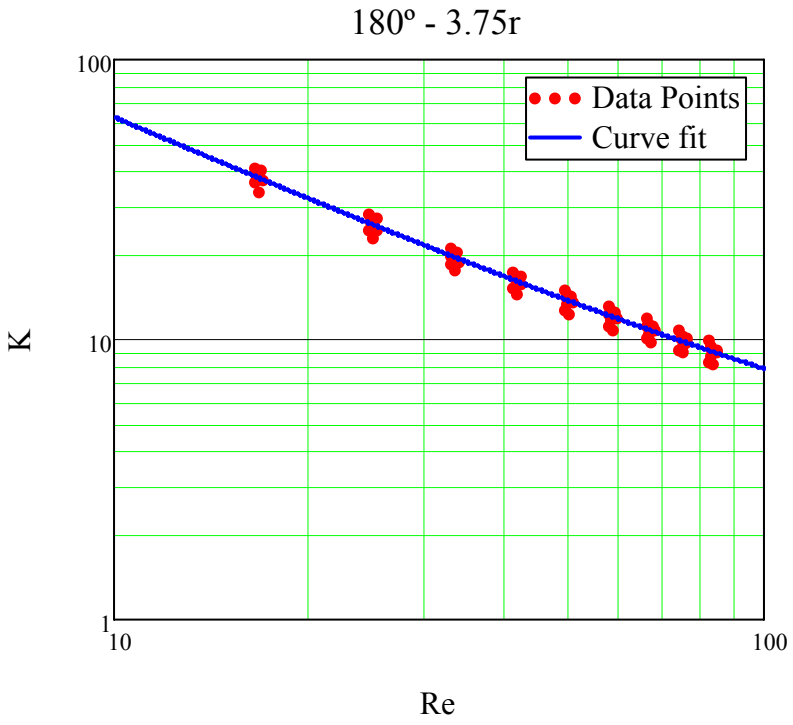
180º - 3.75r
100
10
1
K
10
100
Re
Data Points
Curve fit

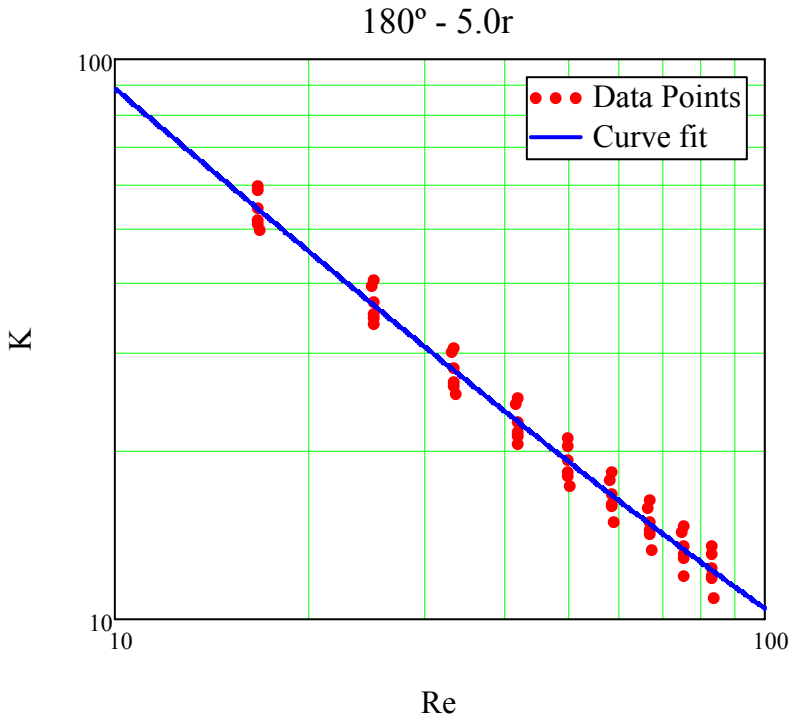
180º - 5.0r
100
10
K
10
100
Re
Data Points
Curve fit

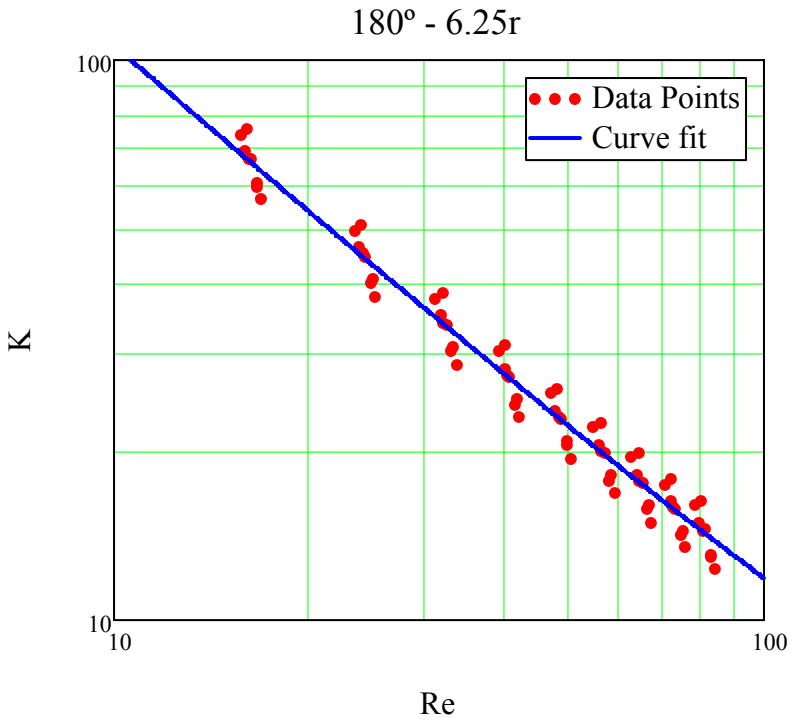
180º - 6.25r
100
10
10
100
K
Re
Data Points
Curve fit

RERFERENCES

[1] P. Gravesen, J. Branebjerg, and O. S. Jensen, "Microfluidics - a review," *J. Micromech. Microeng.*, vol. 3, pp. 168-182, 1993.

[2] S. Shoji and M. Esashi, "Microflow Devices and Systems," *J. Micromech. Microeng.*, vol. 4, pp. 157-171, 1994.

[3] C. Feldt and L. Chew, "Geometry-based micro-tool evaulation of non-moving-part valvular microchannels," *J. Micromech. Microeng.*, vol. 12, pp. 662-669, 2002.

[4] W. Wang and S. A. Soper, *Bio-MEMS: Technologies and applications*: CRC / Taylor & Francis, 2007.

[5] P. Tabeling, *Introduction to Microfluidics*: Oxford University Press, 2005.

[6] W. Qu, G. M. Mala, and L. Dongqing, "Pressure-driven water flows in trapezoidal silicon microchannels," *International Journal of Heat and Mass Transfer*, vol. 43, pp. 353-364, 2000.

[7] G. M. Mala and L. Dongqing, "Flow characteristics of water in microtubes," *International Journal of Heat and Fluid Flow*, vol. 20, pp. 142-148, 1999.

[8] M. Bahrami, M. M. Yovanovich, and J. R. Culham, "Pressure Drop of Fully Developed Laminar Flow in Rough Microtube," *Journal of Fluids Engineering*, vol. 128, pp. 632-637, 2006.

[9] G. P. Celata, M. Cumo, S. McPhail, and G. Zummo, "Characterization of fluid dynamic behaviour and channel wall effects in microtube," *International Journal of Heat and Fluid Flow*, 2005.

[10] R. Xiong and J. N. Chung, "Flow characteristics of water in straight and serpentine micro-channels with miter bends," *Experimental Thermal and Fluid Science*, vol. 31, pp. 805-812, 2007.

[11] C. Rands, B. W. Webb, and D. Maynes, "Characterization of transition to tubulence in microchannels," *International Journal of Heat and Mass transfer*, vol. 49, pp. 2924-2930, 2006.

[12] J. Judy, D. Maynes, and B. W. Webb, "Characterization of frictional pressure drop for liquid flows through microchannels," *International Journal of Heat and Mass transfer*, vol. 45, pp. 3477-3489, 2002.

[13] R. W. Fox, A. T. McDonald, and P. J. Pritchard, *Introduction to Fluid Mechanics*, 6th ed: John Wiley & Sons, Inc., 2004.

[14] J. Koo and C. Kleinstreuer, "Liquid flow in microchannels: experimental observations and computational analyses of microfluidics effects," *Journal of Micromechanics and Microengineering*, vol. 13, pp. 568-579, 2003.

[15] W. Qu and I. Mudawar, "Experimental and Computational Investigation of Flow development and Pressure Drop in a Rectangular Micro-channel," *Journal of Electronic Packaging*, vol. 128, pp. 1-9, 2006.

[16] H. Herwig and O. Hausner, "Critical view on "new results in micro-fluid mechanics": an example," *International Journal of Heat and Fluid Flow*, vol. 46, pp. 935-937, 2003.

[17] J. C. McDonald, D. C. Duffy, J. R. Anderson, D. T. Chiu, H. Wu, O. J. A. Schueller, and G. M. Whitesides, "Fabrication of microfluidic systems in poly(dimethylsiloxane)," *Electrophoresis*, vol. 21, pp. 27-40, 2000.

[18] D. C. Duffy, J. C. McDonald, O. J. A. Schueller, and G. M. Whitesides, "Rapid Prototyping of Microfluidic Systems in Poly(dimethylsiloxane)," *Department of Chemistry and Chemical Biology*, vol. 70, 1998.

[19] R. K. Shah and A. L. London, *Laminar flow forced convection in ducts, A source book for compact heat exchanger analytical data*. New York: Academic press, 1978.

[20] H. Li and M. G. Olsen, "Aspect Ratio Effects on Turbulent and Transitional Flow in Rectangular Microchannels as Measured with MicroPIV," *Journal of Fluids Engineering*, vol. 128, pp. 305-315, 2006.

[21] N.-T. Nguyen and S. T. Wereley, *Fundamentals and Applications of Microfluidics*, Second Edition ed: Artech House, Inc., 2006.

[22] R. Baviere, G. Gamrat, M. Favre-Marinet, and S. L. Person, "Modeling of Laminar Flows in Rough-Wall Microchannels," *Journal of Fluids Engineering*, vol. 128, pp. 734-741, 2006.

[23] A. Goullet, I. Glasgow, and N. Aubry, "Effects of microchannel geometry on pulsed flow mixing," *Mechanics Research Communications*, vol. 33, pp. 739-746, 2006.

[24] M. Niklas, M. Favre-Marinet, and D. Asendrych, "Numerical simulation of microchannel network with complex geometry," *Bulletin of the Polish Academy of Sciences*, vol. 53, 2005.

[25] R. Zengerle and M. Richter, "Simulation of microfluid systems," *J. Micromech. Microeng.*, vol. 4, pp. 192-204, 1994.

[26] H. Schlichting, *Boundary-Layer Theory*: McGraw-Hill, 1979.

[27] W. Y. Lee and M. Wong, "Pressure Loss in Constriction Microchannels," *Journal of Microelectromechanical Systems*, vol. 11, 2002.

[28] B. R. Thompson, D. Maynes, and B. W. Webb, "Characterization of the Hydrodynamically Developing Flow in a Microtube Using MTV," *Journal of Fluids Engineering*, vol. 127, pp. 1003-1012, 2005.

[29] D. Xu, T. Y. Ng, L. S. Pan, K. Y. Lam, and H. Li, "Numerical simulations of fully developed tubulent liquid flows in micro tubes," *Journal of Micromechanics and Microengineering*, vol. 11, pp. 157-180, 2001.

[30] E. Fried and I. E. Idelchik, *Flow Resistance: A Design Guide for Engineers*: Hemisphere Publishing Corp, 1989.

[31] J. J. Bloomer, *Practical Fluid Mechanics for Engineering Applications*: Marcel Dekker, Inc., 2000.

[32] N. P. Cheremisonoff, *Practical Fluid Mechanics for Engineers and Scientists*: Technomic Publishing Company, Inc, 1990.

[33] C. C. E. Division, *Flow of Fluids through Valves, Fittings, and Pipe*. New York: Crance Co., 1969.

[34] R. D. Blevins, *Applied Fluid Dynamics Handbook*. New York: Van Nostrand Reinhold Company Inc., 1984.

[35] C.-H. Tsai, C.-H. Tai, L.-M. Fu, and F.-B. Wu, "Experimental and numberical analysis of the geometry effects of low-dispersion turnsin microfluidic systems," *Journal of Micromechanics and Microengineering*, vol. 15, pp. 277-385, 2005.

[36] M. Yi and H. H. Bau, "The Kinematics of bend-induced mixing in micro-conduits," *International Journal of Heat and Fluid Flow*, vol. 24, pp. 645-656, 2003.

[37] R. Raju and S. Roy, "Hydrodynamic Model for Microscale Flows in a Channel With Two 90 deg Bends," *Journal of Fluids Engineering*, vol. 126, pp. 489-492, 2004.

[38] S. Y. K. Lee, M. Wong, and Y. Zohar, "Gas flow in microchannels with bends," *J. Micromech. Microeng.*, vol. 11, pp. 635-644, 2001.

[39] L. Wang and F. Liu, "Forced Convection in slighly curved microchannels," *International Journal of Heat and Mass Transfer*, vol. 50, pp. 881-896, 2007.

[40] A. P. Sudarsan and V. M. Ugaz, "Fluid mixing in planar spiral microchannels," *The Royal Society of Chemistry*, pp. 74-82, 2006.